

The Islamic University of Gaza
Deanery of Graduate Studies
Faculty of Electrical Engineering
Communication Systems Department



الجامعة الإسلامية-غزة
عمادة الدراسات العليا
كلية الهندسة الكهربائية
قسم أنظمة الاتصالات

M.Sc Thesis

Design of a 4x4 Butler Matrix for Vehicle Radar Beamforming Antenna systems at 24 GHz

By

Hani Abdul Rahman Al Habibi

Supervisor

Dr.Talal F.Skaik

"A Thesis Submitted in Partial Fulfillment of the Requirements for the Degree of
Master of Telecommunication Engineering"

Gaza-Palestine

2014م - 1436هـ

نموذج رقم (1)

إقرار

أنا الموقع أدناه مقدم الرسالة التي تحمل العنوان:

Design of a 4x4 Butler Matrix for Vehicle Radar Beamforming Antenna systems at 24 GHz

أقر بأن ما اشتملت عليه هذه الرسالة إنما هو نتاج جهدي الخاص، باستثناء ما تمت الإشارة إليه حيثما ورد، وإن هذه الرسالة ككل أو أي جزء منها لم يقدم من قبل لنيل درجة أو لقب علمي أو بحثي لدى أي مؤسسة تعليمية أو بحثية أخرى.

DECLARATION

The work provided in this thesis, unless otherwise referenced, is the researcher's own work, and has not been submitted elsewhere for any other degree or qualification

Student's name

Hani A.M Al habibi

Signature

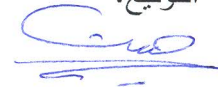
Date:

2015/02/01

اسم الطالب:

هاني عبد الرحمن محمود الحبيبي

التوقيع:



التاريخ:

2015/02/01



مكتب نائب الرئيس للبحث العلمي والدراسات العليا هاتف داخلي 1150

الرقم ج س غ /35/ Ref

التاريخ 2015/01/06 Date

نتيجة الحكم على أطروحة ماجستير

بناءً على موافقة شئون البحث العلمي والدراسات العليا بالجامعة الإسلامية بغزة على تشكيل لجنة الحكم على أطروحة الباحث/ هاني عبدالرحمن محمود الحبيبي لنيل درجة الماجستير في كلية الهندسة قسم الهندسة الكهربائية - أنظمة الاتصالات وموضوعها:

تصميم 4x4 مصفوفة باتلر لأنظمة هوائي رادارات المركبات على تردد 24 جيجا هيرتز
**Design of a 4x4 Butler Matrix for Vehicle Radar Beamforming
Antenna systems at 24 GHz**

وبعد المناقشة العلنية التي تمت اليوم الأربعاء 16 ربيع أول 1436هـ، الموافق 2015/01/06م الساعة الثانية عشرة ظهراً بمبنى القدس، اجتمعت لجنة الحكم على الأطروحة والمكونة من:

.....	مشرفاً ورئيساً	د. طلال فايز سكيك
.....	مناقشاً داخلياً	د. عمار محمد رمضان/أبو هديوس
.....	مناقشاً خارجياً	د. مصطفى حسن أبو نصر

وبعد المداولة أوصت اللجنة بمنح الباحث درجة الماجستير في كلية الهندسة / قسم الهندسة الكهربائية -

أنظمة الاتصالات.

واللجنة إذ تمنحه هذه الدرجة فإنها توصيه بتقوى الله ولزوم طاعته وأن يسخر علمه في خدمة دينه ووطنه.

والله ولي التوفيق ،،،

مساعد نائب الرئيس للبحث العلمي والدراسات العليا

.....
.....
.....
أ.د. فؤاد علي العاجز



Thesis Approval

Abstract

This work presents a design and simulated results for 4x4 butler matrix with 4 inset fed patch antennas for anti-collision radar at 24GHz. The Butler matrix is used as a beam-forming network that allows producing orthogonal beams that can be steered in different directions. The butler matrix consists of 4 couplers, 2 phase shifters, and 2 crossover couplers.

ADS 2011 simulation software has been used in the design of the whole system. Parameters sweep and optimization techniques have been utilized to obtain the best performance.

Best results were picked for overall system at 24 GHz, and the results were as follows: the return loss was below -33 dB, the realized antennas gain was 9.6 dBi, and the power radiated was -29.4 dB (1.14 mw), with bandwidth more than 3 GHz.

The four azimuth was 86° coverage, the directivity was 11.6194 dBi, the max Power intensity was -27.1 dB, the optimized design size was 16.7 mm x 20.7 mm, the phase shift between all output ports was $\pm 45^\circ$, $\pm 135^\circ$ with 6° error, and the overall insertion loss was -6.7 dB.

الملخص

هذا العمل يعرض تصميم ونتائج المحاكات لـ 4 X 4 من مصفوفه باتلر مع 4 شرائح هوائيات التي تستخدم في الرادارات المضادة للتصادم على تردد 24 جيجا هيرتز. مصفوفه باتلر تستخدم كشبكة لتكوين الاشعاع والتي تسمح بتكوين اشعاعات متعامدة التي يمكن ان توجهه في اتجاهات مختلفة. مصفوفه باتلر تتكون من 4 مقرنات و 2 مغيرات الطور و 2 المعاكسات.

لقد تم استخدام برنامج المحاكاة ADS 2011 لإنتاج هذا المشروع. كما وتم استخدام ادوات الطرق الامثلية لبرنامج ADS كالتغيير اليدوي والتغيير التلقائي لقيم المتغيرات للحصول على أفضل النتائج المطلوبة.

اخيرا تم اختيار أفضل النتائج للنظام ككل على تردد 24 جيجا هيرتز والنتائج كانت على النحو التالي: المفاقيد الراجعة اقل من -33 ديسيبل. كسب الهوائيات وصل لـ 9.6 ديسيبل. القدرة المنبعثة وصلت لـ -29.4 ديسيبل. درجة زوايا التغطية وصلت لـ 86 درجة. عرض النطاق الترددي أكبر من 3 جيجا هيرتز. التوجيهية وصلت لـ 11.6194 ديسيبل. أكبر كثافته للقدرة وصلت لـ -27.1 ديسيبل. الحجم الامثل للمشروع هو 16.7م x 20.7 مم. الفرق في الطور بين جميع بوابات الاخراج هو

$\pm 135^{\circ}, \pm 45^{\circ}$ بنسبة خطأ 6 درجات. كما ان المفاقيد المضافة وصلت لـ -6.7 ديسيبل.

Dedication

To my parents,

My wife and my sweet kids,

Aseel, Abdul Rahman and Hala

Acknowledgements

I would like to thank my supervisor Dr. Talal F. Skaik for his cooperation and support. His ideas and help have been a significant factor for success in my thesis. In addition, I would like to express my respects to the electrical engineering department at the Islamic university. Finally, I am highly indebted to my family and friends for their encouragements.

Table of Contents

Chapter 1

Introduction

1.1 Introduction	1
1.2 The History of general Radar Technology.....	1
1.3 Radar system Principle.....	2
1.4 Automotive Radar Evolution	2
1.5 Automotive Radar Applications	3
1.6 The characteristic of automotive applications	4
1.6.1-Adaptive Cruise Control (ACC)	4
1.6.2-Parking Aid	4
1.6.3 Blind Spot Surveillance/ Lane Change Assistant	5
1.6.4 Pre-Crash Warning	5
1.6.5 Collision Avoidance/ Warning	6
1.6.6 Stop & Go system	6
1.7 Thesis objective	6
1.8 Statement of the problem.....	7
1.9 Thesis overview	7
1.10 Thesis methodology.....	8
1.11 Conclusion.....	8
References	9
Chapter 2	10
<i>Antenna theory</i>	
2.1 Introduction	10
2.2 Antennas to Radio Waves	10
2.3 Near-Field and Far-Fields	11
2.4 Radiation Pattern	11

2.4.1 Radiation Pattern Lobes	13
2.5 Beamwidth	14
2.6 Radiation Power Density	15
2.7 Radiation Intensity	15
2.8 Directivity	16
2.8.1 Beam Solid Angle	16
2.9 Antenna Efficiency	16
2.10 Antenna Gain	17
2.11 The Return Loss	17
2.12 Polarization	18
2.13 Types of Antennas	18
2.13.1 Wire Antennas	18
2.13.2 Aperture Antennas	19
2.13.3 Microstrip Antennas	19
2.14 Microstrip Patch Antenna	20
2.14.1 Feeding Methods	20
2.14.1.1 The microstrip-line feed	21
2.14.1.2 Coaxial-Probe feed	21
2.14.1.3 The Proximity-coupled feed	21
2.14.1.4 The Aperture-coupled feed	22
2.15 Methods of Design	22
2.15.1 Transmission-Line Method	23
2.16 Antenna arrays	24
2.16.1 Phased array	25
2.16.2 Two elements array	25
2.16.3 Linear array	26
2.17 Microstrip Discontinuity Compensation	27
2.17.1 The bend allowance (BA)	27

2.18 Design procedure steps	28
2.19 Conclusion	29
References	30
Chapter 3	31
<i>Microwave Couplers and phase shifters</i>	
3.1 Introduction	31
3.2 Scattering Parameters	31
3.2.1 Lossless networks	31
3.2.2 Lossy networks	31
3.2.3 Two-Ports S-Parameters	31
3.2.3.1 Scalar logarithmic gain	32
3.2.3.2 Insertion loss	32
3.2.3.3 Input return loss	32
3.2.3.4 Output return loss	33
3.2.3.5 Reverse gain and Reverse isolation	33
3.2.3.6 Voltage standing wave ratio	33
3.3 ABCD matric of two ports network.....	33
3.4 Directional couplers overview	34
3.5 Hybrid couplers overview	37
3.5.1 90° hybrid couplers functional description	38
3.5.2 Conventional branch-line hybrid coupler	38
3.6 Design of a branch-line hybrid coupler	39
3.7 Analysis of a branch-line hybrid coupler	39
3.8 Crossover (0 dB coupler)	41
3.9 Phase shifter	43
3.10 Conclusion	44
References	45
Chapter 4	46
<i>Design of 4x4 Butler Matrix with 4 patch antennas</i>	
4.1 Introduction.....	46

4.2 Butler matrix with antenna-array	46
4.3 Literature Review.....	48
4.4 Substrate	49
4.5 Computational Electromagnetic Algorithms	50
4.5.1 Method of Moments (MoM)	50
4.5.2 Advanced Design System 2011 (ADS) software.....	52
4.6 Design of single inset fed patch antenna.....	52
4.6.1 Design of inset fed patch antenna by ADS 2011 simulator..	53
4.7 Design of hybrid 3dB coupler.....	54
4.7.1 Design of hybrid 3dB coupler by ADS 2011.....	55
4.8 Design of 0 dB coupler (crossover)	57
4.8.1 Design of 0 dB coupler (crossover) by ADS 2011	57
4.9 Design of phase shifter with ADS 2011	59
4.10 Design of microstrip path connecting butler matrix to antennas	60
4.11 Design of butler matrix without antenna array by ADS 2011	61
4.12 Design of butler matrix with antenna array by ADS 2011	66
4.13 Contribution.....	69
References.....	70
Chapter 5	72
<i>Conclusion and Future Work</i>	
5.1 Conclusion.....	72
5.2 Future Work.....	72

List of Tables

Table 4.1	Mathematical calculation for inset fed patch antenna parameters.	53
Table 4.2	ADS simulated parameters for inset fed patch antenna.	54
Table 4.3	Mathematical calculation for 3dB coupler.	54
Table 4.4	ADS optimized parameters for 3dB coupler.	56
Table 4.5	Mathematical calculation for 0 dB coupler (crossover).	57
Table 4.6	ADS optimized parameters for 0 dB coupler.	58
Table 4.7	ADS optimized parameters for -45° phase shifter.	60
Table 4.8	ADS optimized path to antenna dimensions.	61
Table 4.9	ADS optimized Butler Matrix simulated results	65
Table 4.10	ADS simulated antenna parameters	67
Table 4.11	Results Comparison	70

List of Figures

Figure 1.1	Simple Radar configurations	2
Figure 1.2	Automotive applications for a combined near- and far-distance sensor network	4
Figure 1.3	4x4 Butler matrix with four antennas	7
Figure 2.1	Radio waves generated by a time varying source	11
Figure 2.2	Antenna field regions	12
Figure 2.3	Antenna radiation pattern analysis	13
Figure 2.4	Radiation pattern lobes 3D	13
Figure 2.5	2D radiation pattern lobes	14
Figure 2.6	3D and 2D power patterns	14
Figure 2.7	Geometrical arrangements for defining a steradian	16
Figure 2.8	Reference terminals and losses of an antenna	16
Figure 2.9	Polarization	18
Figure 2.10	Wire antenna shapes	18
Figure 2.11	Aperture antenna shapes	19
Figure 2.12	Common shapes of patch antennas	19
Figure 2.13	Microstrip Patch antenna	20
Figure 2.14	(a) Quarter wavelength feed (b) Inset feed	21
Figure 2.15	Coaxial-Prop feed	21
Figure 2.16	Proximity-coupled feed	22
Figure 2.17	Aperture-coupled feed	22
Figure 2.18	Microstrip line	23
Figure 2.19	Physical and effective length of microstrip patch	23
Figure 2.20	Electric field lines	23
Figure 2.21	Wire, Aperture, and Microstrip array shapes	24
Figure 2.22	Phased arrays	25
Figure 2.23	Two elements array	26

Figure 2.24	Linear array of n elements	26
Figure 2.25	Several shapes of right-angled bends	27
Figure 2.26	Bend allowance	27
Figure 2.27	Inset fed patch antenna	28
Figure 3.1	Two ports network	31
Figure 3.2	ABCD matrix of a two ports network	34
Figure 3.3	(a) An arbitrary power division and (b) power combining	34
Figure 3.4	(a) Symbol for directional couplers and (b) symbol for a directional coupler with port 4 terminated with a matched load	35
Figure 3.5	Symbol of a 90° hybrid coupler	38
Figure 3.6	Geometry of a branch-line hybrid coupler	38
Figure 3.7	Schematic circuit of the normalized branch-line coupler	39
Figure 3.8	(a) Even-mode excitation and (b) Odd-mode excitation	40
Figure 3.9	Geometry of crossover	42
Figure.3.10	Practical crossover	43
Figure.3.11	Ideal phase shifter	43
Figure 4.1	4x4 Butler matrix block diagram	47
Figure 4.2	4x4 Butler matrix with antenna array	47
Figure 4.3	Inset fed patch antenna	52
Figure 4.4	ADS inset fed patch antenna layout.	53
Figure 4.5	ADS simulated return loss S_{11} at 24 GHz.	54
Figure 4.6	Hybrid 3dB coupler.	55
Figure 4.7	ADS 3dB coupler schematic draw.	55
Figure 4.8	ADS 3dB optimized coupler layout	56
Figure 4.9	ADS simulated S-parameters for 3dB coupler at 24 GHz.	56
Figure 4.10	0 dB coupler (crossover).	57
Figure 4.11	ADS 0 dB coupler schematic draw.	57
Figure 4.12	ADS 0 dB (crossover) optimized coupler layout.	58
Figure 4.13	ADS simulated S-parameters at 24 GHz for 0 dB coupler	58

Figure 4.14	ADS -45° phase shifter schematic draw.	59
Figure 4.15	ADS optimized -45° phase shifter layout.	59
Figure 4.16	ADS phase (S_{12}) for -45° phase shifter at 24 GHz.	60
Figure 4.17	ADS optimized path to antenna layout.	61
Figure 4.18	ADS Butler Matrix schematic draw.	62
Figure 4.19	ADS optimized Butler Matrix layout.	62
Figure 4.20	ADS first optimized goal the return loss (S_{11}) < -30 dB at 24 GHz.	63
Figure 4.21	ADS second optimized goal outputs phase shifts (135°) at 24 GHz.	63
Figure 4.22	ADS third optimized goal outputs phase shifts (-45°) at 24 GHz.	63
Figure 4.23	ADS fourth optimized goal outputs phase shifts (45°) at 24 GHz.	64
Figure 4.24	ADS fifth optimized goal outputs phase shifts (-135°) at 24 GHz.	64
Figure 4.25	ADS sixth optimized goal insertion loss at 24 GHz.	64
Figure 4.26	ADS Final optimized design layout.	66
Figure 4.27	Radiation pattern when port 1 is fed.	66
Figure 4.28	Radiation pattern when port 2 is fed.	67
Figure 4.29	Radiation pattern when port 3 is fed.	67
Figure 4.30	Radiation pattern when port 4 is fed.	68
Figure 4.31	Overall beam steering for the Butler matrix.	68

List of Abbreviations and Constants

HPBW	Half Power Beamwidth
AICC	Autonomous Intelligent Cruise Control
ACC	Adaptive Cruise Control
ICC	Intelligent Cruise Control
ABS	Antilock Braking System
EBD	Electronic Brake Distribution
ESP	Electronic Stability Program
SRS	Supplemental Restraint System
VSWR	Voltage Standing Wave Ratio
RL	Return Loss
IL	Insertion Loss
BA	Bend Allowance
WLAN	Wireless Local Area Network
HTS	High Temperature Superconductors
CEM	Computational Electromagnetic
SBR	Shooting and Bouncing Rays
MoM	Method Of Moment
ADS	Advance Design System software
TM	Transverse Electric
TEM	Transverse Electromagnetic
TM	Transverse Magnetic
FDTD	Finite Difference Time Domain
GTD	Geometrical Theory of Diffraction
PTD	Physical Theory of Diffraction
FEM	Finite Element Method
FNBW	First Null Beamwidth

FFT	Fast Fourier Transform
ϵ_{eff}	Effective Dielectric Constant
ρ	Electric Charge
J	Current Density
∇	Curl
H	Magnetic Field
D	Electric Flux Density
B	Magnetic Flux Density
D	Largest dimension of the antenna
D_o	Directivity
E_ϕ, E_θ	Electric Fields in the two planes
f_o	Resonance Frequency
P_r	Radiated Power
$\tan \delta$	Loss Tangent
Z_{in}	Input Impedance
Z_o	Characteristics Impedance
ϵ_r	Dielectric Constant
λ	Wavelength in dielectric
ϕ	Azimuthal angle
θ	Elevation angle
ω	Angular frequency
Γ	Reflection coefficient
dB	Decibel = $10 \log (\text{Value})$
ϵ_o	Permittivity of free space = 8.85419×10^{-12} F/m
μ_o	Permeability of free space = $4\pi \times 10^{-7}$ H/m
η_o	Impedance of free space = 377Ω
c	Velocity of light of free space = 2.997×10^8 m/s

Chapter 1

Introduction

1.1 Introduction

In this chapter, we will talk about the history of general radar technology, then we will present the radar principle, and the automotive Radar evolution. After that, we will give an overview of some automotive radar applications, and their characteristics.

1.2 The History of general Radar Technology

The word radar belongs to the phrase Radio Detection And Ranging and applies to electronic equipment designed for detecting and tracking targets at considerable distances [1]. The scientist, Heinrich Hertz explained in 1886 that radio waves could be reflected from metallic objects [2].

In 1903, a German engineer, Christian Hülsmeyer acquired a patent in many countries for a radio wave device capable of detecting ships by reflection effect. In 1922, Marconi drew attention to the work of Hertz and submitted in marine radar, he gave a fiery speech before the Institute of Radio Engineers (IRE) in London [2].

In the 1930s, there was independent development of radar techniques such as Radar Navigation, especially at sea in USA, Germany, Britain, and France. By 1939, Radar in warships were enhanced and improved [2].

In 1944, marine radar had made an appearance on trader ships and from about the end of the war the development of civil marine radar began. Gradually, it was refined to meet the needs of peacetime navigation and collision avoidance. Nowadays the civil marine radars are different, in size, and in appearance than from their forebears of the 1940s, the basic data that they offer, namely firmness, and target range are determined by exploiting the same fundamental principles unveiled so long ago [2].

In 1950, Radar technology also saw rising fabrication in the component and signal processing sectors. Despite these improvements, the technological improvement of Radar technology was slower than in the consumer goods industry until the 70's. Only after the 70's did the Radar technology experience comparably rapid phase of development through the opening of new fields of usage, as in the fields of sensors and remote sensing [3]. Nowadays, several radar applications are used in military, remote sensing, air traffic control, road traffic control, ships, and space [4].

1.3 Radar system Principle

Radar systems consist of a transmitter and a receiver. The transmitter radiates electromagnetic waves of a particular waveform, and the receiver detects the echo returned from the target [1]. Only short signals of the transmitted energy were re-radiated back to the radar, after that it will be amplified, down-converted and processed. The range to the target is estimated from the travelling time of the wave. The arrival angle of the echoed wave assigns to the target direction. The Doppler shift determines the relative velocity of the target of the returned signal [5].

Generally, when transmitter and receiver share with a common antenna, the system is called a monostatic radar system. For automotive radar applications, splitting between the transmitter and receiver is measly matched to the distance to a target. Therefore, we can say that these systems are monostatic in a classical sense. Nevertheless, when two separate antennas are used for transmit and receive signals, the automotive radar systems are usually indicated to as bistatic, see Figure. 1.1. The duplexer component is required to provide isolation between transmitter and receiver [5].

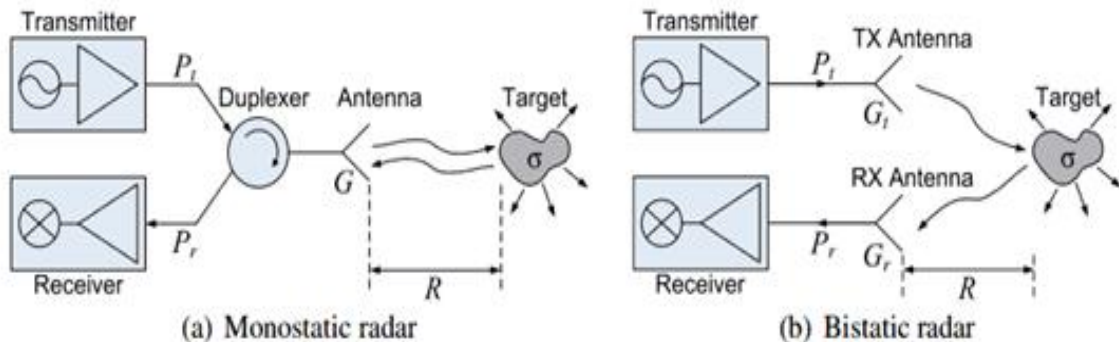


Figure 1.1 Simple Radar configurations [5].

1.4 Automotive Radar Evolution

In 1950, Radar devices were used at the first time in vehicles, since they were able to determine the distance and the velocity of other objects, regardless of weather. Since 1959, General motors' produced simple vehicle radar in Cadillac Cyclone. The Radar was built with tube technology and with very simple target extraction. The distance to the approaching vehicle and the braking distance were indicated on the instrument panel [3].

In 1970, microprocessors and digital signal processing gave a huge development of Radar instrumentation in size reduction of instruments for microwave technology, the radar was operating at 35 GHz, was implemented with transistors [3].

At the mid of 1990's with accessibility MMIC's (Monolithic Microwave Integrated Circuits) allowed for higher level of integration. As a main application, the

automatic distance control appeared in the sense of an intelligent cruise control system (AICC Autonomous Intelligent Cruise Control; ACC Adaptive Cruise Control; and ICC Intelligent Cruise Control)[3].

At the same time frequency range from 76 GHz to 77GHz has been licensed in Europe, USA, and Japan (Technical Standard EN301091 V1.1.1, ETSI) for the use in ACC [6].

Pulse Radar, FM-CW, Pseudo Noise and Multi-frequency CW procedures were used for range determination, whereby the FM-CW was the most frequently used procedure with quasi-optically antennas that the antennas direction were switched electronically [3], and [6].

By 2010, a transportation model was built with several Radar sensors working at 24 GHz. The Radar sensors were used apart from the distance and obstacle controls in the range up to 250 m. They were used additionally for close-range sensing to approximately 5 m such as city traffic, airbag sensors, and used as impact sensors such as airbags, seatbelt control, and for complete angle sensing [3], and [6].

Several additional automotive applications, such as Stop & Go, Pre-Crash, Lane Change Assistant, and Parking Aid, consider a completely different observation area. For these applications, 24 GHz radar sensors are used. Besides the range and velocity parameters, additional information concerning the target type are of great benefit, as one of the main goals of future safety systems will be the increased protection of pedestrians and other road vehicles [7].

1.5 Automotive Radar Applications

Several automotive radar applications such as airbags, ABS (Antilock Braking System) with EBD (Electronic Brake Distribution), brake assistant, ESP (Electronic Stability Program), and SRS (Supplemental Restraint System) became a major topic for automotive companies in recent years, and have been optimized to protect the road users [8].

In automotive radar applications, various sensors such as ultrasonic, infrared, and lidar (light detection and ranging) were used depending on targeted application, each sensor have its own manufacture criteria. Sensors were grouped into three main categories, namely sensor performance, sensor size/visibility, and cost [5], [8].

For automotive applications, the measurements of today's sensors involve range, azimuth angle, velocity, and object size. The sensor performance can be evaluated by its accuracy, resolution, and the maximum unambiguous range [8], [9].

Accuracy is defined as the standard deviation of the measurement relative to its expectation value. The resolution of a sensor is defined as the least necessary condition that leads to a separate detection of two neighboring objects of equal size with equal reflection properties [8].

There are three categories referring to the maximum detectable range of an object. So-called far-distance sensor can achieve a maximum range that lies within 150 and 200 m with a small azimuth angular coverage of about 10°. Near and medium

distance sensors cover a range area up to 20-50 m and have a wider azimuth angular antenna coverage that of about 60°- 120° [8],[9].

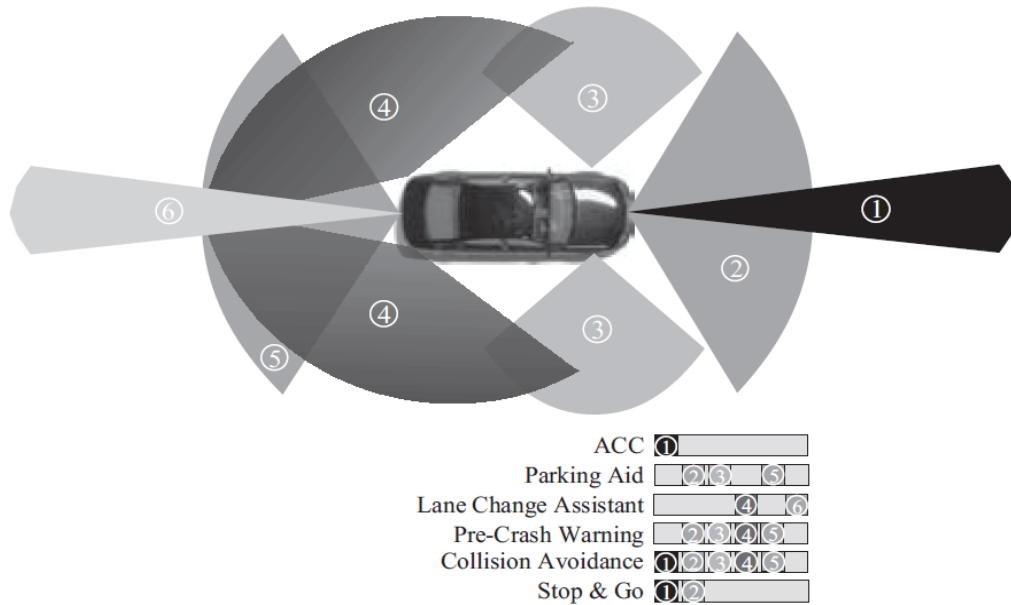


Figure 1.2 Automotive applications for a combined near- and far-distance sensor network [8].

Figure 1.2 shows a variety multi-sensor radar network covering the scan areas of different automotive applications, and summarize the sensor conjunction that are at least demanded by the different automotive applications.

1.6 The characteristic of automotive applications

1.6.1 ACC (Adaptive Cruise Control)

An ACC system is an enhancement of the standard cruise control. It is able to decelerate if the own vehicle is approaching another slower moving car situated in the same lane and to accelerate again if such a slower moving car is changing lanes in order to give way [8].

The required detection area of an ACC system is mainly the own lane as well as the two neighboring lanes at a greater distance in front of the own car [8].

Most of these systems operate with a 77 GHz far-distance radar sensor that can detect targets up to a maximum distance of at least 150m ahead of the own car [8]. The far-distance sensor is mounted in the front bumper, so that the scan area visualized in figure 1.2 is achieved.

1.6.2 Parking Aid

The main idea of a parking aid system is to support the driver in a parking maneuver by moving a vehicle from an area where the traffic flows to an area close to the traffic flow where the vehicle can be left stationary. The sensor checks the size of

the parking lot in comparison to the size of the own car and the own driving capability [8], and [9].

As seen in figure 1.2 ,the required scan area for parking aid system is ideally the whole near-distance area around the car or at least the near-distance area in front and behind the front and rear bumper, respectively [8].

The side-looking sensors measure the size of the parking lot while the car is driving past it. Then, the car informs the driver if a parking maneuver is possible. The driver assistance system is automatically steering the car while the driver is only controlling the speed of the maneuver [8].

1.6.3 Blind Spot Surveillance/ Lane Change Assistant

The aim here is to avoid a classical reason for accidents, a driver has overseen an obstacle being in the blind spot of his car or one that is approaching with high speed on a neighbored lane while the driver is maneuvering in the appropriate direction [8], and [9].

The blind spot surveillance system requires a small detection area with a maximum range of 5 m at the location of the car's blind spot [9].

The lane change assistant system can be considered as the logical extension of the blind spot surveillance system. At this, the driver is informed whether an obstacle will be situated on the right or left lane next to his car in the next moments. If he wants to change lanes in such a situation, a warning signal will appear [8], [9].

Since this application is preferred for highway-driving where high relative velocities may be measured, precise velocity measurements are necessary, see figure 1.2, and the detection area of the side- and back-looking sensors must cover up to 150 m behind the own vehicle for a lane change assistant with full functionality [8].

1.6.4 Pre-Crash Warning

The main idea for pre-crash warning is to react very fast with a pre-crash sensor network and activate all necessary active components such as brakes, airbag, or even steering in the car to avoid an accident or at least minimize consequences of an impact with reduction of the vehicle's kinetic energy. Early activation of airbags is very important [8], and [9].

Since a crash can occur from every direction, the pre-crash warning system requires the whole near-distance area around the car for detection, see figure 1.2.

It is very important, that the pre-crash warning system detect an unavoidable crash as early as possible with an extreme low false alarm rate, so that the system can react properly [8].

1.6.5 Collision Avoidance/ Warning

The main idea for a collision avoidance is to give the driver information that is indicating the need for urgent action to avoid a collision. The warning has to be provided in the advanced phases of a dangerous situation in order to draw the driver's attention to the need of performing an emergency braking, lane changing, or other collision avoidance maneuvers [8], and [9].

Since collisions can occur from every direction, the scan area of the sensors must cover the whole near-distance area around the car, and the update rate of such a safety system must be very high in order to detect possible collisions as early as possible [9]. As seen in figure 1.2, a collision warning/avoidance system requires a far-distance sensor in the front bumper.

1.6.6 Stop & Go system

The stop & go system is a new generation of the adaptive cruise control enabling it to be utilized in more traffic scenarios than a simple ACC system. The main purpose of Stop & Go system is to be able to bring the vehicle to a complete stop and also to accelerate it again. In very dense traffic situations, this application can surely reduce a large amount of accidents [8]. Due to the demands of a close target detection and an early reaction in cut-in situations, the stop & go system requires additional near-distance sensors with a wide azimuthal scan area.

These sensors are mounted in the front bumper as shown in figure 1.2. The update rate must be slightly higher than the one of an ACC system, because the stop & go system should work in dense traffic scenarios, where obstacles can suddenly appear in the driving path from different directions [8].

1.7 Thesis objectives

As mentioned in previous section, Pre-crash vehicle system is a strategic control of an accident being vehicles. The system is designed to prevent the driver and passengers inside the vehicle gets an accident with detect the object in front of them in the safety distance and speed. The pre-crash vehicle Security System is developed by using radar system with application of motor speed control.

In this Research, we will focus on the radar system, so we will design a conformal 4x4 Butler matrix with switched four beam patch antenna array operating at 24 GHz for vehicle anti-crash radar systems, see figure 1.3. The four rectangular inset fed patches will be connected to the outputs of the Butler matrix. The system is based on the microstrip technology.

The Butler matrix is used as a beam forming network that allows producing orthogonal beams that can be steered in different directions. As seen in figure 1.3, conventional components of the Butler matrix like hybrid couplers and crossovers will be studied and designed. ADS 2011 simulation software will be used to design each component of the system.

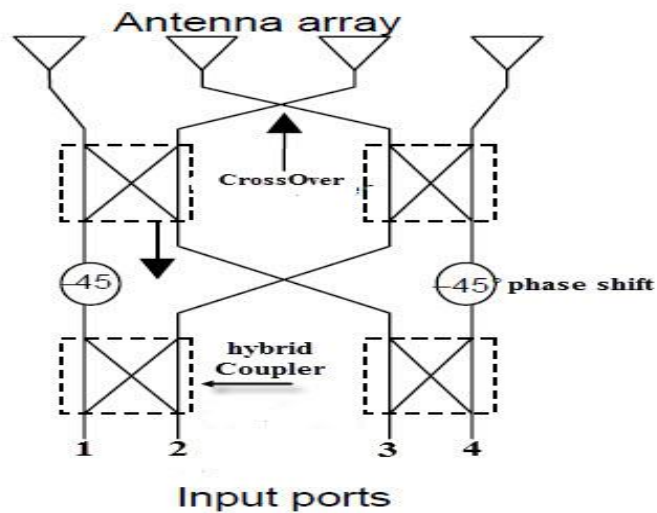


Figure 1.3 4 x 4 Butler matrix with four antennas [10].

1.8 Statement of the problem

Butler matrix consist of several components, as seen in figure 1.3, each component has its own properties and specification to design. When all components are combined, fabrication and optimization are needed. Optimization process will be on overall size reduction, the output ports phase shifts, the return loss, the insertion loss , antenna beam steering, and the distance between all output ports.

1.9 Thesis overview

The main purpose of the proposed work here is the analysis and the design of butler matrix with four-patch antenna array working at 24 GHz for vehicle anti-crash radar systems. Mathematical studies will be carried out firstly then ADS 2011 will be utilized to design the butler matrix.

In chapter two, main antenna parameters with important concepts will be mentioned, the microstrip line, the microstrip patch antennas types, and their main design equations will be explained in the second part of the chapter.

In chapter three, the scattering parameters, microwave couplers, crossovers, and the phase shifters with their mathematical analysis will be reviewed.

In chapter four, the butler matrix will be reviewed, equations explained in previous chapters we will be used for designing the system, the simulation results will be presented at the end of the chapter.

The final chapter will provide summary and conclusions drawn from this work.

1.10 Thesis methodology

Our work will be based on the following design steps:

- Mathematical equations will be used to design each part in the butler matrix.
- ADS 2011 simulator will be used to design each part.
- ADS 2011 schematic draw will be used to get initial results.
- ADS 2011 goals will be defined to start optimization.
- ADS 2011 schematic to layout tool will be used.
- ADS 2011 optimization methods will be used to achieve our goals.
- Beam steering functionality will be tested by ADS 2011.

1.11 Conclusion

We explained in this chapter the history of general radar technology, the radar principle, and automotive radar evolution. Moreover, we gave an overview of some automotive radar applications, and some of their characteristics.

References

- [1] M.Skolnick, Introduction to Radar Systems, Third Edition, McGraw Hill, 2002, ISBN 0-07-290980-3.
- [2] Al.Bole, A. Wall and A. Norris, Radar and ARPA Manual, Third Edition, 2013, ISBN: 978-0-08-097752-2.
- [3] W. Wiesbeck, Radar System Engineering, 15th Edition, Karlsruhe Research University, 2010.
- [4] D.M. Pozar, Microwave Engineering, Fourth Edition, John Wiley & Sons, 2012, ISBN 978-0-470-63155-3.
- [5] V.Issakov, Microwave Circuits for 24 GHz Automotive Radar in Silicon-based Technologies, Springer, 2010, ISBN 978-3-642-13597-2.
- [6] M.Slović, "High Efficiency Patch Antenna for 24 GHz Anti-collision Radar", Microwave journal Review, Jun 2006.
- [7] S.Heuel, "Pedestrian Recognition Based on 24 GHz Radar Sensors", Chapter 10, 2013, Intec, <http://dx.doi.org/10.5772/53007>.
- [8] M.Schiementz, Post processing Architecture for an Automotive Radar Network, Hamburg University of Technology, 2005.
- [9] M.Klotz, "An Automotive Short Range High Resolution Pulse Radar Network", PhD thesis, Hamburg University of Technology, 2002.
- [10] A. Balanis, I. Ioannidis, Introduction to Smart Antennas, Morgan & Claypool Publishers, 2007, ISBN: 1598291777.
- [11] C.Lichtenberg, "Application of radar for automotive collision avoidance." Technical report, NASA tech docs , 1990.
- [12] P.Sanz, I.Slomian , "Four-beam antenna array for 24 GHz applications fed by 4 x 4 butler matrix", Microwave and Telecommunication Technology ,23rd Int. Crimean Conference, IEEE , 2013, ISBN: 978-966-335-395-1.
- [13] M. Meinecke and H. Rohling, "Combination of LFMCW and FSK Modulation principles for Automotive Radar", German Radar Symposium conference, 2000.
- [14] H. Henftling, D. Klotzbücher and, C. Frank: "Ultra Wide Band 24GHz Sequential Lobig Radar for Automotive Applications", conference, 2005.
- [15] M. Schiementz, F. Fölster and H. Rohling, Angle Estimation Techniques for different 24GHz Radar Networks, conference, 2003.
- [16] F. Fölste, H. Rohling, "Signal processing structure for automotive radar", journal, Hamburg University of Technology, 2006.

Chapter 2

Antenna theory

2.1 Introduction

In this chapter, we will review the main antenna parameters, so as we know an antenna is a transformer between a transmission line and free space. To describe an antenna, we must characterize its properties as a transmission line load (input impedance) and the distribution of the electromagnetic energy that it radiates into space (radiation pattern) [1]. There are important parameters and concepts that can be used to describe antenna properties.

An antenna is a device that transmits or receives electromagnetic waves, it has the function of converting one type of wave into another. The basic role of the antenna is to provide a transducer between the free-space propagation and the guided-wave propagation of electromagnetic waves. Most antennas are resonant devices, which operate efficiently over a relatively narrow frequency band [2], and [5].

The transmitting and the receiving antenna can therefore be looked at in the same way (reciprocity principle), and the parameters described below are equally valid for transmission and reception [2].

In the second part of the chapter we will talk about the microstrip line, the microstrip patch antennas types, and their main design equations. Moreover, we will list the design procedure steps.

2.2 Antennas to Radio Waves

At the half of the nineteenth century (1831–1879), James Clerk Maxwell presented a set of equations named as Maxwell's equations that describe the interrelationship between electric fields \mathbf{E} , magnetic fields \mathbf{H} , electric charge ρ , and current density \mathbf{J} [5]. Here we take one case as a single frequency source case (an arbitrary case can be considered the combination of many single-frequency sources), thus Maxwell's equations can be written as [5]:

$$\nabla \times \mathbf{E} = -j\omega\mu \mathbf{H} \quad (2.1)$$

$$\nabla \times \mathbf{H} = \mathbf{J} + j\omega \epsilon \mathbf{E} \quad (2.2)$$

$$\nabla \cdot \mathbf{E} = \frac{\rho}{\epsilon} \quad (2.3)$$

$$\nabla \cdot \mathbf{H} = 0 \quad (2.4)$$

ρ is the charge density, ω is the angular frequency, μ is a scalar quantity, ϵ electric permittivity.

$$\nabla = \mathbf{i} \frac{\partial}{\partial x} + \mathbf{j} \frac{\partial}{\partial y} + \mathbf{k} \frac{\partial}{\partial z} \text{ is a vector operator.}$$

From equations listed a new equation can be derived [5]:

$$\nabla^2 \mathbf{E} + \omega^2 \mu \epsilon \mathbf{E} = j\omega \mu \mathbf{J} + \nabla \left(\frac{\rho}{\epsilon} \right) \quad (2.5)$$

This is an equation, which links the radiated electric field (no magnetic field) directly to the source [5]. To solve this equation, boundary conditions are required for an open boundary, so the field disappears when the distance from the source V to the field point becomes infinite, see figure 2.1.

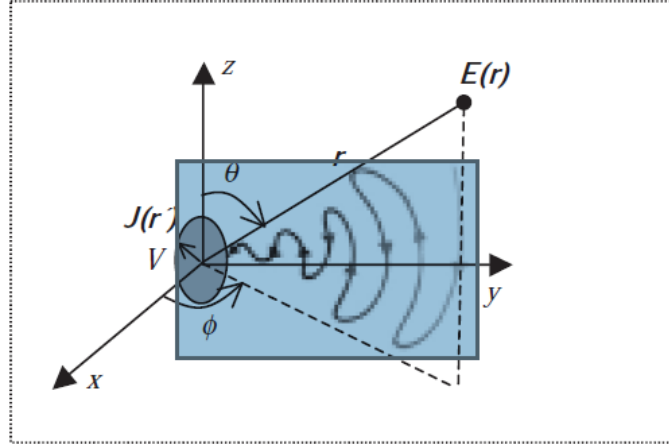


Figure 2.1 Radio waves generated by a time varying source [5].

$$\mathbf{E}(\mathbf{r}) = -j\omega\mu \int_V \mathbf{J}(\mathbf{r}') \frac{e^{-j\beta|\mathbf{r}-\mathbf{r}'|}}{4\pi|\mathbf{r}-\mathbf{r}'|} d\mathbf{v}' + \frac{1}{j\omega\epsilon} \nabla(\nabla \cdot \int_V \mathbf{J}(\mathbf{r}') \frac{e^{-j\beta|\mathbf{r}-\mathbf{r}'|}}{4\pi|\mathbf{r}-\mathbf{r}'|} d\mathbf{v}') \quad (2.6)$$

Equation (2.6) is the solution of Equation (2.5) in a uniformed medium μ and ϵ , where r is the distance vector from the origin to the observation point and \mathbf{r}' is from the origin to the source point [5].

This equation is the most institution of antenna theory, because it shows how the antenna is related to radio waves, and it gives the radiated electric field from a time varying current \mathbf{J} (the time factor $e^{j\omega t}$ is omitted here). Only vibrating (time-varying) current charges as shown in Figure 2.1. It can generate a radio wave (not DC current or static charges) [5]. Antenna design is all about how to control the current distribution \mathbf{J} and hence to obtain the desired radiated field \mathbf{E} . Antenna theory could be summarized by this single complicated equation, which consists of vector partial differentiation and integration [5].

2.3 Near-Field and Far-Fields

Now we want to define three antenna regions as seen in figure 2.2. First region is called the Reactive Near-Field Region and can be defined as the portion of the near-field region immediately surrounding the antenna wherein the reactive field (non-radiating field) predominates [5]. For most antennas, the outer boundary of this region is commonly taken to exist at a distance ($R < 0.62\sqrt{d^3/\lambda}$) from the antenna surface, where λ is the wavelength, and d is the largest dimension of the antenna [3].

The second region is called radiating Near-Field (Fresnel) and can be defined as the region of the field of an antenna between the reactive near-field region and the far-field region wherein radiation fields predominate and wherein the angular field distribution is dependent upon the distance from the antenna. If the antenna has a maximum dimension that is not large compared to the wavelength, this region may not exist [5]. The inner boundary is taken to be the distance ($R \geq 0.62\sqrt{d^3/\lambda}$) and the outer boundary the distance ($R < 2d^2/\lambda$) where d is the largest dimension of the antenna [3].

The third region is called Far-Field (Fraunhofer) and can be defined as the region of the field of an antenna where the angular field distribution is essentially independent of the distance from the antenna [5]. The far-field regions commonly taken to exist at distances ($R > 2d^2/\lambda$) from the antenna, λ being the wavelength [3]. And, $r_1 = 0.62\sqrt{d^3/\lambda}$, $r_2 = 2d^2/\lambda$, d = Largest dimension of the antenna, see figure 2.2.

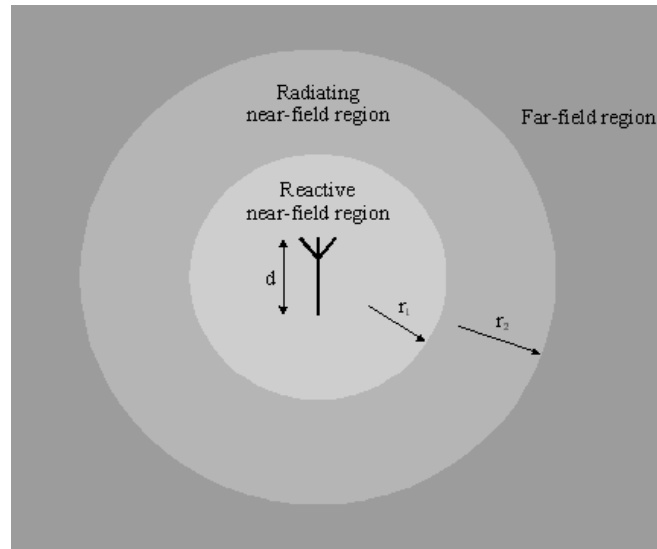


Figure 2.2 Antenna field regions [5].

2.4 Radiation Pattern

The radiation pattern is defined as a graphical representation of the radiation properties of the antenna as a function of space coordinates, and can be drawn with three-dimensions (3D) [3]. As seen in figure 2.3, the 3D pattern is a good way for the radiated field distribution as a function of angle θ and φ in space. The radiation patterns in the two main planes are the E-plane, and the H-plane. The E-plane belongs to the electric field E plane, and the H-plane belongs to the magnetic field H plane.

In ideal current element case, the electric field is E_θ and the magnetic field is H_φ , so the E-plane pattern is the field E_θ measured as a function of θ when the angle φ and the distance are fixed [5]. The H-plane pattern is the field, E_θ measured as a function of φ when the angle θ and the distance are fixed. It should be pointed out that the radiation patterns in figure 2.3 are plotted on a logarithmic scale (dB plot) that helps us to see details of the field or power over a large dynamic range, especially some minor side lobes [5].

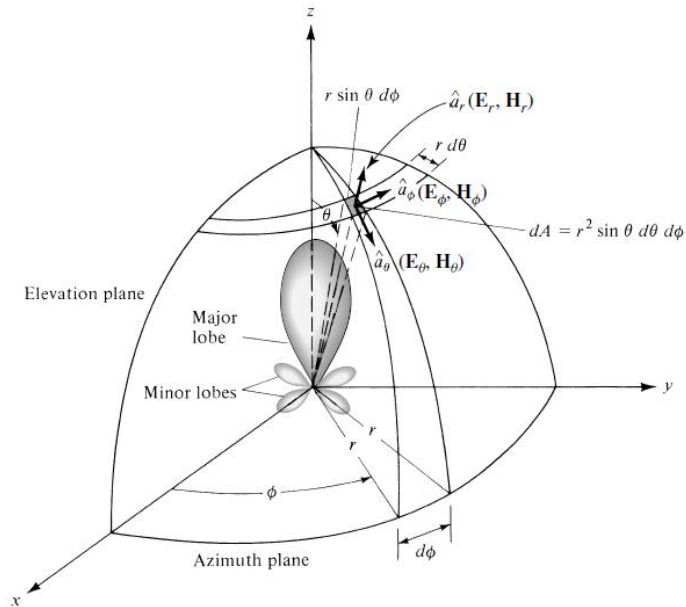


Figure 2.3 Antenna radiation pattern analysis [3].

2.4.1 Radiation Pattern Lobes

A radiation lobe is a portion of the radiation pattern bounded by regions of relatively weak radiation intensity [4], and [5]. As seen in figure 2.3, and 2.4, radiation pattern can be divided to main lobe, minor lobes, side lobes and back lobes.

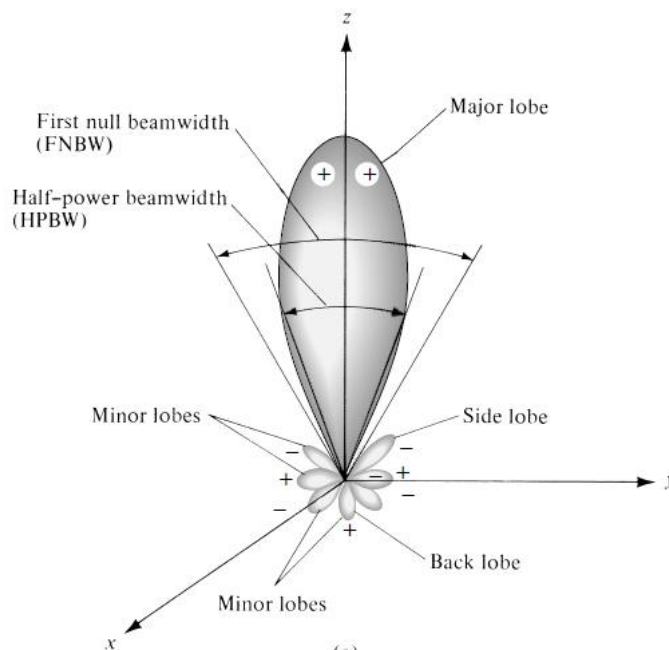


Figure 2.4 radiation pattern lobes 3D [3].

Minor lobes usually represent radiation in undesired directions, and they should be minimized. The Side lobes are the biggest of the minor lobes. The level of minor lobes is defined as a ratio of the power density, often termed the side lobe level [5]. In several radar systems, low side lobe ratios are very important to minimize false target

indications through the side lobes [3]. Figure 2.5 describes the radiation pattern lobes with two-dimensions (2D) plot. The most common resolution criterion states that the resolution capability of an antenna to distinguish between two sources is equal to half the first-null beamwidth (FNBW/2), which is usually used to approximate the HPBW [4], see figure 2.3.

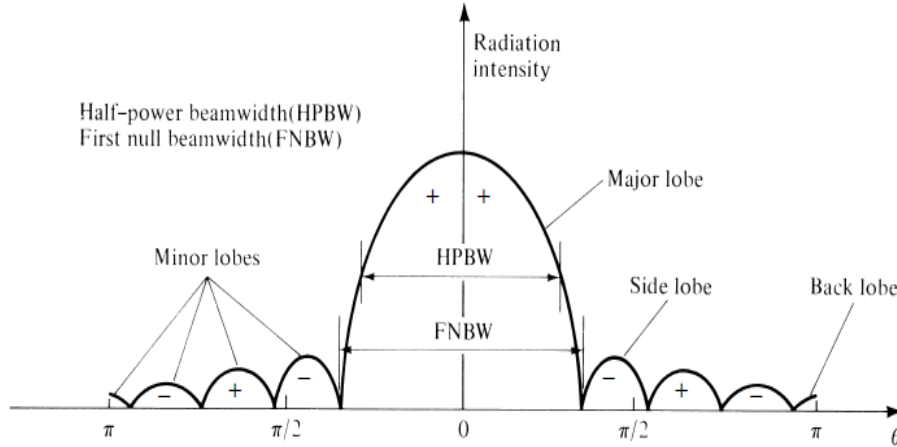


Figure 2.5 2D radiation pattern lobes [3].

2.5 Beamwidth

The beamwidth of an antenna is a very important figure and often is used as a trade-off between it and the side lobe level. As seen in figure 2.6 it is also used to describe the resolution capabilities of the antenna to distinguish between two adjacent radiating sources or radar targets [3], and [5].

There are two types of beamwidth, the first type is called Half-Power Beam Width (HPBW), and it can be defined as the angle between the two directions in which the radiation intensity is one-half value of the beam, or the angular width of the main beam at the half-power points [3]. The second type is called First-Null Beam width (FNBW) and it can be defined as an Angular separation between the first nulls of the pattern [3], and [5], see figure 2.6.

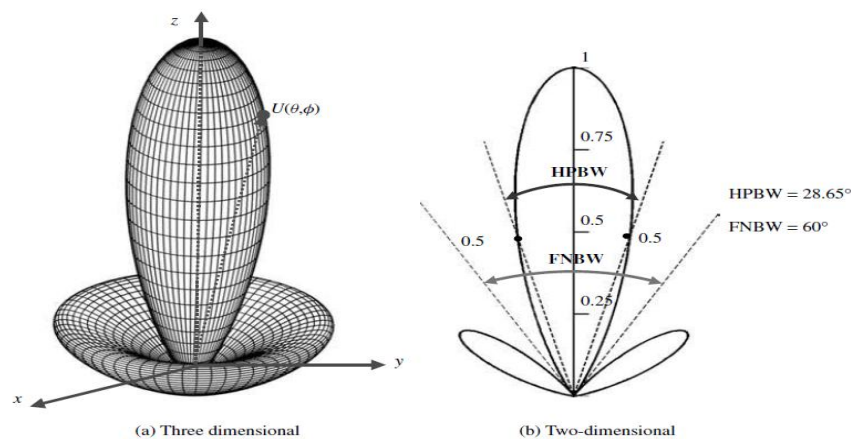


Figure 2.6 3D and 2D power patterns [3].

2.6 Radiation Power Density

First, the radiation density can be defined as the power density of an antenna in its far field region. The instantaneous Poynting Vector \vec{W} is defined as the quantity used to describe the power associated with an electromagnetic wave [3]:

$$\vec{W} = \vec{E} \times \vec{H} \quad (2.7)$$

\vec{W} : instantaneous Poynting vector (W/m²)

\vec{E} : instantaneous electric field intensity (V/m)

\vec{H} : instantaneous magnetic field intensity (A/m)

Since the Poynting vector is a power density, then the total power crossing a closed surface can be obtained by integrating the normal component of the Poynting vector over the entire surface, and be written as [3], and [5]:

$$P = \oint_S \vec{W} \cdot \vec{n} da \quad (2.8)$$

Where

P = instantaneous total power crossing a closed surface (W).

\vec{n} = unit vector normal to the surface.

W = instantaneous Poynting vector (W/m²)

da = infinitesimal area of the closed surface (m²).

The average power density (time average Poynting vector) can be written as [3], and [5]:

$$\vec{W}_{av}(\mathbf{x}, \mathbf{y}, \mathbf{z}) = [\vec{W}(\mathbf{x}, \mathbf{y}, \mathbf{z}; t)]_{av} = [\vec{E} \times \vec{H}^*]/2 \quad (\text{W/m}^2) \quad (2.9)$$

The real average power density is represented by the real part of $[\vec{E} \times \vec{H}^*]/2$, and the reactive power density is represented by the imaginary part of $[\vec{E} \times \vec{H}^*]/2$. From (2.9) the average power radiated can be written as [3]:

$$P_{rad} = P_{av} = \oint_S \vec{W}_{rad} \cdot d\vec{s} = \oint_S \vec{W} \cdot \vec{n} da = \frac{1}{2} \oint_S \text{Re} [\vec{E} \times \vec{H}^*] \cdot d\vec{s} \quad (2.10)$$

2.7 Radiation Intensity

Radiation Intensity is defined as radiated power from any antenna per solid angle (radiated power normalized to a unit sphere) [2], and [3]. the radiation intensity is a far field parameter, so it can be obtained by multiplying the radiation density by the square of the distance.

$$U = r^2 W_{rad} \quad (2.11)$$

Where

U = radiation intensity (W/solid angle)

W_{rad} = radiation density (W/m²)

From (2.11) the power pattern is also a measure of the radiation intensity, so the total power is obtained by integrating the radiation intensity over the entire solid angle of 4π .

$$P_{rad} = \int_0^{2\pi} \int_0^\pi U(\theta, \phi) \sin\theta d\theta d\phi = \int_0^{2\pi} \int_0^\pi U(\theta, \phi) d\Omega \quad (2.12)$$

and $d\Omega = \sin\theta d\theta d\phi$ is defined as the differential solid angle. The radiation intensity of isotropic source is found by dividing the radiation intensity by the area of the unit sphere (4π) which gives [3]:

$$U_0 = \frac{\iint_{00}^{2\pi\pi} U(\theta,\phi) d\Omega}{4\pi} = \frac{P_{rad}}{4\pi} \quad (2.13)$$

2.8 Directivity

It can be defined as the ratio of the radiation intensity in a given direction from the antenna to the radiation intensity averaged over all directions [3], and [5].

$$D = D(\theta, \phi) = \frac{U(\theta, \phi)}{U_0} = \frac{4\pi U(\theta, \phi)}{P_{rad}} \quad (2.14)$$

2.8.1 Beam Solid Angle

The beam solid angle (steradian) Ω_A is define as the solid angle with its vertex at the center of sphere radius r that subtended by a spherical surface area r^2 , or can be defined as the solid angle through which all the power of the antenna would flow if its radiation intensity were constant and equal to the maximum value of U for all angles within Ω_A [3], and [5]. A steradian is a solid angle measurement unit, see figure 2.7. Thus, the directivity can be written as:

$$D = \frac{4\pi}{\Omega_A} \quad (2.15)$$

and solid angle $\Omega_A = \int r^2 \sin\theta d\theta d\phi$

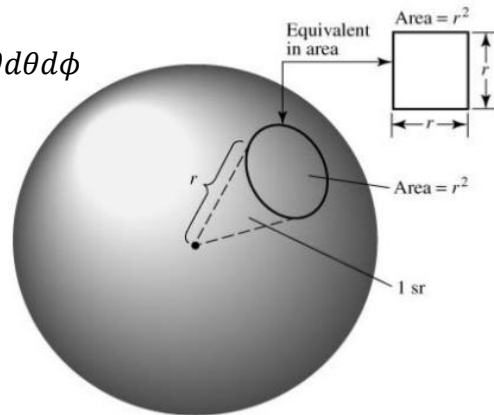


Figure 2.7 Geometrical arrangements for defining a steradian [3].

2.9 Antenna Efficiency

The total antenna efficiency e_0 is used to take into account losses at the input terminals and within the structure of the antenna, and e_0 is due to the combination of number of efficiencies [3], see figure 2.8

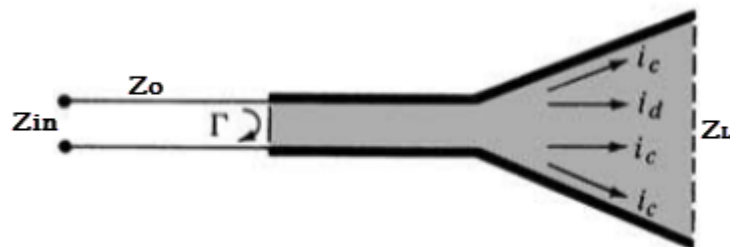


Figure 2.8 Reference terminals and losses of an antenna [3].

The overall efficiency can expressed as:

$$e_o = e_r e_c e_d \quad (2.16)$$

where

e_o = total efficiency.

e_r = reflection (mismatched with input), $e_r = (1 - |\Gamma|^2)$.

e_c = conduction efficiency.

e_d = dielectric efficiency.

$$\Gamma = \frac{Z_{in} - Z_o}{Z_{in} + Z_o} = \frac{Z_L - Z_o}{Z_L + Z_o} \quad (2.17)$$

$$VSWR = \frac{1 + |\Gamma|}{1 - |\Gamma|} \quad (2.18)$$

and Γ = voltage reflection coefficient at the input terminals of the antenna, Z_{in} = antenna input impedance, Z_o = characteristic impedance of the transmission line. VSWR = voltage standing wave ratio, usually e_c and e_d are very difficult to compute, but they can be determined experimentally [3].

2.10 Antenna Gain

Antenna Gain is the ratio of the radiation intensity in a given direction to the radiation intensity that would be obtained if the power accepted by the antenna were radiated isotropically [3], and [5]. In addition, the gain of the antenna is related to the directivity.

$$\text{Gain} = 4\pi \frac{\text{radiation intensity}}{\text{total input accepted power}} = 4\pi \frac{U(\theta, \phi)}{P_{in}} \quad (\text{dimensionless}) \quad (2.19)$$

The antenna gain can be expressed as the ohmic losses (e_{cd}) in the antenna multiplied by the antenna directivity $D(\theta, \phi)$.

$$G(\theta, \phi) = e_{cd} D(\theta, \phi) \quad (2.20)$$

2.11 The Return Loss

The return loss (RL) can be defined by the ratio of the incident power of the antenna P_{inc} to the power reflected back from the antenna of the source P_{ref} [5]. Return loss tells us how much of the input signal is reflected. The Return Loss (RL) may also be explained as the difference between the power of a transmitted signal and the power of the signal reflections caused by variations in link and channel impedance [9], and [10].

Return loss is the negative of the reflection coefficient expressed in decibels. In terms of the voltage standing wave ratio (VSWR). High return loss values mean a close impedance match, which results in greater differentiation between the powers of transmitted and reflected signals, can be expressed as [5], [9], and [10]:

$$RL = 10 \log_{10} \frac{P_{inc}}{P_{ref}} = 20 \log_{10} \left| \frac{VSWR+1}{VSWR-1} \right| = -20 \log_{10} |\Gamma| \quad (dB) \quad (2.21)$$

2.12 Polarization

Polarization of an antenna in a given direction could be defined as the polarization of the wave transmitted (radiated) by the antenna or the property of an electromagnetic wave describing the time varying direction and relative magnitude of the electric-field vector [3]. Polarization is the curve traced by the end of the arrow representing the instantaneous electric field [3], and [5], see figure 2.9.

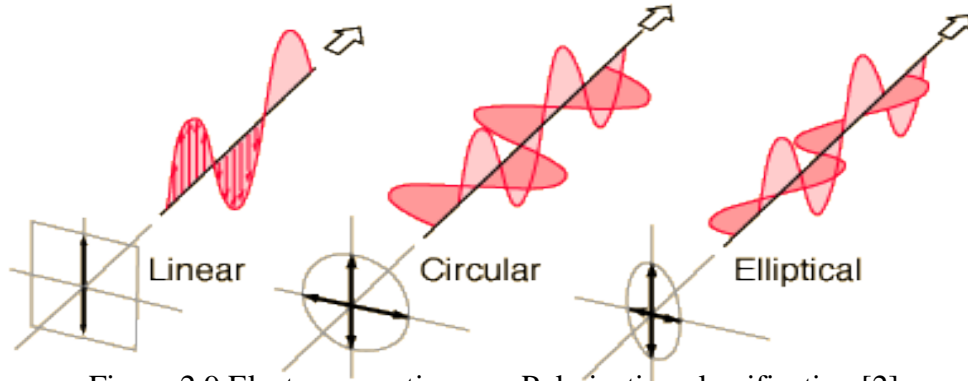


Figure 2.9 Electromagnetic wave Polarization classification [2].

Electromagnetic wave Polarization can be classified as [3]:

Elliptical polarization if the figure that electric field traces is an ellipse, see figure 2.9. Linear polarized if the vector that describes the electric field at a point in space as a function of time is always directed along a line. Circular polarized if the figure of the electric field is traced as a circle, and can be Clockwise (CW), or Counterclockwise (CCW).

2.13 Types of Antennas

Different types of antennas are available named such as wire, aperture, microstrip, and array. Each type has its own forms in order to achieve the desired radiation characteristics for the particular applications [3], [7], and [17].

2.13.1 Wire Antennas

It is the simplest type of antennas, there are various shapes of wire antennas such as a straight wire (dipole), circular or square loop, and helix [3], and [7], which are shown in figure 2.10.

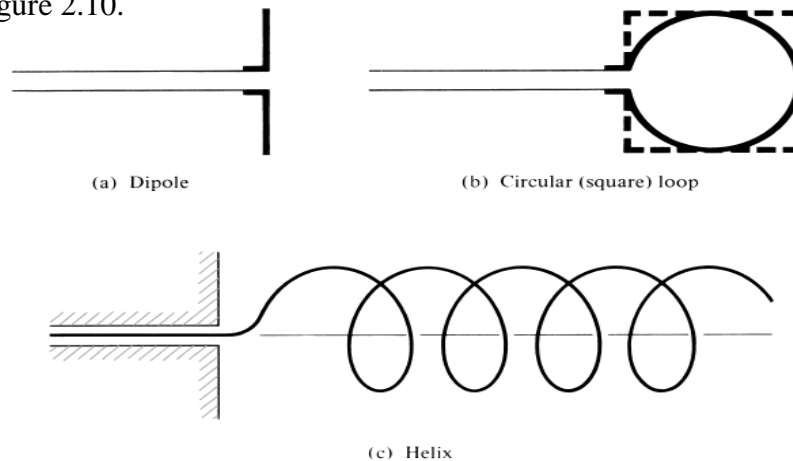


Figure 2.10 Wire antenna shapes [3].

2.13.2 Aperture Antennas

This type of antennas is used in high frequencies, and is very useful for aircraft and spacecraft applications. There are several shapes of aperture antennas such as Pyramidal, Conical horns, and waveguides [3], see figure 2.11.

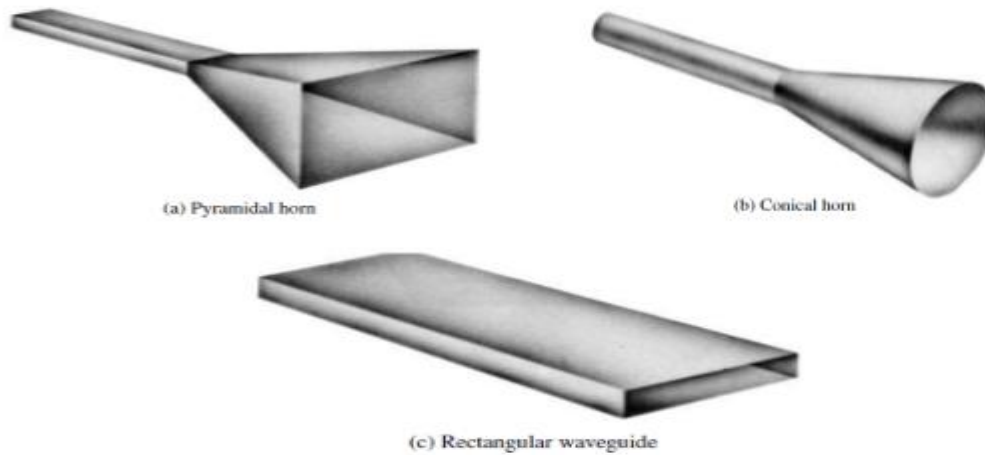


Figure 2.11 Aperture antenna shapes [3].

2.13.3 Microstrip Antennas

Microstrip antennas are the most popular antennas in these days, because they are used in different commercial applications. There are several shapes of microstrip patch antennas, and the shape changes depending on the design application. Some of the common shapes are shown in figure 2.12, for millimeter wave frequencies. The most common types are rectangular, square, and circular patches [3], [10], and [17].

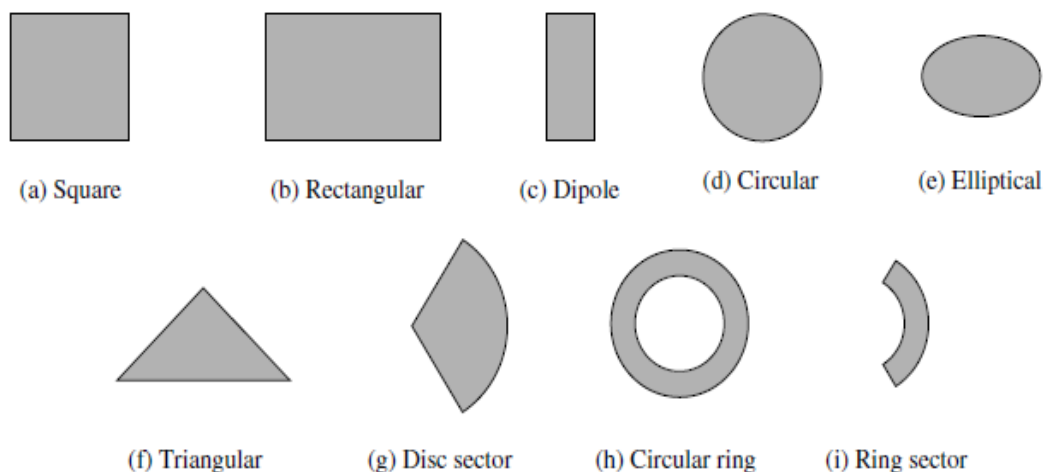


Figure 2.12 Common shapes of patch antennas [3].

2.14 Microstrip Patch Antennas

A Microstrip patch antenna is famed as a rectangular microstrip antenna. It is a type of radio antenna with a low profile that can be mounted on a flat surface. The Microstrip Patch Antenna is a single-layer design that consists generally of four parts: the patch, a ground plane, the substrate, and the feeding point [8], and [10], see figure 2.13.

Patch antennas are simple to fabricate and easy to modify and customize. They are the original type of microstrip antenna described by Howell in 1972 [4], and [11]. The two metal sheets together form a resonant piece of microstrip transmission line with a length of approximately one-half wavelength of the radio waves [10].

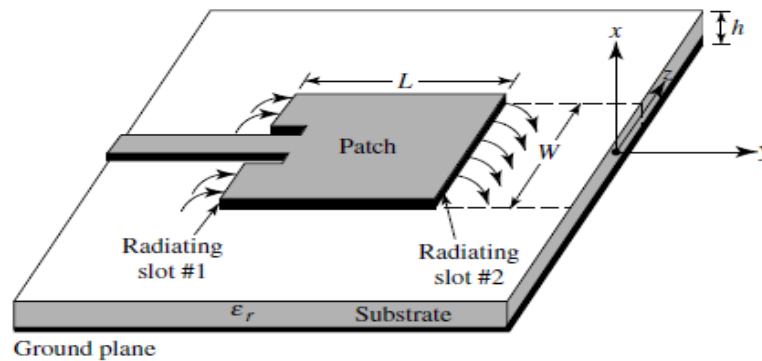


Figure 2.13 Microstrip Patch antenna [3].

The radiation at the edges causes the antenna to work slightly larger electrically than its physical dimensions, so in order for the antenna to be resonant, a length of microstrip transmission line slightly shorter than one-half a wavelength at the frequency is used. A patch antenna is usually erected on a dielectric substrate, using the same materials and lithography processes used to make printed circuit [10].

As seen in figure 2.13. The thickness of the substrate h has a big effect on the resonant frequency f_r and bandwidth BW of the antenna. Bandwidth of the microstrip antenna will increase with increasing of substrate thickness h but with limits, otherwise the antenna will stop resonating [12].

There are several advantages of the microstrip antennas such as small size, low profile, lightweight, and conformable to planar and non-planar surfaces. They are simple and cheap to manufacture using modern printed circuit technology. Nevertheless, the main disadvantages of the microstrip antennas are low efficiency, and low RF power due to the small separation between the radiation patch and the ground plane [8], and [12].

2.14.1 Feeding Methods

There are many methods of feeding a microstrip antenna [7]. The most popular methods are:

1. Microstrip-Line feed.
2. Coaxial Probe feed.
3. Proximity-coupled feed.
4. Aperture-coupled feed.

2.14.1.1 The microstrip-line feed

This is simplest feeding method, and it is widely used to design and fabricate. There are two types of microstrip line feed; one is called Fed with a Quarter Wavelength Transmission line and the other is called inset feed [3], and [7], see figure 2.14.

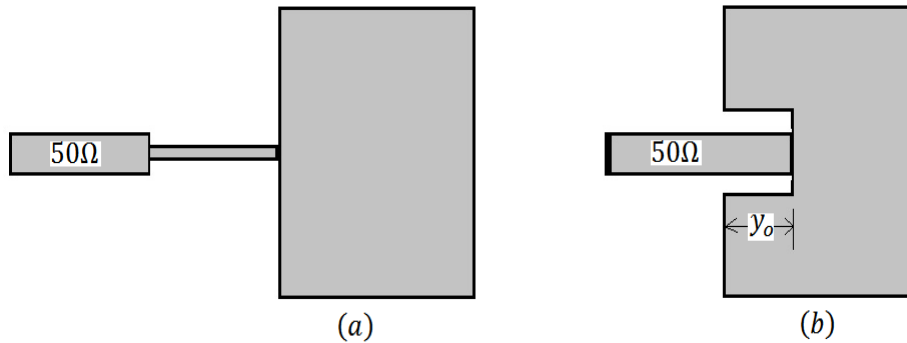


Figure 2.14 (a) Quarter wavelength feed (b) Inset feed [3].

2.14.1.2 Coaxial-Probe feed

As seen in figure 2.15, the inner conductor of the coax is attached to the radiation patch while the outer conductor is connected to the ground plane. The coaxial probe feed is also easy to fabricate and match, and it has low spurious radiation. In addition, the probe will also radiate, which can lead to radiate in undesirable directions [3], and [7].

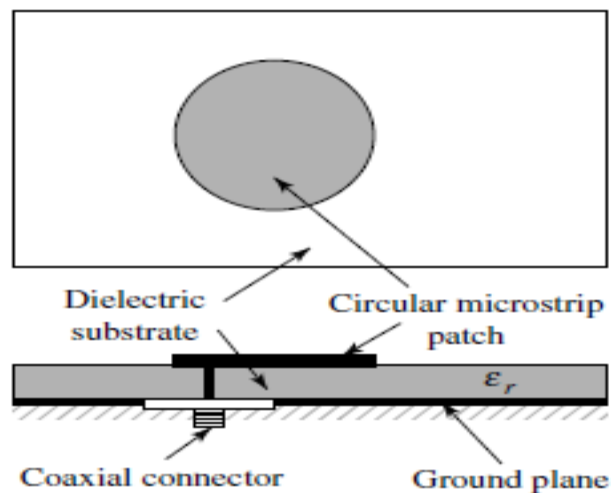


Figure 2.15 Coaxial-Prop feed [3].

2.14.1.3 The Proximity-coupled feed

The proximity coupling has the largest bandwidth as seen in figure 2.16. The patch is located on the top, the ground plane is in the bottom and a microstrip line is connected to the power source and laying between the two substrates. It is little easy to model. Moreover, it has low spurious radiation. However, its fabrication is somewhat more difficult [3], [7], and [13]. The power from the feed network is coupled to the patch electromagnetically, as opposed to a direct contact. This form of microstrip patch is sometimes referred to as an electromagnetically coupled patch antenna [3].

A key attribute of the proximity coupled patch is that its coupling mechanism is capacitive in nature. This is in contrast to the direct contact methods, which are predominantly inductive. The difference in coupling significantly affects the obtainable impedance bandwidth, because the inductive coupling of the edge and probe-fed geometries limits the thickness of the material useable. Thus, bandwidth of a proximity coupled patch is inherently greater than the direct contact feed patches [3], and [7].

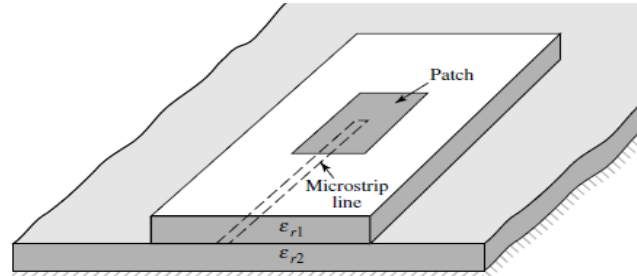


Figure 2.16 Proximity-coupled feed [3], and [13].

2.14.1.4 The Aperture-coupled feed

In this technique, the feed circuitry (transmission line) is shielded from the antenna by a conducting plane with a hole (aperture) to transmit energy to the antenna [3], as shown in figure 2.17.

The upper substrate can be made with a lower permittivity to produce loosely bound fringing fields, yielding better radiation. The lower substrate can be independently made with a high value of permittivity for tightly coupled fields that do not produce spurious radiation. The disadvantage of this method is the difficulty in fabrication [7], [13], and [16].

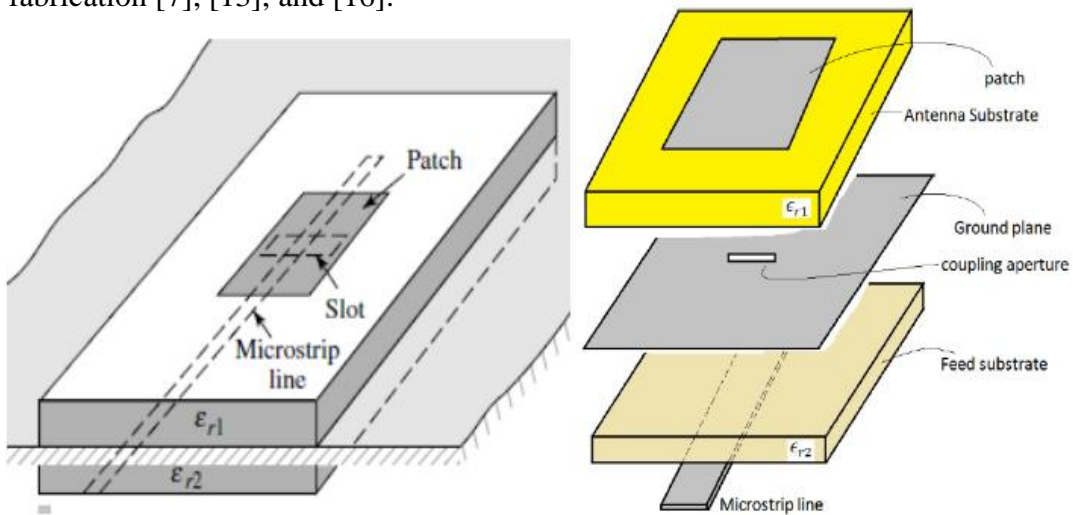


Figure 2.17 Aperture-coupled feed [3], [13].

2.15 Methods of Design

There are variety methods to design the microstrip antennas; the most popular models are transmission line, cavity and full wave. The transmission-line model is the simplest one, due to best physical insight, but is less accurate and it is more difficult to model coupling [3],[14], and [16]. In our work, we will constrain on the transmission line method.

2.15.1 Transmission-Line Method

In this method the transmission line model represents the microstrip patch antenna by two slots, Separated by a low-impedance transmission line of length L [3], [7], and [16].

To study the theory of microstrip transmission line we have two different cases:

Case (1): $W/h < 1$ suitable for narrow strip line.

Case (2) $W/h \gg 1$ and $\epsilon_r > 1$ wider transmission line, see figure 2.18.

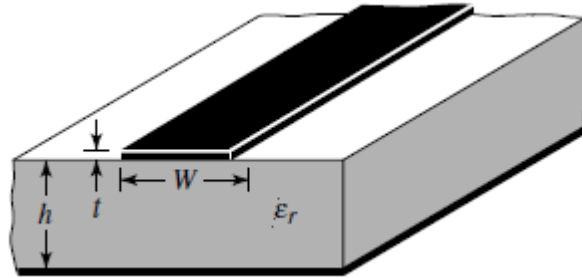


Figure 2.18 Microstrip line [3].

Assuming that the thickness of the conductor t has no effect in our design because it is very thin compared with the substrate height h .

Now some parameters must be determined such as the width W , the length L , the height h , and the dielectric constant ϵ_r of the substrate [3], and [16], see figures 2.18, and 2.19.

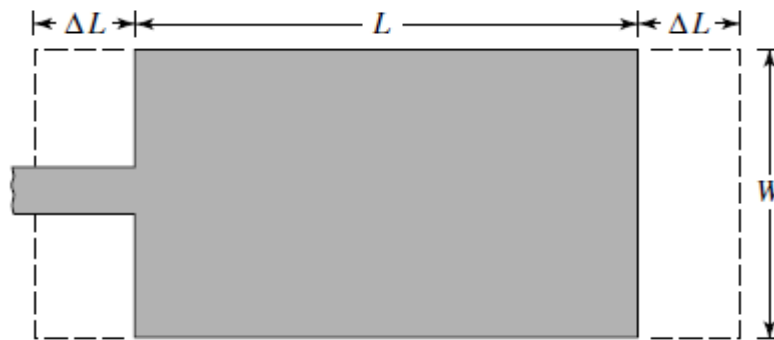


Figure 2.19 Physical and Effective length of a microstrip patch [3].

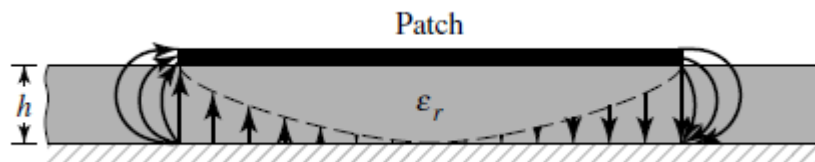


Figure 2.20 Electric field lines [3].

The characteristic impedance of the microstrip line can be written as [2], [3], and [8]

$$Z_o = \frac{120\pi}{\sqrt{\epsilon_{reff}} \left(1.393 + \frac{W}{h} + \frac{2}{3} \ln \left(\frac{W}{h} + 1.444 \right) \right)} \quad (2.22)$$

and, ϵ_{reff} is the effective dielectric constant.

The width of the microstrip line is given by [2],[3], [8]

$$W = \frac{1}{2fr\sqrt{\mu_0\epsilon_0}} \sqrt{\frac{2}{\epsilon_r+1}} = \frac{c}{2fr} \sqrt{\frac{2}{\epsilon_r+1}} \quad (2.23)$$

and, c is free space velocity of light, f_r is resonant frequency.

The microstrip patch antenna in figure 2.19 looks longer than its physical dimensions because of the effect of fringing. The effective length therefore is differing from the physical length by ΔL . A very popular approximation to calculate the extension of the length of the patch is given by [2], [3], and [8].

$$\frac{\Delta L_{eff}}{h} = 0.412 \frac{(\epsilon_{reff}+0.300)(\frac{W}{h}+0.264)}{(\epsilon_{reff}-0.258)(\frac{W}{h}+0.8)} \quad (2.24)$$

Equation (2.24) shows that the extension of the length ΔL is a function of the ratio W/h ,

and ϵ_{reff} . To calculate the effective length, we add the length L to the extension of the length ΔL [3].

$$L_{eff} = (L + 2\Delta L_{eff}) \quad (2.25)$$

For patch antennas air is above the substrate, this will lead to [3], and [10]:

$$1 < \epsilon_{reff} < \epsilon_r.$$

From equation (2.26), the effective dielectric constant is also a function of frequency, f_r is the resonant frequency for the TM_{100} mode that equals [2], [3], and [8]:

$$f_r = \frac{v_0}{2\sqrt{\epsilon_{reff}}(L+2\Delta L_{eff})} \quad (2.26)$$

The effective dielectric constant ϵ_{reff} can be calculated from the formula [2], [3], and [8]:

$$\epsilon_{reff} = \frac{\epsilon_r+1}{2} + \frac{\epsilon_r-1}{2\sqrt{1+\frac{12h}{W}}} \quad (2.27)$$

2.16 Antenna arrays

This type can be defined as a set of two or more antennas. As seen in figure 2.21, the signals from the antennas are combined or processed in order to improve performance of the single antenna. The performance could be increasing the overall gain or reducing the interference or to steer the array [3], [7], and [17].

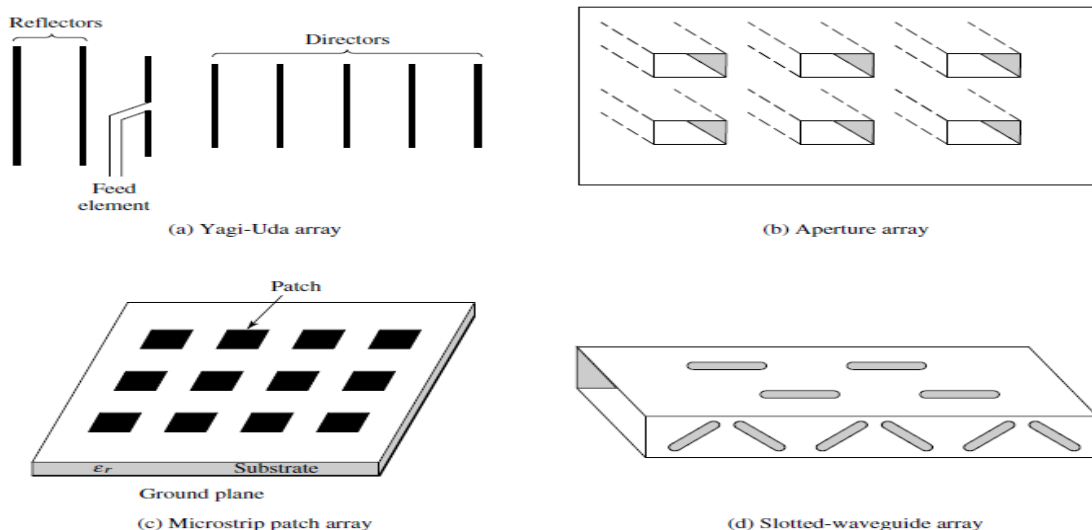


Figure 2.21 Wire, Aperture, and Microstrip array shapes [3].

Antennas with a given radiation pattern may be arranged in a pattern such as a line or a circle or a plane to yield a different radiation pattern. Linear array antenna elements arranged along a straight line. Circular array antenna elements arranged around a circular ring [3]. Planar array antenna elements arranged over some planar surface such as a rectangular array. Conformal array antenna elements arranged to conform to some non-planar surface such as an aircraft skin. There are several array design variables which can be changed to achieve the overall array pattern design [23], such as: general array shape (linear, circular, planar, etc.), element spacing, element excitation amplitude, element excitation phase, and patterns of array elements [3], and [23].

2.16.1 Phased array (Multibeam antenna)

Phased array or multibeam antenna, which consists of either a number of fixed beams with one beam turned on towards the desired signal or a single beam (formed by phase adjustment only) that is steered toward the desired signal[6],[23].See figure 2.22. Phased arrays can be used to steer the main beam of the antenna without physically moving the antenna. Given an antenna array of identical elements, the radiation pattern of the antenna array may be found according to the pattern multiplication theorem [23]. The Pattern multiplication theorem can be expressed as [3], [16], and [23]:

$$\text{Array pattern} = \text{Array element pattern} \times \text{Array factor (AF)} \quad (2.28)$$

and, array element pattern: is the pattern of the individual array element, array factor: is a function dependent only on the geometry of the array and the excitation (amplitude, phase) of the elements.

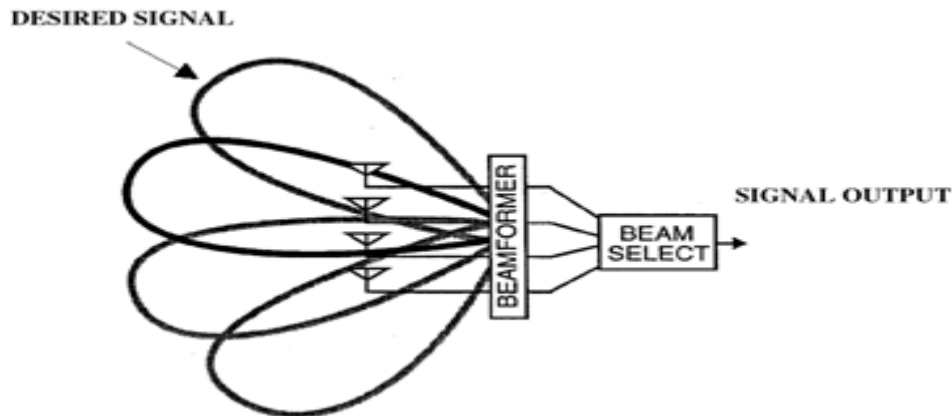


Figure 2.22 Phased array [23].

2.16.2 Two Elements Array

Suppose that two antenna elements occurred to make an array as in figure 2.23, the two elements are fed with current I_1 and I_2 , which are equal in magnitude but out of phase. If $I_1 = I_2 \angle \alpha$. The point of observation is in the far field, the path length difference is $l \cos \alpha$, where l is the distance between the two elements. The radiation of element 1 at P will lead the radiation of element 2 with angle ψ where [16], and [23]:

$$\psi = \beta l \cos \phi + \alpha \quad (2.29)$$

β : Phase constant of the transmitted wave.

The total electric field at P is:

$$E = E_1 [1 + \exp(j\psi)] \quad (2.30)$$

E_1 : is the field at P due to element 1.

The magnitude of the electric field at P is:

$$|E_\phi| = 2E_1 \cos\left(\frac{1}{2}\psi\right) = 2E_1 \cos\left(\frac{\pi l}{\lambda} \cos \phi + \frac{\alpha}{2}\right) \quad (2.31)$$

From (2.31), we found that for a given phase difference and distance we can change the radiation pattern by changing $\left(\frac{l}{\lambda}\right)$.

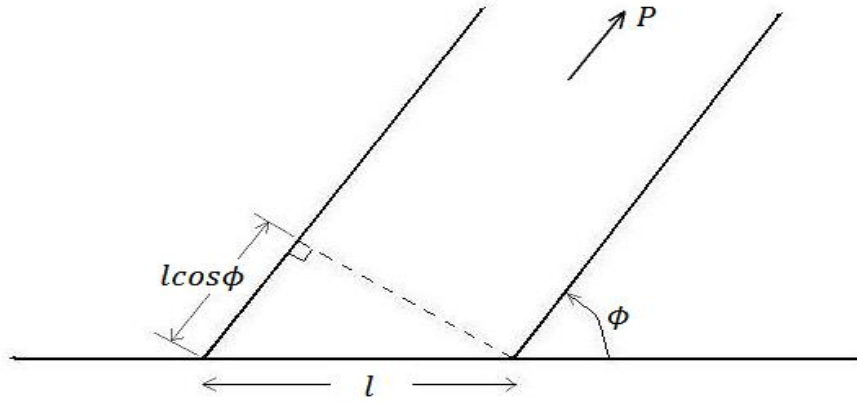


Figure 2.23 two- element array [16].

2.16.3 Linear Array

Previous section we explained a simple array that consist of two antenna elements, now if we put more elements in the line of our two elements array, we will build a linear array, see figure 2.24.

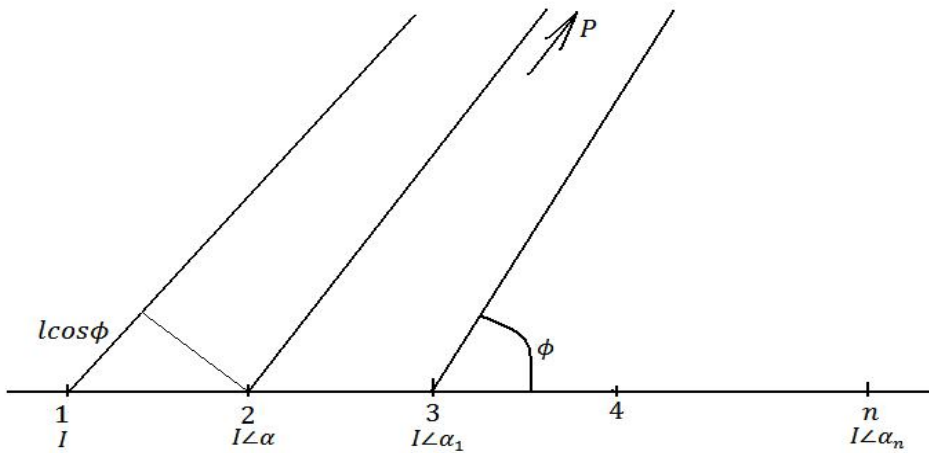


Figure 2.24 linear array of n elements [16].

Consider a simple linear array with equal separation between elements l and equal current in magnitude and equal difference in phase I , see figure 2.24, the currents are: $I, I\angle\alpha, I\angle\alpha_1, I\angle\alpha_2, \dots, I\angle\alpha_n$.

The total electric field at P is [16]:

$$E = E_1 [1 + e^{j\psi} + e^{j2\psi} + e^{j3\psi} + \dots + e^{jn\psi}] \quad (2.26)$$

The magnitude of E is [16]:

$$E = E_o \cos \left[\frac{\sin \frac{n\psi}{2}}{\sin \frac{\psi}{2}} \right], \psi = \beta l \cos \phi + \alpha \quad (2.27)$$

$\left| \frac{\sin \frac{n\psi}{2}}{\sin \frac{\psi}{2}} \right|$: Array factor (AF) that determines the shape of the radiation pattern.

Equation (2.27) reached the maximum value when $\psi = 0$ then $\beta l \cos \phi = -\alpha$, so we can reach the maximum as we wish by choosing α correctly. The phase of each element in this array can be controlled by phase shifter, and the amplitude of each element is adjusted by an amplifier or attenuator [16].

2.17 Microstrip Discontinuity Compensation

The inescapable discontinuities at bends, step changes in widths, and junctions can cause regression in microstrip circuit performance [3]. In general, compensated discontinuities enhance the circuit behavior and the bandwidth. Usually chamfered bends or rounded corners are used in microstrip circuits. Several shapes of bends such as right-angled bends were designed to enhance the microstrip circuits' performance [10],[14], and [22], see figure 2.25.

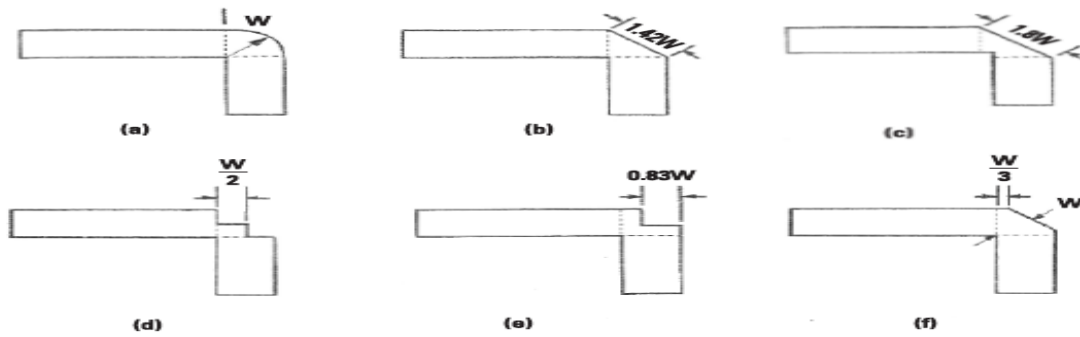


Figure 2.25 Several shapes of right-angled bends [14], [22].

2.17.1 The bend allowance (BA)

Bend allowance comes from the fact that when sheet metal is bent, the inside surface of the bend is compressed and the outer surface of the bend is stretched, see figure 2.26, and can be calculated from the formula [19]:

$$(BA) \text{ Length} = \text{Bend Angle} * (\pi / 180) * (\text{Inside Radius} + K\text{-factor} * \text{Thickness}) \quad (2.28)$$

and $K\text{-factor} = (0 \text{ to } 0.5)$ depend on metal .

or from the approximated formula [20]:

$$(BA) \text{ Length} = [(0.01743 * \text{Inside Radius}) + (0.0078 * \text{Thickness})] * (\text{Bend Angle}) \quad (2.29)$$

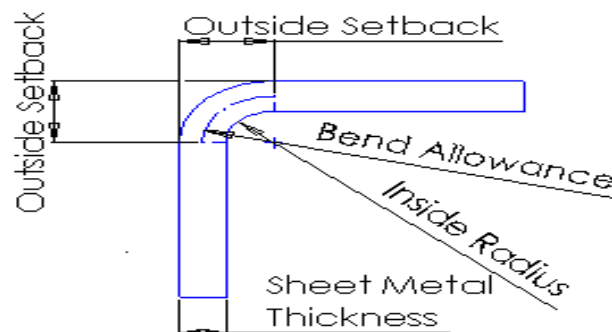


Figure 2.26 Bend allowance [19].

2.18 Design procedure steps

In our project, we will design an inset fed antenna as seen in figure 2.27, and additional parameters should be calculated.

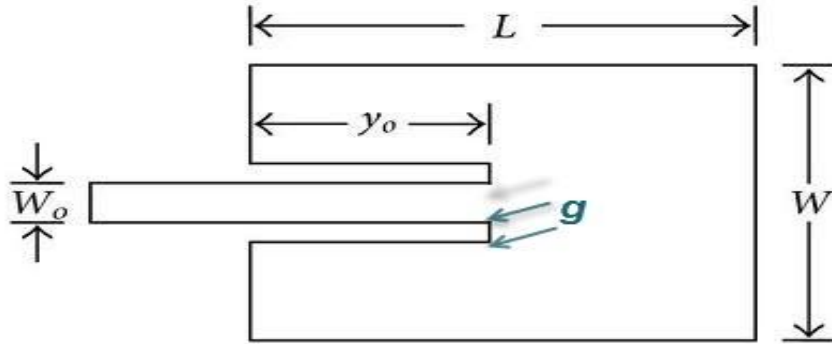


Figure 2.27 Inset fed patch antenna [3], and [5].

The procedure assumes that the specified information includes the dielectric constant of the substrate (ϵ_r), the resonant frequency (f_r), and the height of the substrate h , so the design procedure could be as follows [3]:

1. Calculate the patch width (W): use (2.23)

$$W = \frac{c}{2f_r} \sqrt{\frac{2}{\epsilon_r + 1}}$$

c = free space velocity of light. 3×10^8 m/s.

2. Calculate the effective dielectric constant of the patch antenna (ϵ_{reff}) use (2.27)

$$\epsilon_{reff} = \frac{\epsilon_r + 1}{2} + \frac{\epsilon_r - 1}{2} \left(\frac{1}{\sqrt{1 + \frac{12h}{W}}} \right)$$

3. Calculate the actual length of the patch (L): use (2.25)

$$L = L_{eff} - 2\Delta L$$

and, effective length (L_{eff})

$$L_{eff} = \frac{c}{2f_r \sqrt{\epsilon_{eff}}}$$

4. Calculate the length extension ΔL use (2.24):

$$\frac{\Delta L}{h} = 0.412 \frac{(\epsilon_{eff} + 0.3) \left(\frac{W}{h} + 0.264 \right)}{(\epsilon_{eff} - 0.258) \left(\frac{W}{h} + 0.8 \right)}$$

5. Calculate the patch feeder width (W_o) [3], and [10]:

As we know, the feeder is a simple transmission line, so we can use the transmission line equations to find the feeder width.

$$\frac{W}{h} = \begin{cases} \frac{8e^A}{8e^{2A}-2} & \text{for } w/h < 2 \\ \frac{2}{\pi} \left[B - 1 - \ln(2B - 1) + \frac{\epsilon_r - 1}{2\epsilon_r} \left(\ln(B - 1) + 0.39 - \frac{0.61}{\epsilon_r} \right) \right] & \text{for } w/h > 2 \end{cases} \quad (2.30)$$

$$\text{where } A = \frac{Z_o}{60} \sqrt{\frac{\epsilon_r + 1}{2}} + \frac{\epsilon_r - 1}{\epsilon_r + 1} \left(0.23 + \frac{0.11}{\epsilon_r} \right), \text{ and } B = \frac{377\pi}{2Z_o\sqrt{\epsilon_r}}$$

6. Calculate the feeder length (L_o) [3], and [5]:

The feeder electrical length must be $L_o = \frac{\lambda}{2}$

$$L_o = \frac{(\phi)(\pi/180)(3 \times 10^8)}{(2\pi f)\sqrt{\epsilon_{eff}}} \quad (2.31)$$

7. Calculate the cut depth (y_o) [3], and [5]:

$$R_{in}(y = y_o) = R_{in}(y = 0) \cos^2\left(\frac{\pi}{L} y_o\right) \quad (2.32)$$

Where

$$R_{in}(y = 0) = \frac{1}{2G_1} \text{ and } G_1 = \frac{1}{90} \left(\frac{W}{\lambda_o}\right)^2 \text{ for } W \ll \lambda_o \text{ we have } R_{in}(y = y_o) = 50\Omega.$$

8. Calculate the cut width (gap) (g):

Several approaches for $g \approx \frac{W_o}{N}$ where N takes (10, 15, 20, 25, 30, 35, 40...) [18].

2.19 Conclusion

In this chapter, several antenna parameters were reviewed. Microstrip line and patch antennas with their feeding techniques were explained. Microstrip patch antenna equations were written. Design steps were listed that will be used in chapter 4.

References:

- [1] A. Balanis, Advanced engineering electromagnetic, New York, Wiley, cop. 1989, ISBN 0-471-62194-3.
- [2] C.Rohner, Antenna basics, Rohde & Schwarz, <http://www.rohde-schwarz.com/>.
- [3] C. A. Balanis, Antenna theory: analysis and design, third edition, Hoboken, NJ: Wiley, 2005.
- [4] C. A. Balanis, Modern Antenna Handbook, first edition, Wiley, 2008.
- [5] Y.Huang, Antennas from Theory to Practice, first edition, Wiley, Oct.2008.
- [6] T. A. Milligan, Modern Antenna Design, Second Edition, Wiley, OCR.7.0-2.6.LotB, 2005.
- [7] L .Godara, Handbook of Antennas in Wireless Communications, first edition, CRC, 2002.
- [8] R.Garg, Microstrip antenna design handbook, first edition, Artech House, Inc., USA, 2001, ISBN 0-89006-513-6.
- [9] L.Meyer, "Calculating Antenna System Return Loss as Viewed through the RF Path.", Whitepaper, Andrew Communication Scope, TP-102660-EN, <http://www.andrew.com>, December 2009.
- [10] D.M .Pozar, Microwave Engineering, Third Edition, John Wiley & Sons, 2005,Inc. ISBN 0-471-44878-8.
- [11] F. Yang , Y. Sami, Electromagnetic Band Gap Structures in Antenna Engineering, The Cambridge RF and Microwave Engineering Series, Cambridge University Press, 2009. ISBN: 9780521889919.
- [12] D.M. Pozar, H.schaubert ,Microstrip Antennas: The Analysis and Design of Microstrip Antennas and Arrays, first edition, Wiley, ISBN 0-7803-1078-0.
- [13] Available on ["http://www.antenna-theory.com/antennas/patches/patch3.php"](http://www.antenna-theory.com/antennas/patches/patch3.php), 2014.
- [14] Available on: ["http://www.madmadscientist.com/html/Theory.htm"](http://www.madmadscientist.com/html/Theory.htm), 2014.
- [15] M.demerdash, A. M. Abdin, "Effect of Mutual Coupling on the Performance of Four Elements Microstrip Antenna Array Fed by a Butler Matrix", 29th National Radio Science conference, Cairo, Egypt, 2012.
- [16] A. Alsager,"Design and Analysis of Microstrip Patch Antenna Arrays", Master thesis, University College of Borås, Sweden, 2011.
- [17] I.Bahl, Lumped Elements for RF and Microwave Circuits, London, 2003, ISBN 1-58053-309-4.
- [18] M. Matin,A. Sayeed,"A Design Rule for Inset-fed Rectangular Microstrip Patch Antenna". West-seas transactions on communications, Department of Electrical Engineering and Computer Science North South University, January 2010,
- [19] Available on ["http://www.oemenclosure.com/blog/sheet-metal-bending-bend-allowance-and-k-factor"](http://www.oemenclosure.com/blog/sheet-metal-bending-bend-allowance-and-k-factor).2014.
- [20] Available on : ["http://ehflyers.com/AeroLaulima/SheetMetal/help.html"](http://ehflyers.com/AeroLaulima/SheetMetal/help.html).2014.
- [21] N. Nasimuddin, Microstrip Antennas, first edition, Intec, April 4, 2011, ISBN 978-953-307-247-0.
- [22] K.Gupta, R.Garg Microstrip Lines and Slotlines, Second Edition, Artech House,USA,1996,ISBN 0-89006-766.
- [23] A. Balanis, I. Ioannidis, Introduction to Smart Antennas, first edition, Morgan &Claypool Publishers, 2007, ISBN: 1598291777.

Chapter 3

Microwave Couplers and phase shifters

3.1 Introduction

In this chapter, we will talk about the scattering parameters, and then we will talk about couplers, their analysis, crossovers, and the phase shifters.

3.2 Scattering Matrix Parameters

The first published description of S-matrix parameters was in the thesis of Vitold Belevitch in 1945[1]. The name used by Belevitch was repartition matrix and limited consideration to lumped-element networks. The term scattering matrix was used by physicist and engineer Robert Henry Dicke in 1947 who independently developed the idea during war time work on radar S-parameters or scattering parameters (the elements of a scattering matrix or S-matrix) describe the electrical attitude of linear electrical networks when undergoing various steady state motivation by electrical signals. The parameters are useful for electrical engineering, electronics, communication systems design, and especially for microwave engineering [1], and [2].

Consider that we have n -ports network, and a_n is the amplitude of the voltage wave incident on port n and b_n is the amplitude of the voltage wave reflected from port n . The scattering matrix, or [S] matrix, can be derived in relation to these incident and reflected voltage waves as [2],[18]:

$$[b_n] = [S][a_n] \quad (3.1)$$

3.2.1 Lossless networks

A lossless network is one that does not dissipate any power, or $\sum |a_n|^2 = \sum |b_n|^2$ the sum of the incident powers at all ports is equal to the sum of the reflected powers at all ports. This implies that the S-parameter matrix is unitary, that is $(S)^H(S) = (I)$ where $(S)^H$ the conjugate transpose of (S) is and (I) is the identity matrix [1], [2], and [4].

3.2.2 Lossy networks

A lossy passive network is one in which the sum of the incident powers at all ports is greater than the sum of the reflected powers at all ports. It therefore dissipates power, or: $\sum |a_n|^2 \neq \sum |b_n|^2$. In this case $\sum |a_n|^2 > \sum |b_n|^2$, and $(I) - (S)^H(S)$ is positive definite [1], and [2].

3.2.3 Two-Ports S-Parameters

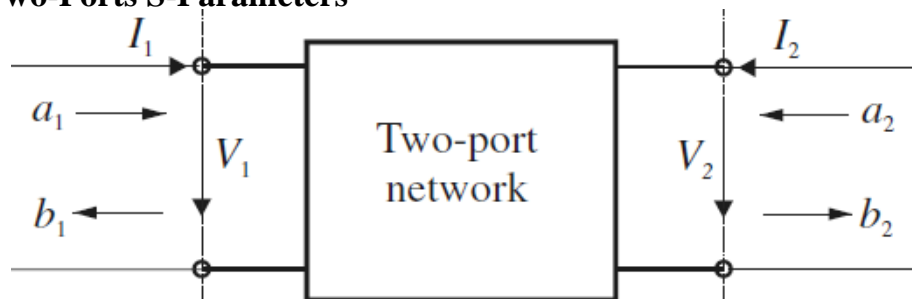


Figure 3.1 Two ports network [1], and [18].

The S-parameters of a two ports network shown in figure 3.1 are as follow, which give relationship between the reflected and incident power waves [1], [3], and [18]:

$$\begin{bmatrix} b_1 \\ b_2 \end{bmatrix} = \begin{bmatrix} S_{11} & S_{12} \\ S_{21} & S_{22} \end{bmatrix} \begin{bmatrix} a_1 \\ a_2 \end{bmatrix} \quad (3.2)$$

Where:

$$b_1 = s_{11}a_1 + s_{12}a_2 \quad (3.3)$$

$$b_2 = s_{21}a_1 + s_{22}a_2 \quad (3.4)$$

S_{11} : is the input port voltage reflection coefficient (Port 1 reflection coefficient = b_1/a_1).

S_{12} : is the reverse voltage gain (Port 2 to Port 1 transmission coefficient/gain = b_1/a_2).

S_{21} : is the forward voltage gain (Port 1 to Port 2 transmission coefficient/gain = b_2/a_1).

S_{22} : is the output port voltage reflection coefficient (Port 2 reflection coefficient = b_2/a_2).

We will assume that the input and output connections are to ports 1 and 2 respectively which is the most common convention. The nominal system impedance, frequency and any other factors, which may influence the device, such as temperature, must also be specified [1], and [8].

3.2.3.1 Scalar logarithmic gain

The scalar logarithmic (decibel or dB) expression for gain (g) is:

$$g = 20\log_{10}|S_{21}| \text{ dB.} \quad (3.5)$$

This is used more than scalar linear gain and a positive quantity is normally understood as simply a 'gain'. A negative quantity is expressed as a 'negative gain' or more usually as a 'loss' equivalent to its magnitude in dB [1], [3].

3.2.3.2 Insertion loss

When the two measurement ports use the same reference impedance, the insertion loss (IL) is the dB expression of the transmission coefficient $|S_{21}|$ [1]. It can be expressed as:

$$IL = -20\log_{10}|S_{21}| \text{ dB} \quad (3.6)$$

3.2.3.3 Input return loss

Input return loss RL_{in} is a scalar measure of how close the actual input impedance of the network to the nominal system impedance value, and is expressed in logarithmic scale as [1]:

$$RL_{in} = |20\log_{10}|S_{11}|| \text{ dB} \quad (3.7)$$

3.2.3.4 Output return loss

The output return loss (RL_{out}) has a similar definition to the input return loss but applies to the output port (port 2) instead of the input port [1]. It is given by:

$$RL_{out} = |20\log_{10}|S_{22}|| \text{ dB} \quad (3.8)$$

3.2.3.5 Reverse gain and Reverse isolation

The scalar logarithmic (decibel) expression for reverse gain g_{rev} is written as [1]:

$$g_{rev} = 20\log_{10}|S_{12}| \text{ dB} \quad (3.9)$$

3.2.3.6 Voltage standing wave ratio

The voltage standing wave ratio (VSWR) at a port, represented by the lower case 's', is a similar measure of port match to return loss but is a scalar linear quantity, the ratio of the standing wave maximum voltage to the standing wave minimum voltage. It therefore relates to the magnitude of the voltage reflection coefficient and hence to the magnitude of either for S_{11} the input port or S_{22} for the output port [2], and [3].

At the input port, the VSWR (S_{in}) is given by

$$S_{in} = \frac{1+|S_{11}|}{1-|S_{11}|} \quad (3.10)$$

At the output port, the VSWR (S_{out}) is given by

$$S_{out} = \frac{1+|S_{22}|}{1-|S_{22}|} \quad (3.11)$$

3.3 ABCD matrix of two-port network

There are sundry benefits of using the $ABCD$ matrix representation when designing microwave components [21]. They allow simulating entire structures made of a cascade of lumped elements, such as capacitors, inductors, and transformers. In addition, S parameters can be converted to $ABCD$ parameters, and vice versa. When analyzing a microwave structure element, it is easier to model the element as a combination of lumped elements rather than interpreting the S parameters directly. The $ABCD$ matrix of a two-port is defined by using voltages and currents as shown in figure 3.2. The $ACBD$ matrix is defined by [2], and [21]:

$$V_1 = AV_2 + B(-I_2) \quad (3.12)$$

$$I_1 = CV_2 + D(-I_2) \quad (3.13)$$

Equations (3.12), and (3.13) explain the relation between voltages and currents, thus given V_1 , I_1 , V_2 and I_2 can be found if the $ABCD$ matrix is known, previous relations can be written in matrix form as [2], and [21]:

$$\begin{bmatrix} V_1 \\ I_1 \end{bmatrix} = \begin{bmatrix} A & B \\ C & D \end{bmatrix} \begin{bmatrix} V_2 \\ -I_2 \end{bmatrix} \quad (3.14)$$

In practice, many microwave circuits consist of a cascade connection of two or more than two-port network. The $ABCD$ matrix of the cascade connection can be easily found by multiplying the $ABCD$ matrices of the individual two-ports networks [2], and [21].

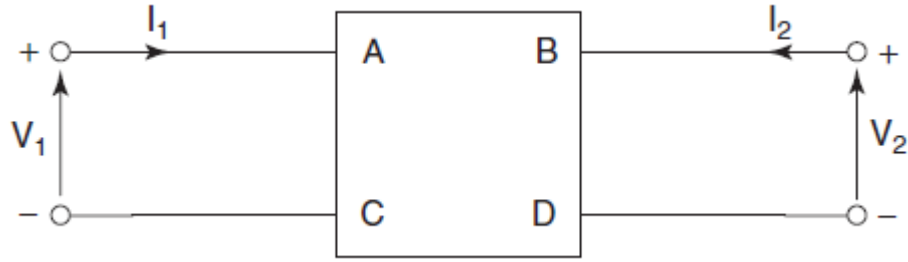


Figure 3.2 $ABCD$ matrix of a two-port system.

For conversion from $ABCD$ to S parameters, equation (3.15) can be used [2], and [21]:

$$\begin{bmatrix} S_{11} & S_{12} \\ S_{21} & S_{22} \end{bmatrix} = \frac{1}{Z_o A + B + Z_o^2 C + Z_o D} \begin{bmatrix} Z_o A + B + Z_o^2 C - Z_o D & 2Z_o(AD - BC) \\ 2Z_o & -Z_o A + B + Z_o^2 C + Z_o D \end{bmatrix} \quad (3.15)$$

where, Z_o is the characteristic impedance of the transmission lines connected to the $ABCD$ network, usually equals 50Ω .

For conversion from S to $ABCD$ parameters, equation (3.16) can be used [2], and [21]:

$$\begin{bmatrix} A & B \\ C & D \end{bmatrix} = \frac{1}{2S_{21}} \begin{bmatrix} (1 + S_{11})(1 - S_{22}) + S_{12}S_{21} & Z_o[(1 + S_{11})(1 + S_{22}) - S_{12}S_{21}] \\ \frac{1}{Z_o}[(1 - S_{11})(1 - S_{22}) - S_{12}S_{21}] & (1 - S_{11})(1 + S_{22}) + S_{12}S_{21} \end{bmatrix} \quad (3.16)$$

3.4 Directional couplers overview

Directional couplers are passive microwave devices used for power division or power combining, figure 3.3 (a) shows an arbitrary power division, where an input signal is divided by the coupler into two signals of lesser power. When it is also used as a combiner, the coupler takes two signals to provide only one output [2], and [6], as seen in figure 3.3 (b). The coupler may be a three-port component as illustrated in figure 3.4, or maybe a four-port component.

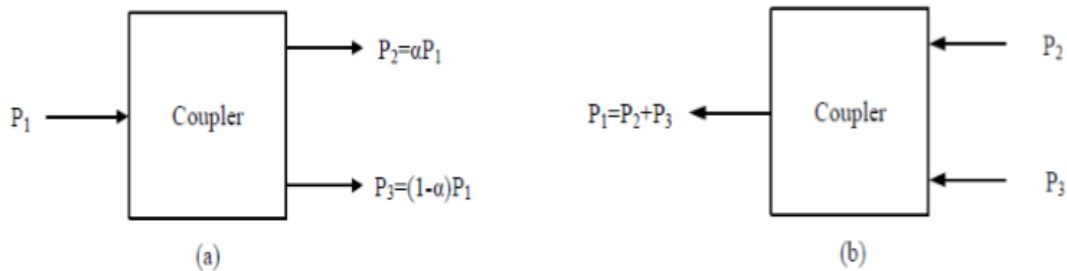


Figure 3.3 (a) An arbitrary power division and (b) power combining [2].

With reference to figure 3.4 (a), which is a commonly used symbol for directional couplers, the ideal directional coupler has the property that a wave incident in port 1 couples power into ports 2 and 3 but not into port 4. For the wave incident in port 4, the power is coupled into ports 2 and 3 but not into port 1. Thus, ports 1 and 4 are uncoupled. Similarly, ports 2 and 3 are also uncoupled. However, port 4 is usually terminated with a matched load and not accessible to the user [2], and [6]. This results in a three-port component as shown in figure 3.4 (b).

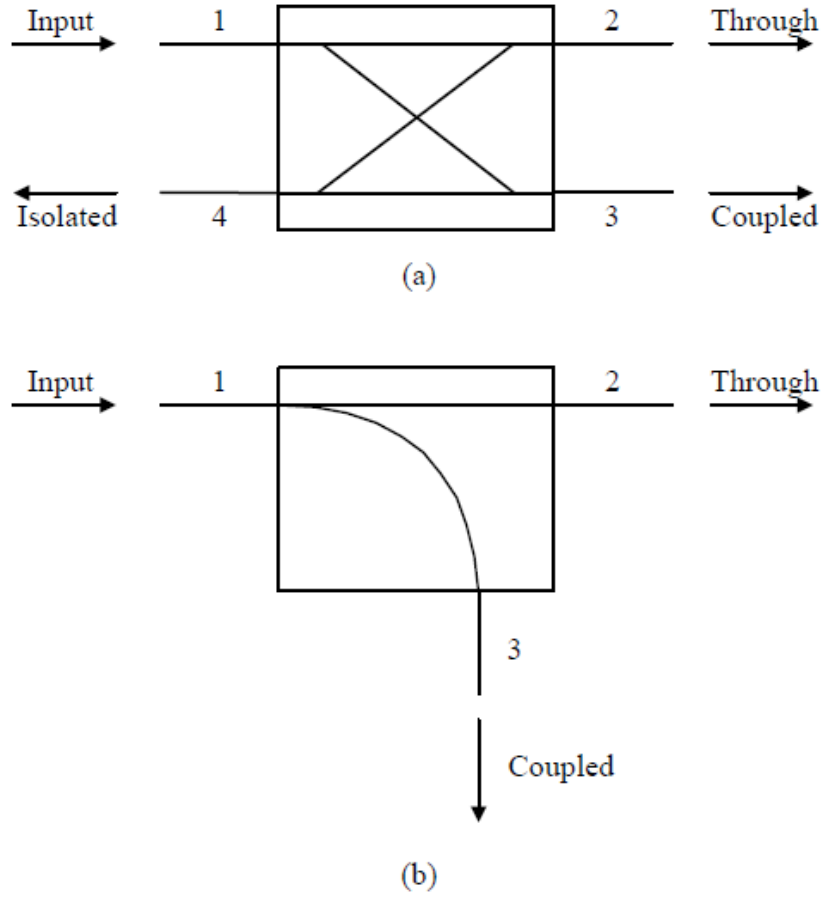


Figure 3.4 (a) Symbol for directional couplers and (b) symbol for a directional coupler with port 4 terminated with a matched load [2].

The performance of a directional coupler is characterized by two parameters: the coupling and the directivity. The coupling factor indicates the fraction of the input power that is coupled to the output port, and the directivity is a measure of how well the power is coupled in the desired direction. Let P_1 be the power supplied to port 1, P_3 be the coupled power in the forward direction in port 3 and P_4 be the power coupled in the backward direction in port 4 [2], and [6]. The coupling in decibels is then given by:

$$C = 10 \log \frac{P_1}{P_3} \quad (3.17)$$

The directivity can be defined as

$$D = 10 \log \frac{P_3}{P_4} \quad (3.18)$$

Ideally, the power P_4 coupled in port 4 should be zero, and therefore the directivity of the coupler would be infinite.

The ideal directional coupler, as illustrated in figure 3.4 (a), is a lossless reciprocal four-port network matched at all ports with $S_{14} = S_{23} = 0$. Thus, the scattering matrix [1], and [2] has the form:

$$[S] = \begin{bmatrix} 0 & S_{12} & S_{13} & 0 \\ S_{12} & 0 & 0 & S_{24} \\ S_{13} & 0 & 0 & S_{34} \\ 0 & S_{24} & S_{34} & 0 \end{bmatrix} \quad (3.19)$$

Several properties of the ideal directional coupler can be deduced from the symmetry and unitary properties of its scattering matrix [1], and [2]. If we take the product of row 1 with the conjugate of row 4 in (3.19), and similarly row 2 with the conjugate of row 3, we obtain:

$$S_{12}S_{24}^* + S_{13}S_{34}^* = 0 \quad (3.20)$$

$$S_{12}S_{13}^* + S_{24}S_{34}^* = 0 \quad (3.21)$$

If we note that $|S_{12}S_{24}^*| = |S_{12}||S_{24}|$, (3.14) and (3.21) are seen to give:

$$|S_{12}||S_{24}| = |S_{13}||S_{34}| \quad (3.22)$$

$$|S_{12}||S_{13}| = |S_{24}||S_{34}| \quad (3.23)$$

Now if we divide (3.22) by (3.23) we obtain:

$$\frac{|S_{24}|}{|S_{13}|} = \frac{|S_{13}|}{|S_{24}|} \quad (3.24)$$

which implies that

$$|S_{13}| = |S_{24}| \quad (3.25)$$

So that the coupling between ports 1 and 3 equals that between ports 2 and 4 [1], and [2].

Use of (3.25) in (3.22) gives

$$|S_{12}| = |S_{34}| \quad (3.26)$$

So that the coupling between ports 1 and 2 is the same as that between ports 3 and 4.

Then the product of the first row with its conjugate in (3.19) yields:

$$|S_{12}|^2 + |S_{13}|^2 = 1 \quad (3.27)$$

Similarly,

$$|S_{12}|^2 + |S_{24}|^2 = 1 \quad (3.28)$$

By properly choosing the terminal planes on ports 1 and 3, we can adjust the phase angle of scattering parameters [2], so that:

$$S_{12} = S_{34} = C_1 \quad (3.29)$$

$$S_{13} = C_2 e^{j\alpha} \quad (3.30)$$

$$S_{24} = C_2 e^{j\beta} \quad (3.31)$$

where C_1 and C_2 are real and α and β are phase constants to be determined.

Use of (3.29) and (3.30) in (3.28) gives:

$$C_1^2 + C_2^2 = 1 \quad (3.32)$$

Substituting (3.29) to (3.31) into (3.32) yields a relation between the two-phase constants as:

$$\alpha + \beta = \pi \pm 2n\pi \quad (3.33)$$

In practice [2], and [6], there are two particular choices:

1. The 90° coupler: The phase constants are chosen equal, $\alpha = \beta = \pi/2$. Then the scattering matrix has the form

$$[S] = \begin{bmatrix} 0 & C_1 & jC_2 & 0 \\ C_1 & 0 & 0 & jC_2 \\ jC_2 & 0 & 0 & C_1 \\ 0 & jC_2 & C_1 & 0 \end{bmatrix} \quad (3.34)$$

2. The 180° coupler: The phase constants are chosen to be 180° apart, $\alpha = 0$, $\beta = \pi$. Then the scattering matrix has the form

$$[S] = \begin{bmatrix} 0 & C_1 & C_2 & 0 \\ C_1 & 0 & 0 & -C_2 \\ C_2 & 0 & 0 & C_1 \\ 0 & -C_2 & C_1 & 0 \end{bmatrix} \quad (3.35)$$

3.5 Hybrid couplers overview

Directional couplers can be designed for arbitrary power division. However, hybrid couplers [2] are special cases of directional couplers with equal power division (3dB), which implies:

$$C_1 = C_2 = 1/\sqrt{2} \quad (3.36)$$

Hybrid couplers have either a 90° or a 180° phase shift between the output ports.

3.5.1 90° hybrid couplers functional description

The 90° hybrid coupler, also known as the quadrature hybrid coupler, is a 3 dB directional coupler with 90° phase difference in the two output ports [2]. With reference to a 90° hybrid symbol shown in figure 3.5, a signal applied to port 1 will be evenly split into two components with a 90° phase difference at ports 2 and 3, and port 4 will be isolated.

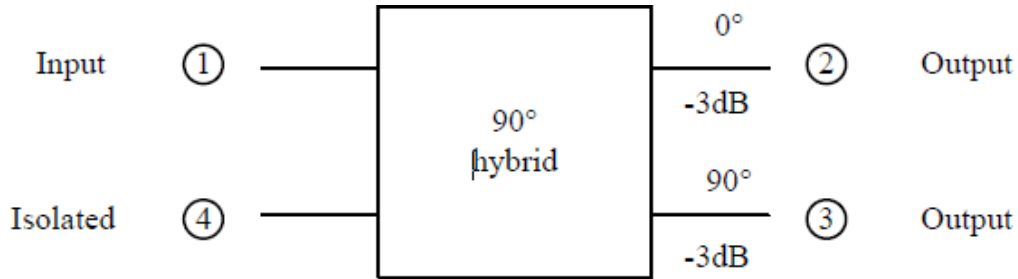


Figure 3.5 Symbol of a 90° hybrid coupler [2].

The branch-line hybrid coupler [2], and [6] has a 90° phase difference between ports 2 and 3 when fed at port 1, and is an example of the 90° hybrid coupler. Its scattering matrix has the form [2]:

$$[S] = \frac{1}{\sqrt{2}} \begin{bmatrix} 0 & 1 & j & 0 \\ 1 & 0 & 0 & j \\ j & 0 & 0 & 1 \\ 0 & j & 1 & 0 \end{bmatrix} \quad (3.37)$$

3.5.2 Conventional branch-line hybrid coupler

The branch-line hybrid coupler [2], and [5] shown in figure 3.6 can easily be constructed in planar (microstrip or stripline) form. As illustrated in Figure 3.5, the branch-line hybrid has four ports with the terminal impedance Z_0 . It consists of two quarter-wavelength transmission line sections of characteristic impedance Z_{01} . Two transmission line sections are connected by two shunt branches, which are both quarter-wavelength transmission line sections of characteristic impedance Z_{02} , at both ends [2]. With reference to figure 3.6. A signal applied to port 1 will be evenly split into two components with a 90° phase difference at ports 2 and 3, and port 4 will be isolated [5]. Observe that the branch-line hybrid is symmetrical, so any port can be used as the input port.

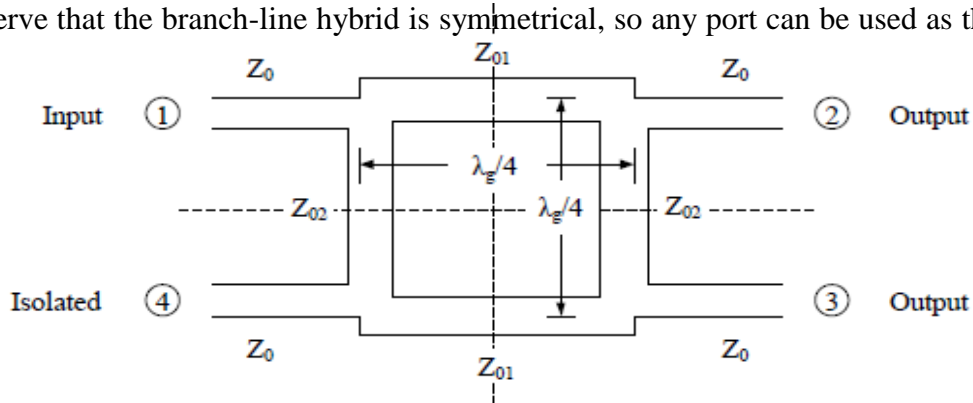


Figure 3.6 Geometry of a branch-line hybrid coupler [2].

3.6 Design of a branch-line hybrid coupler

At the center frequency, scattering parameters of the branch-line hybrid are given by [5], and [6]:

$$S_{21} = -j \frac{Z_{01}}{Z_0} \quad (3.38)$$

$$S_{31} = -\frac{Z_{01}}{Z_{02}} \quad (3.39)$$

$$S_{11} = S_{41} = 0 \quad (3.40)$$

Thus, the complete scattering matrix can be expressed as [5], and [6]:

$$[S] = \begin{bmatrix} 0 & -jZ_{01} & -\frac{Z_{01}}{Z_{02}} & 0 \\ -j\frac{Z_{01}}{Z_0} & 0 & 0 & -\frac{Z_{01}}{Z_{02}} \\ \frac{-Z_{01}}{Z_{02}} & 0 & 0 & -j\frac{Z_{01}}{Z_0} \\ 0 & -\frac{Z_{01}}{Z_{02}} & \frac{-jZ_{01}}{Z_0} & 0 \end{bmatrix} \quad (3.41)$$

From (3.41) and (3.34), we have:

$$Z_{01} = Z_0 C_1 \quad (3.42)$$

$$Z_{02} = \frac{Z_{01}}{C_2} \quad (3.43)$$

Then using (3.36) in (3.42) and (3.43) gives:

$$Z_{01} = \frac{1}{\sqrt{2}} Z_0 \quad (3.44)$$

$$Z_{02} = Z_0 \quad (3.45)$$

3.7 Analysis of a branch-line hybrid coupler

The analysis of the branch-line hybrid can be carried out using the even- and odd-mode approach [2], [5], and [8]. As shown in figure 3.7, we first draw the schematic circuit of branch-line coupler in normalized form, where each line represents a transmission line with the characteristic impedance normalized to Z_0 . We then assume that a wave of unit amplitude $A_1=1$ is incident at port 1.

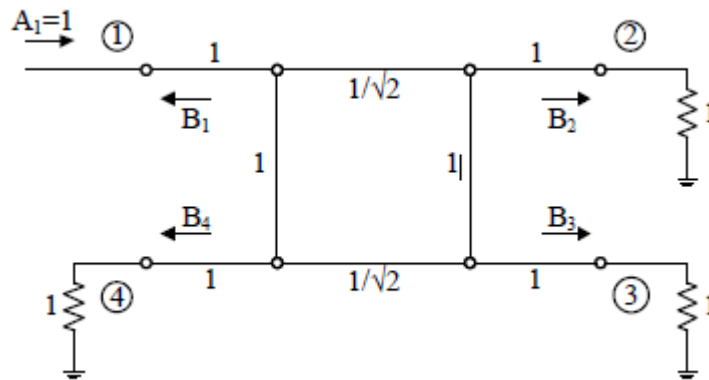


Figure 3.7 Schematic circuit of the normalized branch-line coupler [2].

The circuit of figure 3.7 can be decomposed into the superposition of an even-mode Excitation and an odd-mode excitation, as shown in figure 3.8.

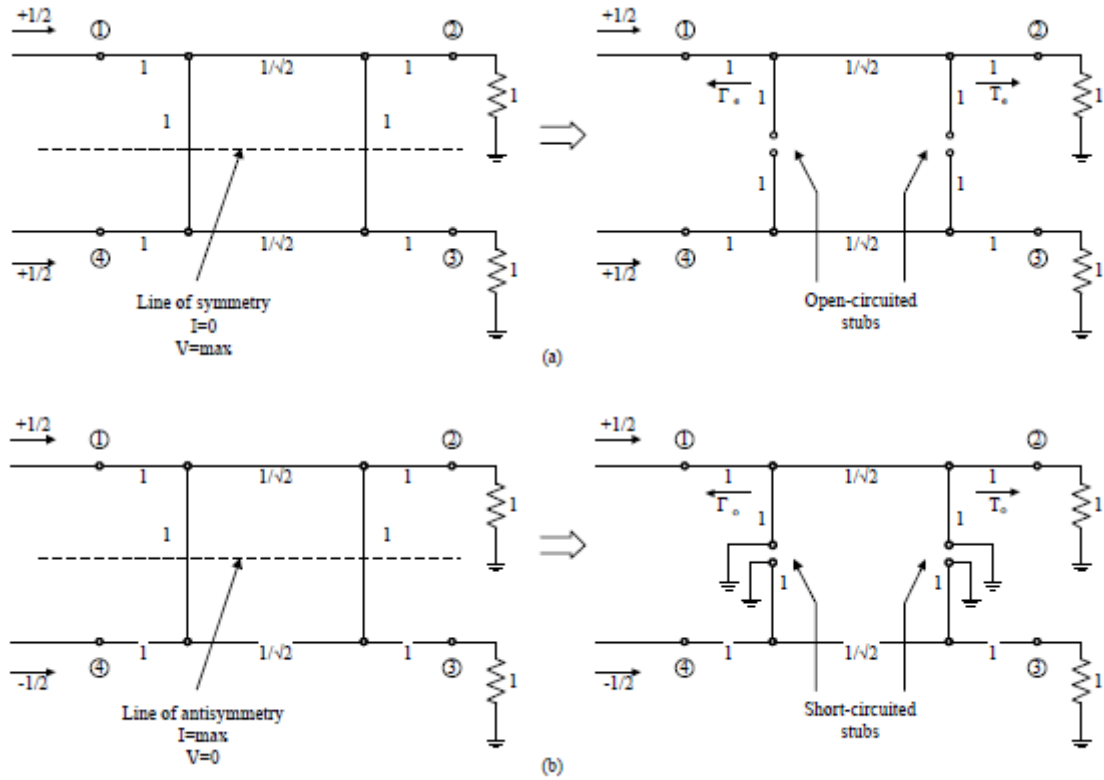


Figure 3.8 (a) Even-mode excitation and (b) Odd-mode excitation [2].

Because the circuit is linear, the actual response of figure 3.7 can be obtained from the sum of the responses to the even-mode and odd-mode excitations. The amplitude of the emerging wave at each port of the branch-line hybrid coupler (B_1, B_2, B_3, B_4) can be expressed [5], [6], and [8] as:

$$B_1 = \frac{1}{2}\Gamma_e + \frac{1}{2}\Gamma_o \quad (3.46)$$

$$B_2 = \frac{1}{2}T_e + \frac{1}{2}T_o \quad (3.47)$$

$$B_3 = \frac{1}{2}T_e - \frac{1}{2}T_o \quad (3.48)$$

$$B_4 = \frac{1}{2}\Gamma_e - \frac{1}{2}\Gamma_o \quad (3.49)$$

where $T_{e,o}$ and $\Gamma_{e,o}$ are the even- and odd- mode transmission and reflection coefficients for the two port networks of figure 3.8. For the even-mode two-port circuit shown in figure 3.8 (a), T_e and Γ_e can be calculated from multiplying the $ABCD$ matrices of each cascade component in the circuit [2], and [7]. Assume the branch-line hybrid coupler has a center frequency of f_o , which implies that each branch has the length

$$l = \frac{\lambda_o}{4} = \frac{c/f_o}{4} = \frac{\pi c}{2\omega_o} \quad (3.50)$$

where λ_0 and ω_0 are the wavelength and radian frequency corresponding to the center Frequency f_o , respectively. With reference to [2], [7], and [21], the $ABCD$ matrix of a transmission line section of length l and characteristic impedance Z_c can be expressed as:

$$\begin{bmatrix} A & B \\ C & D \end{bmatrix} = \begin{bmatrix} \cos \beta l & jZ_c \sin \beta l \\ jY_c \sin \beta l & \cos \beta l \end{bmatrix} \quad (3.51)$$

where $\beta = \omega/c$ is the phase constant. Substituting the impedance of figure 3.8 into (3.51) gives the $ABCD$ matrix of the main branch as [21]:

$$\begin{bmatrix} A & B \\ C & D \end{bmatrix} = \begin{bmatrix} \cos \frac{\omega \pi}{\omega_o 2} & j \frac{1}{\sqrt{2}} \sin \frac{\omega \pi}{\omega_o 2} \\ j\sqrt{2} \sin \frac{\omega \pi}{\omega_o 2} & \cos \frac{\omega \pi}{\omega_o 2} \end{bmatrix} \quad (3.52)$$

However, for the open-circuited stub, the impedance is given as:

$$Z_{oc} = -jZ_c \cot \beta l \quad (3.53)$$

where the length of each stub is $l = \frac{\lambda_o}{8} = \frac{\pi \omega}{4 \omega_o}$

The $ABCD$ matrix of the shunt open-circuited stub can be obtained as [21]:

$$\begin{bmatrix} A & B \\ C & D \end{bmatrix} = \begin{bmatrix} 1 & 0 \\ j \tan \frac{\omega \pi}{\omega_o 4} & 1 \end{bmatrix} \quad (3.54)$$

Thus for the two-port even-mode excitation, the $ABCD$ matrix is found [2], [7], and [21] as:

$$\begin{bmatrix} A & B \\ C & D \end{bmatrix}_e = \begin{bmatrix} 1 & 0 \\ j \tan \frac{\omega \pi}{\omega_o 4} & 1 \end{bmatrix} \begin{bmatrix} \cos \frac{\omega \pi}{\omega_o 2} & j \frac{1}{\sqrt{2}} \sin \frac{\omega \pi}{\omega_o 2} \\ j\sqrt{2} \sin \frac{\omega \pi}{\omega_o 2} & \cos \frac{\omega \pi}{\omega_o 2} \end{bmatrix} \begin{bmatrix} 1 & 0 \\ j \tan \frac{\omega \pi}{\omega_o 4} & 1 \end{bmatrix} \quad (3.55)$$

The transmission and reflection coefficients can be converted from the $ABCD$ matrix [2], [7], and [21] as:

$$T_e = \frac{2}{A+B+C+D} \quad (3.56)$$

$$\Gamma_e = \frac{A+B-C-D}{A+B+C+D} \quad (3.57)$$

Similarly, for the odd-mode excitation, we obtain the $ABCD$ matrix for the two port network [2], [7], and [21]:

$$\begin{bmatrix} A & B \\ C & D \end{bmatrix}_o = \begin{bmatrix} 1 & 0 \\ -j \cot \frac{\omega \pi}{\omega_o 4} & 1 \end{bmatrix} \begin{bmatrix} \cos \frac{\omega \pi}{\omega_o 2} & j \frac{1}{\sqrt{2}} \sin \frac{\omega \pi}{\omega_o 2} \\ j\sqrt{2} \sin \frac{\omega \pi}{\omega_o 2} & \cos \frac{\omega \pi}{\omega_o 2} \end{bmatrix} \begin{bmatrix} 1 & 0 \\ -j \cot \frac{\omega \pi}{\omega_o 4} & 1 \end{bmatrix} \quad (3.58)$$

which gives the transmission and reflection coefficients as [2], and [7]:

$$T_o = \frac{2}{A+B+C+D} \quad (3.59)$$

$$\Gamma_o = \frac{A+B-C-D}{A+B+C+D} \quad (3.60)$$

So, the scattering parameters of the branch-line hybrid coupler are obtained as [2], [7], and [21]:

$$S_{11} = \frac{B_1}{A_1} = B_1 = \frac{1}{2}(\Gamma_e + \Gamma_o) \quad (3.61)$$

$$S_{21} = \frac{B_2}{A_1} = B_2 = \frac{1}{2}(T_e + T_o) \quad (3.62)$$

$$S_{31} = \frac{B_3}{A_1} = B_3 = \frac{1}{2}(T_e - T_o) \quad (3.63)$$

$$S_{41} = \frac{B_4}{A_1} = B_4 = \frac{1}{2}(\Gamma_e - \Gamma_o) \quad (3.64)$$

3.8 Crossover (0 dB coupler)

The crossover can be built by cascading two 90° hybrid couplers network with 2 inputs and 2 outputs [2], [10], and [11], see figure 3.9. This type of coupler is also called 0 dB coupler. The perfect design of crossover is accomplished if every adjacent ports are isolated such that if port 1 is fed, the output of ports 2 and 4 should be equal to 0 and if port 4 is fed, the output of ports 1 and 3 should be 0, and $(Z_{02} = Z_{03} = Z_0, Z_{01} = \frac{Z_0}{\sqrt{2}})$ [10]. The S-matrix for the crossover can be obtained by extending the even-odd Mode analysis for the quadrature hybrid [2], [8], and [11]. The (S) matrix will have the following form [10]:

$$[S] = \begin{bmatrix} 0 & 0 & j & 0 \\ 0 & 0 & 0 & j \\ j & 0 & 0 & 0 \\ 0 & j & 0 & 0 \end{bmatrix} \quad (3.65)$$

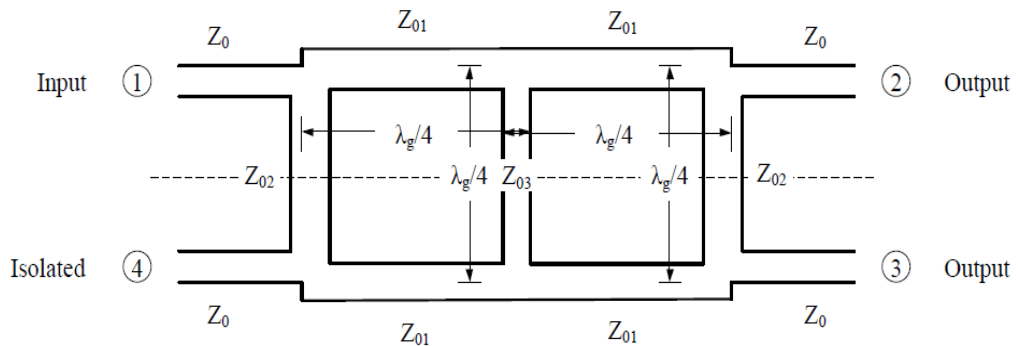


Figure 3.9 Geometry of crossover [6].

Note: Crossover can be implemented by microstrip transmission line equations, and in practical cascading of two 90° hybrids to implement a crossover did not give the required performance [10-13] of its scattering matrix parameters, so the geometry will be modified to implement the practical crossover as shown in figure 3.10.

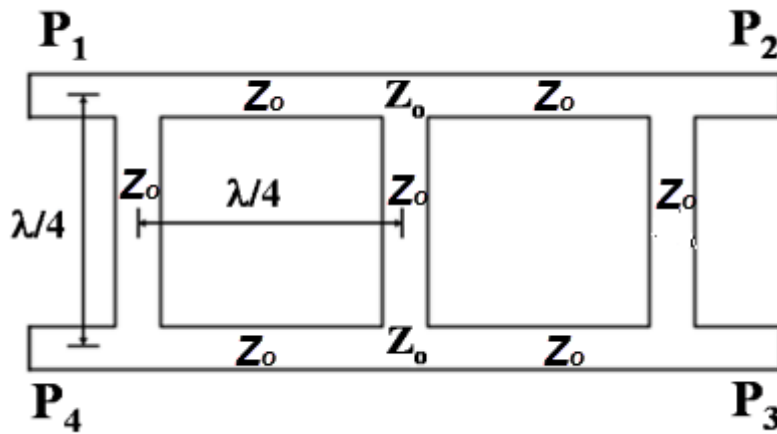


Figure.3.10 Practical crossover [12-13].

3.9 Phase shifter

The phase shifter is implemented using microstrip transmission line. As seen in figure 3.11, the length of the line corresponding to -45° phase shift is given by the formula [9-12]:

$$\phi = \frac{2\pi}{\lambda} L \quad (3.66)$$

where L is the length in meters, ϕ is in radians, λ is the wavelength in the microstrip line, and the wavelength in the microstrip transmission line is given by:

$$\lambda = \lambda_0 / \sqrt{\epsilon_{\text{reff}}} \quad (3.67)$$

where λ_0 is the free space wavelength, and ϵ_{reff} is the effective dielectric constant of the microstrip line. Since the phase shift is implemented using simple transmission line, therefore it is linearly frequency dependent [9-11].

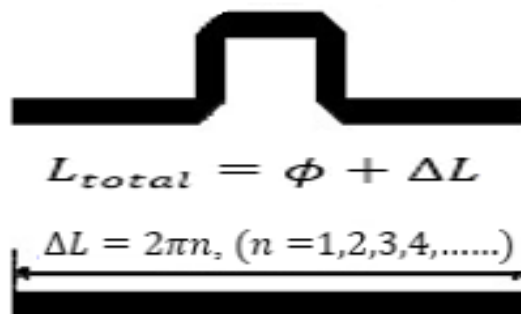


Figure 3.11 Ideal phase shifter [13].

Note: In practice [10-13] we can design the phase -45° shifter by equation (3.68), and add another an extra line length ΔL without changing the desired phase.

$$L_{total} = \frac{\lambda}{8} + \Delta L \quad (3.68)$$

where $\Delta L = 2\pi n$, ($n = 1, 2, 3, 4, \dots$)

3.10 Conclusion

In this chapter, the scattering parameters and their meanings were explained. The chapter introduced couplers types and the derivation of the S-matrix. Moreover, the crossover coupler was reviewed. Finally, microstrip phase shifter was presented. All of these components will be used in chapter 4.

References

- [1] Hp, "S Parameter circuit analysis and Design", Hewlett-Packard Application Note 5A, 1973.
- [2] D. M. Pozar, Microwave Engineering, Third Edition, John Wiley & Sons, 2005, Inc. ISBN 0-471-44878-8.
- [3] J.Choma, W.Chen, Feedback networks: theory and circuit applications, Vol 5, ISBN 10: 9810227701, 2007.
- [4] A.Tager, M.Eleiwa, "Design and Implementation of a Smart Antenna Using Butler Matrix for ISM-band", Electromagnetics Research Symposium, Electronics Department, M. T. C., Cairo, Egypt, 2009.
- [5] W. M. Fathelbab, "The Synthesis of a Class of Branch-Line Directional Couplers," Microwave Theory and Techniques, IEEE Transactions on, vol. 56, no. 8, pp. 1985-1994, Aug.2008.
- [6] S. LU, "Design Of Microwave Hybrid Couplers Using Inter-Coupled Resonators", master thesis, Electrical and Computer Engineering, the University of Birmingham, 2012.
- [7] Jia. Hong, M. J. Lancaster, Microstrip Filters for RF/Microwave Applications, John Wiley & Sons, Inc., 2001, ISBN: 978-0-470-40877-3.
- [8] J.Reed, G.J.Wheeler, "A Method of Analysis of Symmetrical Four-Port Networks", Microwave Theory and Techniques , IEEE Transactions on, ISSN: 0097-2002, 1956.
- [9] Z. Zhang, Y. Jiao, "Modified Broadband Schiffman Phase Shifter using Dentate Microstrip And Patterned Ground Plane", Progress In Electromagnetics Research Letters, Vol. 24, 9-16, 2011.
- [10] E. H. Fooks, R. Zakarevicius, Microwave engineering using microstrip circuits, Prentice Hall, New York , ISBN-13: 978-0136916505 ,1990.
- [11] S. Ahmad, F.Seman, "4-Port Butler Matrix for Switched Multibeam Antenna Array", conference of applied electromagnetics, ISBN: 0-7803-9431-3, 2005.
- [12] M.Aldemerdash, A. M. Abdin, "Effect of Mutual Coupling on the Performance of Four Elements Microstrip Antenna Array Fed by a Butler Matrix", 29th National Radio Science Conference, Cairo Egypt, 2012.
- [13] W. Bhowmik, S.Srivastava , "Optimum Design of a 4x4 Planar Butler Matrix Array for WLAN Application", Journal of Telecommunications, Volume 2, 2010.
- [14] T.Mazri, F.Riouch, "Application of Butler Matrix to a Tree Structure of Microstrip Antenna Array", International Journal of Computer Science, ISSN (Online): 1694-0814, July 2011.
- [15] Agilent, "S-Parameter Design", AN 154 Application Note, Agilent Technology, 2000.
- [16] R. E. Collin, Foundations for microwave engineering, Second edition, Wiley-IEEE Press, ISBN: 978-0-7803-6031-0, 2000.
- [17] M. hefnawy "Microstrip Antennas for Indoor Wireless Dynamic Environments", Sains University, Microstrip Antennas, InTech, Malaysia, April 2011.
- [18] Yi. Huang, Antennas from Theory to Practice, first edition, Wiley, Oct.2008.
- [19] J. Hong, M. Lancaster, Microstrip Filters for RF/Microwave Applications, Wiley, New York 2001.
- [20] G. Matthaei, L. Young, and E, Microwave Filters, Impedance-Matching Networks, and Coupling Structures, McGraw-Hill, New York, 1964.
- [21] P.Jarry , J.Beneat ,Advanced Design Techniques and Realizations of Microwave and RF Filters, John Wiley & Sons, Inc.,2008

Chapter 4

Design of 4x4 Butler Matrix with 4 patch antennas

4.1 Introduction

In this chapter, we will explain the butler matrix, and how to design it, and then we will use equations explained in previous chapters to design the overall system. Finally, we will use the ADS 2011 simulator to design and optimize the desired goals.

4.2 Butler matrix with antenna-array

In several applications, antennas are designed with very directive characteristics to meet demands for long distance communication. This can only be done by increasing the electrical size of the antenna. Another way is to form an assembly of radiating elements in a geometrical and electrical configuration, without necessarily increasing the size of the individual elements. Such a multi-element radiation device is defined as an antenna array [1].

Antenna arrays can be one, two, and three-dimensional. By using basic array geometries, the analysis and synthesis of their radiation characteristics can be simplified. In an array of identical elements, we can find at least multi individual controls (degrees of freedom) that can be used to shape the overall pattern of the antenna [1].

Smart antenna is one of the most favorable technologies that will enable a higher capacity in wireless networks by effectively reducing interference. This is accomplished by focusing the radiation only in the desired direction. A switched beam technique is the simplest one in smart antenna systems. It is similar to an antenna-array system that forms multiple-fixed beams with enhanced sensitivity in a specific area. This antenna system detects signal strength pick out one of the predetermined fixed beams, and switches from one beam to another as the user moves [2].

The supply system of the switched beam is named as the Butler matrix. Feeding an N -element antenna array performs a spatial Fast Fourier Transform (FFT) using an $N \times N$ Butler matrix, N orthogonal beams can be generated where N should be an integer power of 2 (i.e. $N = 2^n$, $n \in \mathbb{Z}^+$), and each beam has a gain of the whole array [2-4].

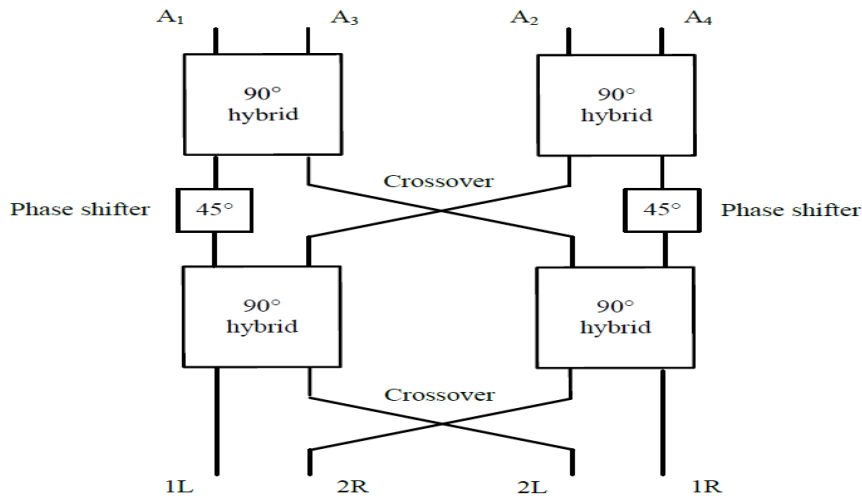


Figure 4.1 4 x 4 Butler matrix block diagram [20].

The Butler matrix was first qualified by Jesse Butler and Ralph Lowe [4]. As seen in figure 4.1, the Butler matrix divides the input power into 4 outputs with same amplitude but with linear phase taper. The phase taper is different for each input port. The outputs are linearly combinations of the inputs and can expressed as [4], and [22]:

$$1L = \frac{1}{4}(A_1\angle 225^\circ + A_2\angle 270^\circ + A_3\angle 315^\circ + A_4\angle 0^\circ) \quad (4.1)$$

$$2R = \frac{1}{4}(A_1\angle 270^\circ + A_2\angle 45^\circ + A_3\angle 180^\circ + A_4\angle 315^\circ) \quad (4.2)$$

$$2L = \frac{1}{4}(A_1\angle 315^\circ + A_2\angle 180^\circ + A_3\angle 45^\circ + A_4\angle 270^\circ) \quad (4.3)$$

$$1R = \frac{1}{4}(A_1\angle 0^\circ + A_2\angle 315^\circ + A_3\angle 270^\circ + A_4\angle 225^\circ) \quad (4.4)$$

Butler matrix works the same when it transmits energy as when it receives energy because it is a passive reciprocal network. Each beam can be used by a dedicated transmitter or receiver. We can see it in figure 4.2, a 4x4 Butler matrix used as a feed circuit for an antenna array [20], and [22].

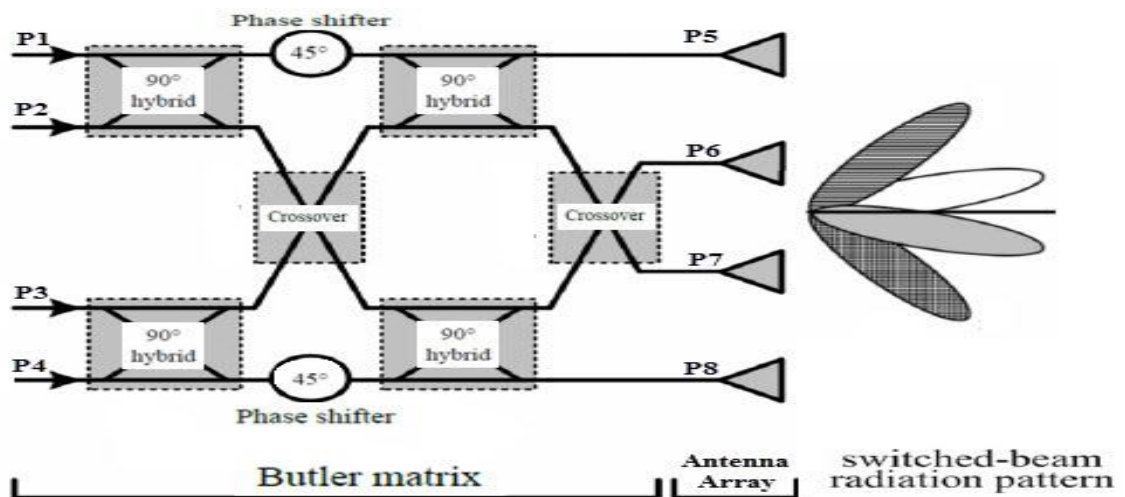


Figure 4.2 4x4 Butler matrix with antenna array [11].

The block diagram of a 4 x 4 butler matrix as shown in Figure 4.2 consists of four -3dB (90°) hybrids couplers , two crossovers , two 45° phase shifters and four antennas [4], and [11].

4.3 Literature Review

There have been several researches in butler matrix with antenna arrays in different applications and various frequency bands.

Here is a list of some previous researches interested in butler matrix design:

1. In [7], for vehicle anti-crash systems an 8-port wide-band Butler matrix with antenna arrays at 24 GHz for front-end radars has been successfully built using micro machined techniques. Best simulation results were written.
2. In [8], a four-beam antenna array operating within 24 GHz frequency range was developed with low cost design. The designed matrix was integrated and manufactured with the four-element linear antenna array confirming the usability of the utilized Butler matrix in beam-scanning applications.
3. In [9], a 4x4 Butler matrix was studied, designed and simulated successfully. The simulated results show that the 4x4 butler matrix produces four orthogonal beams in the required directions. Taken into account the 3dB beam width, the four beams effectively cover the required 120-azimuth angle.
4. In [10], a four-element microstrip antenna array fed by a Butler matrix over spiral EBG structure has been designed and simulated using Ansoft Designer. The antenna array was manufactured and measured showing good results and confirming antenna array's usability.
5. In [11], a 60-GHz switched-beam antenna with Butler matrix network is developed for 60-GHz wireless communication applications. The Butler matrix is integrated with the antenna elements on the same substrate. It provides a cost-effective approach to implement adaptive antennas for the 60-GHz wireless communications.
6. In [12], an optimum design of a 4x4 planar Butler matrix array for WLAN applications is presented. Initially all the necessary formulae for dimensions of hybrid coupler, crossover, phase shifter and radiating elements are evaluated using MATLAB. Then all the components are designed and simulated using commercial software SONNET.
7. In [13], a laboratory project on 4x4 Butler Matrix was presented. It was designed, implemented, and measured at the Microwave Lab of Indian Institute of Science, Bangalore. Cutting the ground techniques are used to reduce the resonance frequency, and the size of antenna. The use of crossover by cutting the ground plane made the Butler matrix compact.
8. In [14], a 4x4 Butler matrix has been designed in Ku-band with a central frequency of 12.5 GHz. Based on Substrate Integrated Waveguide (SIW) technology. SIW technology based on planar dielectric substrates with top and bottom metal layers perforated with metalized holes, the proposed system has the advantages of low cost, light weight and ease of fabrication and integration. SIW structures offer a compact, low loss, flexible, and cost-effective solution for integrating active circuits, passive components and radiating elements on the same substrate.

9. In [15], a branch-line coupler using two-step stub impedance operating at 2.45 GHz was designed based on size reduction, which gives the same performance in terms of reflection coefficient and S-parameter analysis as compared to the normal branch-line coupler.
10. In [16], a high temperature superconductors (HTS) Butler matrix beam-forming network was described. Reasonably good agreement between the simulated results. The Butler matrix demonstrates the possibility of making HTS Butler matrices without having crossovers, which is a benefit to reduce overall size.
11. In [17], a 4 x 4 X-Band Butler Matrices for antenna beam forming were designed, where theoretical basis, design specifications, tolerance analysis, and simulation building were included.
12. In [27], a 24 GHz 4-ways Butler Matrix Monolithic Microwave Integrated Circuit (MMIC) in CMOS technology was presented for smart antenna systems. The multi-layer structure of CMOS process was utilized to reduce the size and the overall return loss. The output relative phases were less than 6° deviation from the desired $\pm 135^\circ$, $\pm 45^\circ$, four orthogonal beams were pointing to $\pm 49^\circ$, $\pm 15^\circ$.
13. In [28], a steerable antenna array at 24 GHz Using Butler matrices with Micro Electro Mechanical Systems was presented, the designed 4 x 4 Butler matrix provided four different possible phase shifts at the output $\pm 45^\circ$, and $\pm 135^\circ$ with 2° error. The steering angles of approximately were $\pm 13^\circ$, and $\pm 43^\circ$.
14. In [29], a low loss 24-26 GHz 4x4 Butler Matrix for Beam Forming Antenna Systems Based on integrated passive device (IPD) was presented. The proposed Butler matrix occupied a chip area 2.2 x 1.9 mm², the outputs phase difference were $\pm 43^\circ$, $\pm 137^\circ$.

4.4 Substrate

RO4000 Series High Frequency Circuit Materials are glass-reinforced hydrocarbon/ceramic laminates designed for performance sensitive, high volume commercial applications. RO4000 laminates are designed to offer superior high frequency performance and low cost circuit fabrication. The result is a low loss material, which can be fabricated using standard epoxy/glass (FR4) processes offered at competitive prices [18].

Features [18]:

1. Excellent high frequency performance due to low dielectric tolerance and loss.
2. Stable electrical properties versus frequency.
3. Low thermal coefficient of dielectric constant.
4. Low Z-Axis expansion.
5. Low in-plane expansion coefficient.
6. Excellent dimensional stability.
7. Volume manufacturing process.

In our design, we took one standard model (RO4003C) from Roger standards substrates:

RO4003C -substrate properties [18]:

- Dielectric Constant $\epsilon_r = 3.38$
- Standard thickness = 0.203 mm
- Standard Copper Cladding = 35 μ m
- Dissipation Factor $\tan \delta = 0.0021$
- Volume Resistivity = 1.7 X 10¹⁰ M Ω •cm
- Surface Resistivity = 4.2 X 10⁹ M Ω
- Thermal Coefficient of $\epsilon_r = +40$
- Thermal Conductivity = 0.64 W/m/°K at 100°C

4.5 Computational Electromagnetic Algorithms

As the power of the computer continues to grow, computational electromagnetic (CEM) were used to tackle electromagnetic problems that could not be solved analytically. CEM also helps to provide fundamental insights into electromagnetic problems through the power of computation and computer visualization, making it one of the most important areas of engineering today [23], and [24].

Today, Several CEM algorithms are used, and are typically classified as so-called “exact” or “low-frequency” and “approximate” or “high-frequency” methods and further sub-classified into time- or frequency-domain methods [24].

Finite Difference Time Domain Method (FDTD), Finite Element Method (FEM), Method of Moments (MoM), Geometrical Theory of Diffraction (GTD), Physical Theory of Diffraction (PTD), and Shooting and Bouncing Rays (SBR) are common examples for the computational electromagnetic algorithms [24], and [25].

4.5.1 Method of Moments (MoM)

This technique is used to solve Maxwell's electromagnetic equations for planar structures embedded in a multilayered dielectric substrate by transforming them into integral equations [25]. The basic idea is to transform an integral or differential equation into a set of simultaneous linear algebraic equations (or matrix equation) which may then be solved by numerical techniques [23].

Equation (4.5) is a linear equation that explained the general case of the Method of Moments.

$$L(F) = g \quad (4.5)$$

where L is a known linear operator, g is a known excitation function, and F is the unknown function to be determined. In physics, L means the system transfer function and g represents the source. The objective is to determine F once L and g are specified. First, the function F is expanded using a series of known basis functions (or expansion Functions) f_1, f_2, f_3, \dots . In the domain of operator L , we have [23]:

$$F = \sum_n I_n f_n \quad (4.6)$$

where I_n are unknown complex coefficients to be determined and $n = 1, 2, \dots, N$. N should be infinite in theory but is a limited number in practice. We can replace F in Equation (4.5) by Equation (4.6) and use the linearity of L to give [23]:

$$\sum_n I_n L(f_n) = g \quad (4.7)$$

The problem becomes how to determine these unknown coefficients I_n . Secondly, a set of weighting functions (or testing functions) W_1, W_2, W_3, \dots in the domain of L is chosen and then the inner product is formed as [23]:

$$\sum_n I_n \langle W_m, L(f_n) \rangle = \langle W_m, g \rangle \quad (4.8)$$

where $m = 1, 2, \dots, M$. Again, M should be infinite in theory but is a finite number in practice and a typical, but not unique, inner product is defined as [23]:

$$\langle x(z), y(z) \rangle = \langle y(z), x(z) \rangle = \int_L x(z)y(z)dz \quad (4.9)$$

Thirdly, the inner product is performed on Equation (4.8) for $m = 1$ to M to give the matrix equation [23]:

$$\begin{bmatrix} \langle W_1, L(f_1) \rangle & \langle W_1, L(f_2) \rangle & \dots & \langle W_1, L(f_N) \rangle \\ \langle W_2, L(f_1) \rangle & \langle W_2, L(f_2) \rangle & \dots & \langle W_2, L(f_N) \rangle \\ \vdots & \vdots & \vdots & \vdots \\ \langle W_m, L(f_1) \rangle & \dots & \dots & \langle W_m, L(f_N) \rangle \end{bmatrix} \begin{bmatrix} I_1 \\ I_2 \\ \vdots \\ I_N \end{bmatrix} = \begin{bmatrix} \langle W_1, g \rangle \\ \langle W_2, g \rangle \\ \vdots \\ \langle W_m, g \rangle \end{bmatrix} \quad (4.10)$$

or, in other form [23]:

$$[Z_{mn}][I_n] = [V_m] \quad (4.11)$$

where

$$Z_{mn} = \langle W_m, L(f_n) \rangle \quad (4.12)$$

and

$$V_m = \langle W_m, g \rangle \quad (4.13)$$

Now the unknown coefficients can be yielded as [23]:

$$[I_n] = [Z_{mn}]^{-1}[V_m] \quad (4.15)$$

The unknown function F can therefore be obtained approximately using Equations (4.6) and (4.15).

The election of the basis functions and weighting functions is a key to obtaining accurate solutions efficiently and successfully. In general, the basis functions should have a capability to accurately represent and resemble the anticipated unknown function. There are several possible basis/weighting function sets, but only a limited number are used in practice. The N equations in Equation (4.10) must be linearly independent and give a unique solution [23].

In addition, they should be chosen to minimize the computations required to evaluate the inner product. If both the basis functions and weighting functions are the same, then this special procedure is known as Galerkin's method [23].

4.5.2 Advanced Design System 2011 (ADS) software

Advanced Design System is the world's leading electronic design automation software for RF, microwave, and high speed digital applications. In a powerful and easy-to-use interface, ADS pioneers the most innovative and commercially successful technologies, such as S-parameters and 3D EM simulators, used by leading companies in the wireless communication & networking and aerospace & defense industries [5],and [25].

ADS 2011 features made it easier for engineers to design multiple RF and microwave integrated circuits (implemented with a variety of technologies), assemble them in a package or on a multilayer laminate, and simulate electrical and 3D electromagnetic performance, all within a single platform [5]. Simulation models (microwave and RF) included in ADS 2011 are both based on MoM technique. Using different variations of the same technology are good ways to achieve best results [25].

4.6 Design of single inset fed patch antenna.

Refer to chapter two, the inset fed patch antenna equations were used to calculate the initial design parameters as seen in figure 4.3. The parameters were listed in table 4.1.

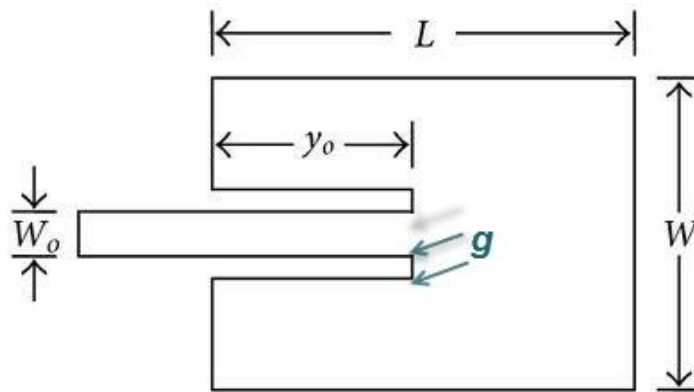


Figure 4.3 Inset fed patch antenna [23].

As we mentioned at previous section, the substrate will be Roger RO4003C.

- Operating frequency, $f_r=24$ GHz.
- Substrate thickness, $h = 0.203$ mm.
- Dielectric constant, $\epsilon_r = 3.38$.
- The characteristic impedance, $Z_o = 50 \Omega$.

Table 4.1 Mathematical calculation for inset fed patch antenna parameters.

Parameters	Calculated Dimension	Units
Dielectric (ϵ_r)	3.38	-
Effective (ϵ_{reff})	3.1376	-
Loss tangent ($\tan\delta$)	0.0021	-
Thickness (h)	0.203	mm
Operating frequency	24	GHz
Wavelength (λ)	12.5	mm
Effective wavelength (λ_{eff})	6.79	mm
Length (L)	3.33	mm
Effective length (L_{eff})	3.5311	mm
Width (W)	4.223	mm
Feeder width (W_o)	0.469	mm
Feeder Length (L_o)	3.807	mm
Cut depth (y_o)	1.105	mm
Gap (g)	0.22	mm

4.6.1 Design of inset fed patch antenna by ADS 2011 simulator

Single inset fed patch antenna was drawn with parameters listed in table 4.1 in the ADS 2011 layout. A single port with TLM calibration (50Ω), and adaptive frequency plan from [23-25] GHz with 100 points were configured. Then simulation options with mesh frequency 24 GHz, and mesh density 30 cells/wavelength were added. Roger 4003C substrate ($\epsilon_r = 3.38$), and sheet copper conductor thickness 0.035mm were selected. The layout of the patch antenna is shown in figure 4.4.

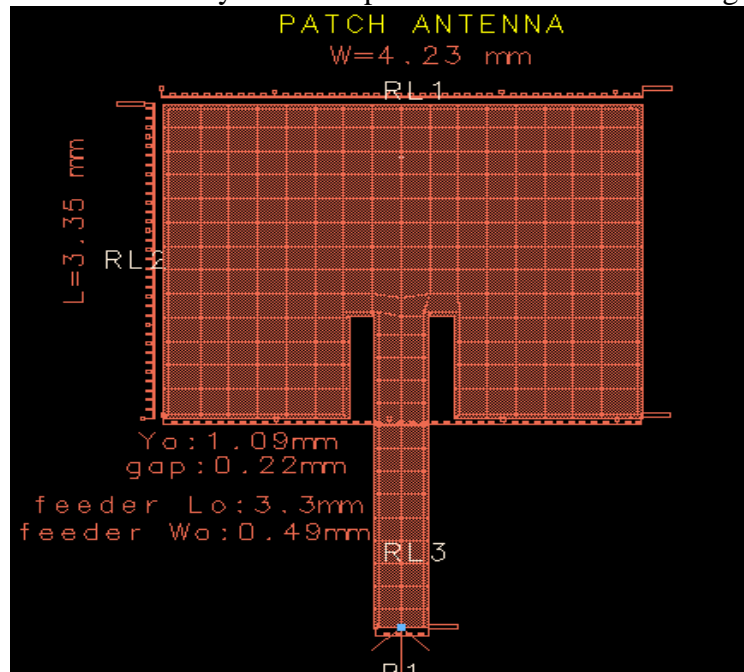


Figure 4.4 ADS inset fed patch antenna layout.

A goal of $S_{11} < -25$ dB was defined in simulation and the following parameters are obtained as shown in table 4.2.

Table 4.2 ADS simulated parameters for inset fed patch antenna.

Dimension	mm
Length (L)	3.35
Width (W)	4.23
Feeder width (W_o)	0.49
Feeder Length (L_o)	3.3
Cut depth (y_o)	1.09
Gap (g)	0.22

The simulation results show that the return loss: (S_{11}) = -30.139 dB at center frequency 24 GHz as depicted in figure 4.5.

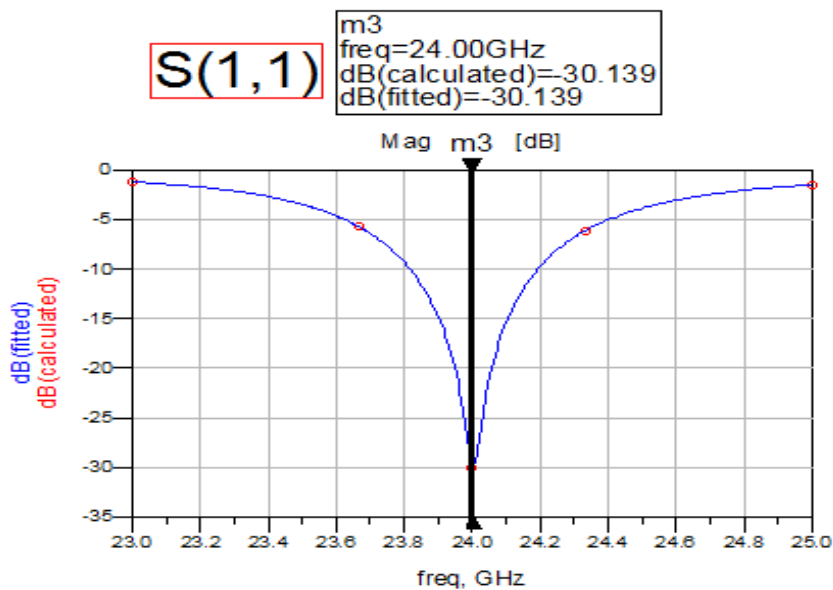


Figure 4.5 ADS simulated return loss S_{11} at 24 GHz.

4.7 Design of hybrid 3dB coupler

As seen in figure 4.6 the hybrid coupler consists of eight transmission lines with electrical length $L = \frac{\lambda}{4}$ with two different characteristic impedances $Z_{01} = 35.35\Omega$ and $Z_{02} = Z_o = 50\Omega$.

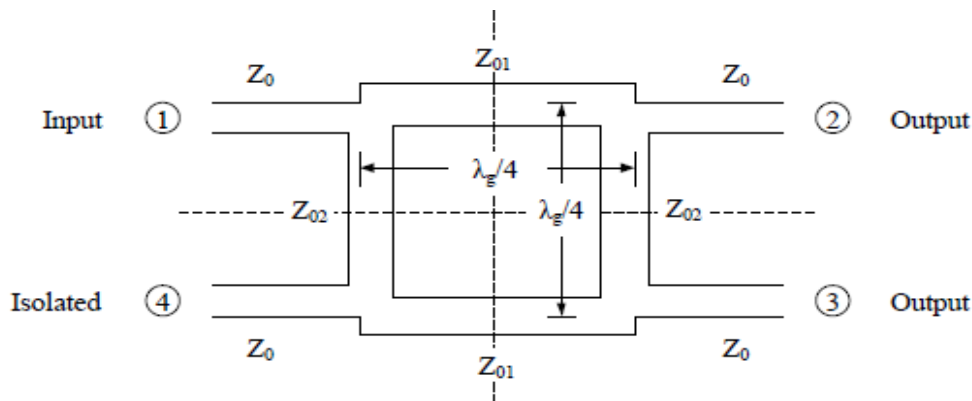


Figure 4.6 Hybrid 3dB coupler.

Now referred to equations missioned in chapter two we got:

Table 4.3 Mathematical calculation for 3dB coupler.

Dimensions	Transmission line Z_{01}	Transmission line Z_{02}, Z_0
Length	1.875 mm	1.912mm
Width	0.7582 mm	0.47 mm

4.7.1 Design of hybrid 3dB coupler by ADS 2011

The Line-Calc- tool listed in ADS 2011 was used to draw the initial eight transmission lines.

As seen in figure 4.7 the eight transmission lines were combined to get the 3dB coupler.

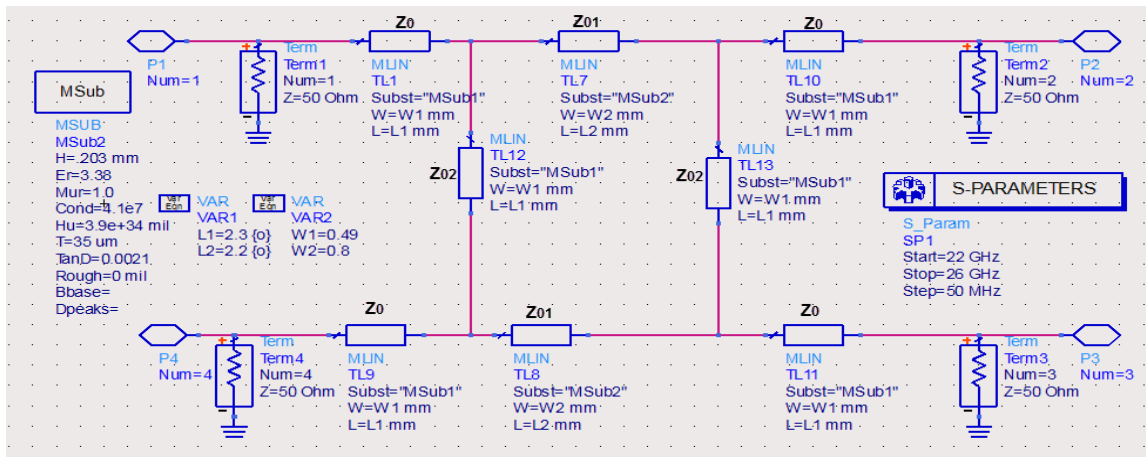


Figure 4.7 ADS 3dB coupler schematic draw.

The main goals to design 3dB coupler is to get excellent return loss (S_{11}) at center frequency 24 GHz, to get a phase difference between ports 2 and 3 of 90° , and magnitude of $S_{12} = -3\text{dB}$.

The design goals in ADS were defined such that $(S_{11} < -45)\text{dB}$, $\text{phase}(S(1, 2)) - \text{phase}(S(1, 3)) = 90^\circ$, and the simulation starts from 22 GHz to 26 GHz with 50 MHz step.

The ADS optimizer was run to get excellent results, and then it was converted to layout design by ADS layout generator, see figure 4.8. Four ports were configured with TLM calibration (50Ω). adaptive frequency plan was added from [23-25] GHz with 100

points, simulation option with mesh frequency of 24 GHz, and mesh density 25 cells/wavelength were configured.

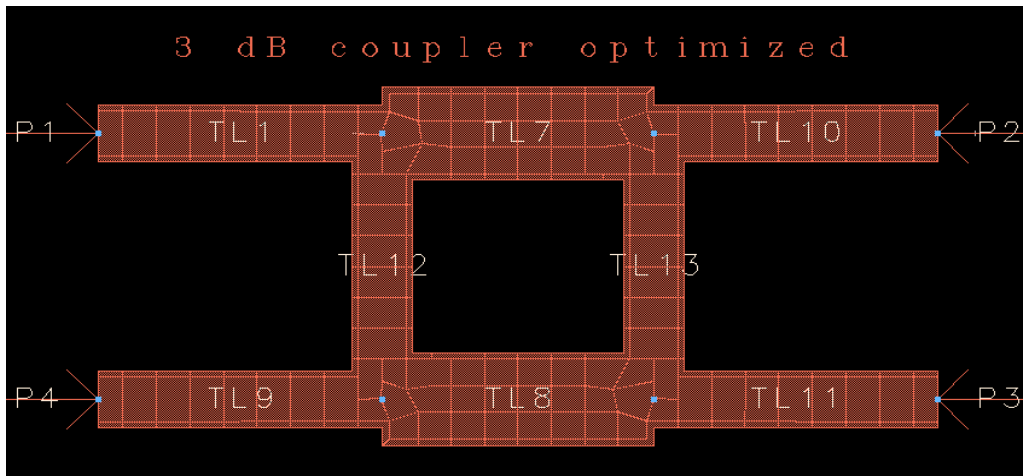


Figure 4.8 ADS 3dB optimized coupler layout.

The Optimized lengths and widths for the 3dB transmission lines by ADS layout optimizer are shown in table 4.4.

Table 4.4 ADS optimized parameters for 3dB coupler.

Dimensions	Transmission line Z_{01}	Transmission line Z_{02}, Z_{0}
Length	2.2 mm	2.3 mm
Width	0.8 mm	0.49 mm

From simulated results we got Return Loss (S_{11}) = -45.34dB, Insertion Loss (S_{12}) = - 2.8 dB as seen in figure 4.9.

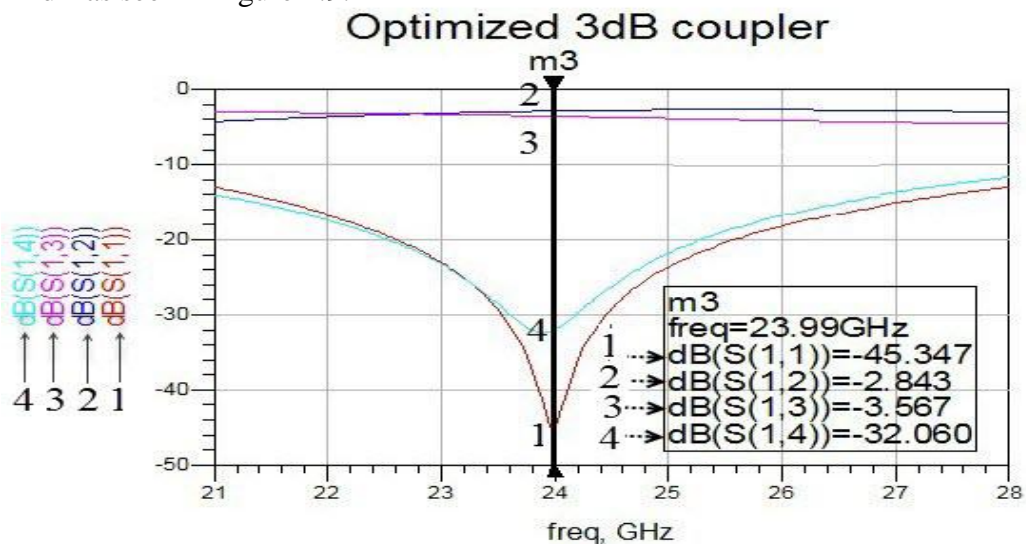


Figure 4.9 ADS simulated S-parameters for 3dB coupler at 24 GHz.

4.8 Design of 0 dB coupler (crossover)

In figure 4.10 the 0 dB coupler consists of 11 transmission lines with electrical length $L = \frac{\lambda}{4}$ and two different characteristic impedances $Z_{01} = 35.35\Omega$, $Z_{02} = Z_{03} = Z_0 = 50\Omega$.

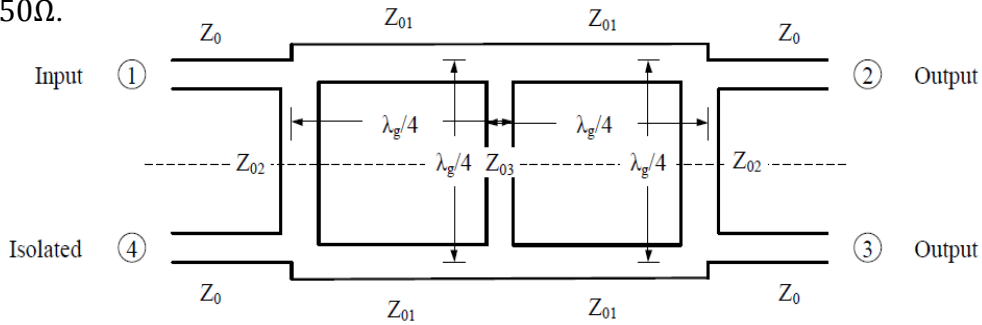


Figure 4.10 0 dB coupler (crossover).

Now refer to equations in chapter two we got the calculated dimensions as shown in table 4.5:

Table 4.5 Mathematical calculation for 0 dB coupler (crossover).

Dimensions	Transmission line Z_{01}	Transmission line Z_{02}, Z_{03}, Z_0
Length	1.875 mm	1.912 mm
Width	0.7582 mm	0.47 mm

4.8.1 Design of 0 dB coupler (crossover) by ADS 2011

As mentioned in chapter 3, cascading of two 90° hybrids to implement a crossover did not give the required performance and we need to modify the geometry of the 0 dB coupler, see figure 4.11.

The 11 transmission lines, and 4 Curved bends were combined to obtain the 0dB schematic draw seen in figure 4.11.

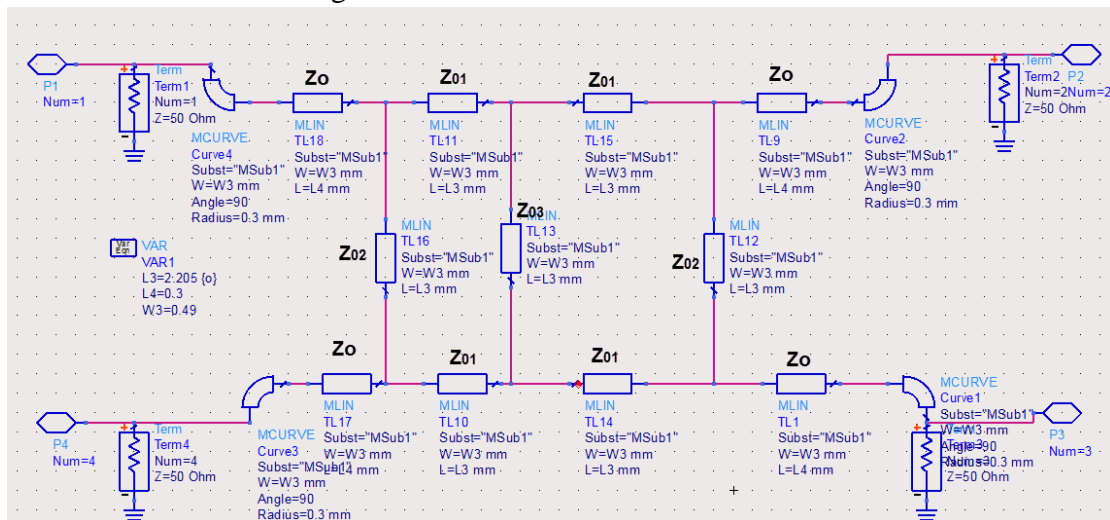


Figure 4.11 ADS 0 dB coupler schematic draw.

The main goals here in the design is to get magnitude of (S_{11}) , (S_{12}) , (S_{14}) less than -40 dB at the center frequency 24 GHz, and to get the magnitude of $(S_{13})=0$ dB at the center frequency 24 GHz.

Four ports were defined, with same configurations mention in previous section 4.7.1, then ADS optimizer was run to get excellent results, and was converted to layout design, see figure 4.12.

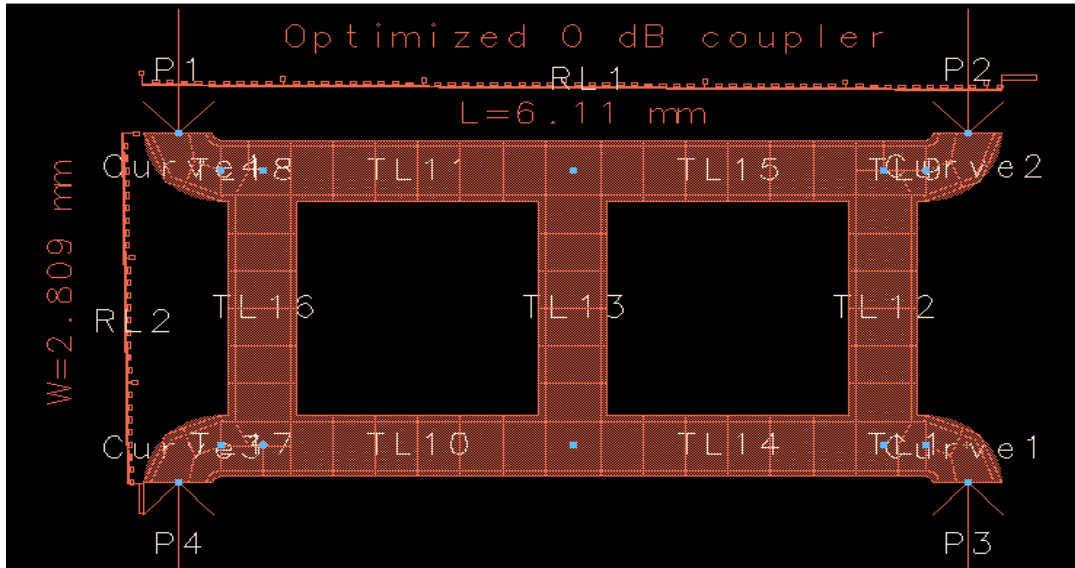


Figure 4.12 ADS 0 dB (crossover) optimized coupler layout.

The optimized lengths and widths for the 0 dB transmission lines by ADS layout optimizer are presented in table 4.6.

Table 4.6 ADS optimized parameters for 0 dB coupler.

Dimensions	Transmission line Z_{01}, Z_{02}, Z_{03}	Transmission line Z_0	Curved bend
Length	2.2 mm	0.3 mm	0.55 mm
Width	0.49 mm	0.49 mm	0.49 mm

The simulation results show Return Loss $(S_{11}) = -30.706$ dB, Insertion Loss $(S_{12}) = -52.7$, $(S_{13}) = -0.209$ dB, $(S_{14}) = -33.136$ as shown in figure 4.13.

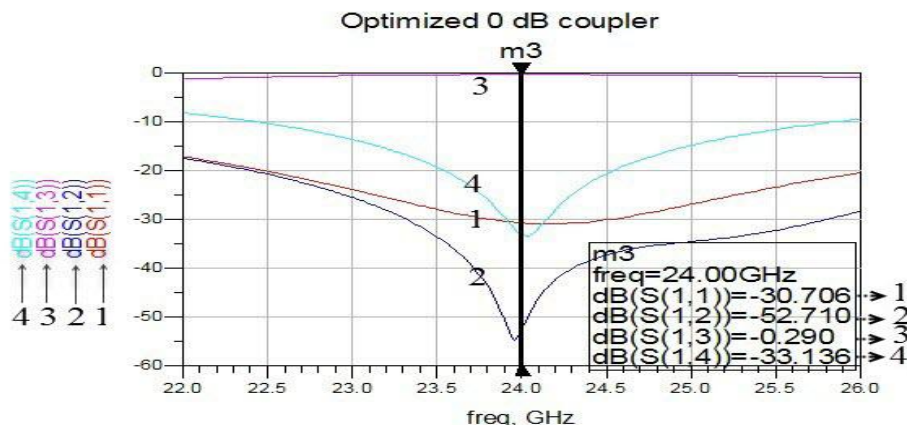


Figure 4.13 ADS simulated S-parameters at 24 GHz for 0dB coupler.

4.9 Design of phase shifter with ADS 2011

In our project, we want to design -45° phase shift, so equations mentioned in chapter three were used to find the initial electrical length for the phase shifter.

Note: To design the phase shifter first we have to build the whole system to determine the distance between two-phase shifter terminals then design your own shape phase shifter. In our design the initial distance between to phase shifter terminals was 2.8 mm, see figure 4.14.

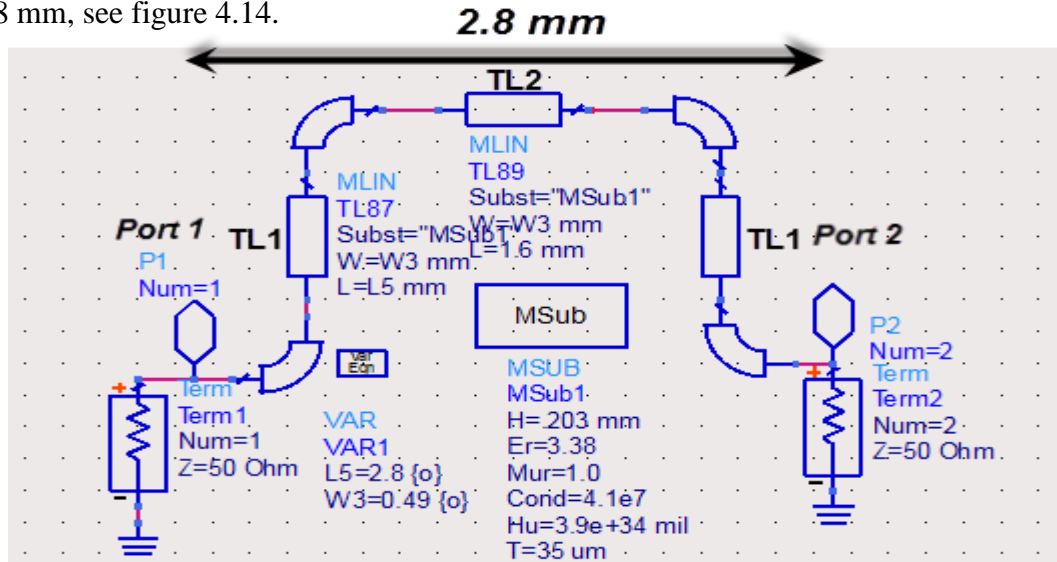


Figure 4.14 ADS -45° phase shifter schematic draw.

The main goal here is to get phase $(S_{12}) = -45^\circ$ at center frequency 24 GHz.

The ADS optimizer was run with two ports, and same configurations mention in previous section 4.7.1, and then was converted to layout design, see figure 4.15.

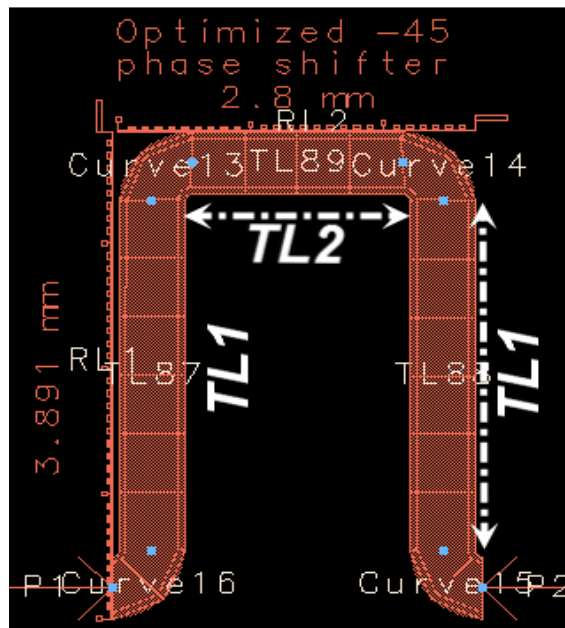


Figure 4.15 ADS optimized -45° phase shifter layout.

The Optimized lengths and widths for the -45° transmission lines by ADS layout optimizer are listed in table 4.7:

Table 4.7 ADS optimized parameters for -45 phase shifter.

Dimensions	Transmission line 1 Zo	Transmission line 2 Zo	Curved bend	Overall length
Length	2.8 mm	1.6 mm	0.55 mm	9.4 mm
Width	0.49 mm	0.49 mm	0.49 mm	0.49 mm

The simulated insertion loss phase shift (S_{12}) = -45° at center frequency 24 GHz is presented in figure 4.16.

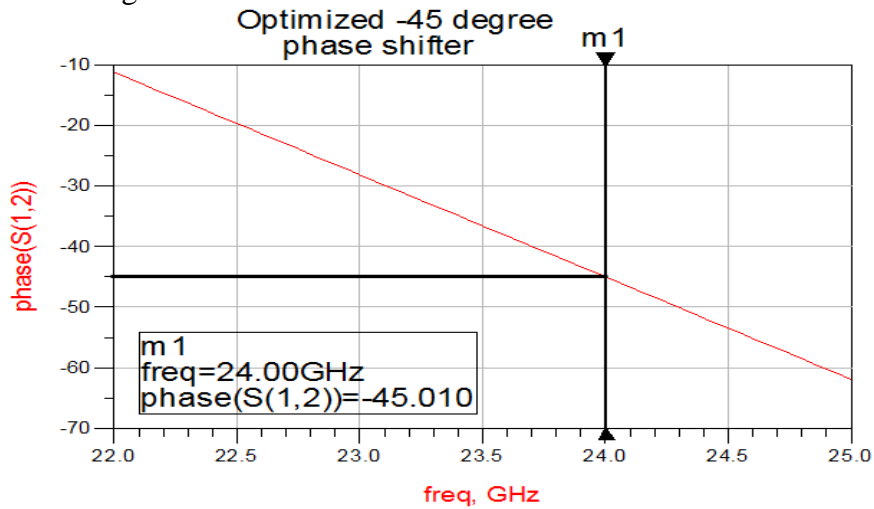


Figure 4.16 ADS phase (S_{12}) for -45° phase shifter at 24 GHz.

4.10 Design of microstrip path connecting butler matrix to antennas

The main two considerations to design the path between butler matrix and antenna are the length of the path and the distance between the butler matrix output ports, see figure 4.17.

We will use (4.16) to find the initial electrical length for the connecting butler matrix path length that its ($\text{phase}(S_{12})=0$) [26], and [27].

$$L = n\lambda \quad (4.16)$$

Where n is integer and λ is the effective wavelength.

We will use (4.17) to get the distance between butter matrix output ports [1], [26], and [27].

$$D \approx \frac{\lambda}{2} \quad (4.17)$$

Now back to ADS 2011 transmission lines with curve bends were defined and optimization goal that the phase (S_{12}) = 0 was added.

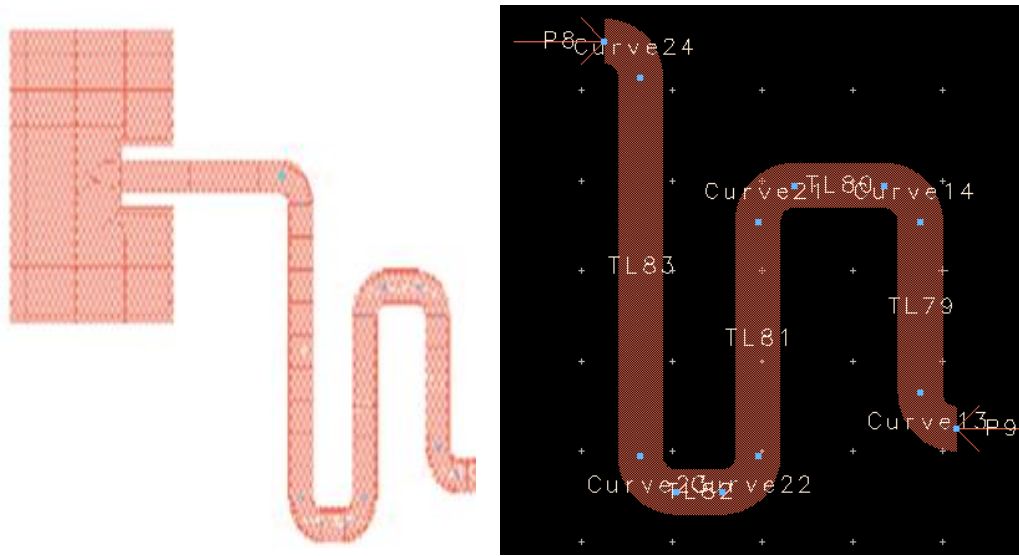


Figure 4.17 ADS optimized path to antenna layout.

The optimized path to antenna is presented in figure 4.17, and the overall length and width are listed in table 4.8.

Table 4.8 ADS optimized path to antenna dimensions.

Dimensions	Overall length
Length	13.18 mm
Width	0.49 mm

4.11 Design of butler matrix without antenna array by ADS2011

After each part was designed, the parts were combined together to get the butler matrix layout without antennas.

The main design goals are as follows:

1. The Return Loss (S_{11}) < -30 dB at center frequency 24 GHz.
2. If input at port 1 the phase shift between four output ports = 135°.
3. If input at port 2 the phase shift between four output ports = -45°.
4. If input at port 3 the phase shift between four output ports = 45°.
5. If input at port 4 the phase shift between four output ports = -135°.
6. The butler matrix insertion loss from input port to output port at most = -8 dB (we have two cascaded - 3dB couplers with crossover).
7. The butler matrix size reduction.
8. The output ports spacing distance $D \approx \frac{\lambda}{2}$.

Therefore, the schematic design in ADS 2011 with parametric lengths was drawn as shown in figure 4.18, and then eight objective goals were defined.

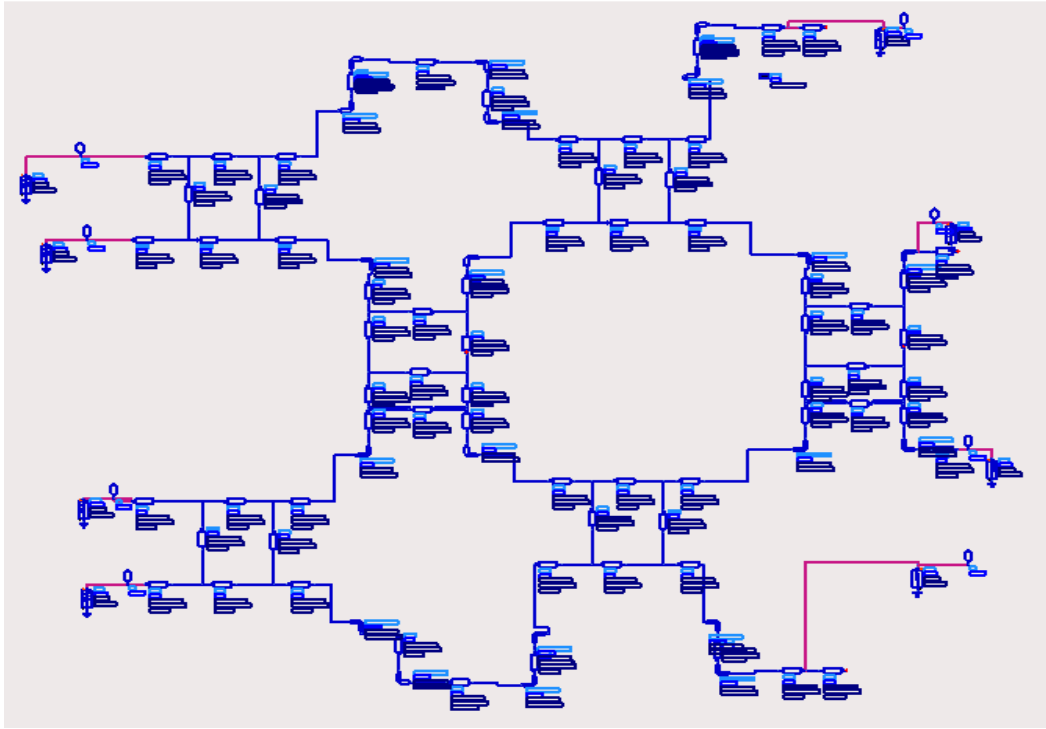


Figure 4.18 ADS Butler Matrix schematic draw.

The layout of the whole butler matrix is shown in figure 4.19 and the optimized goals are shown in figure 4.20 to 4.25.

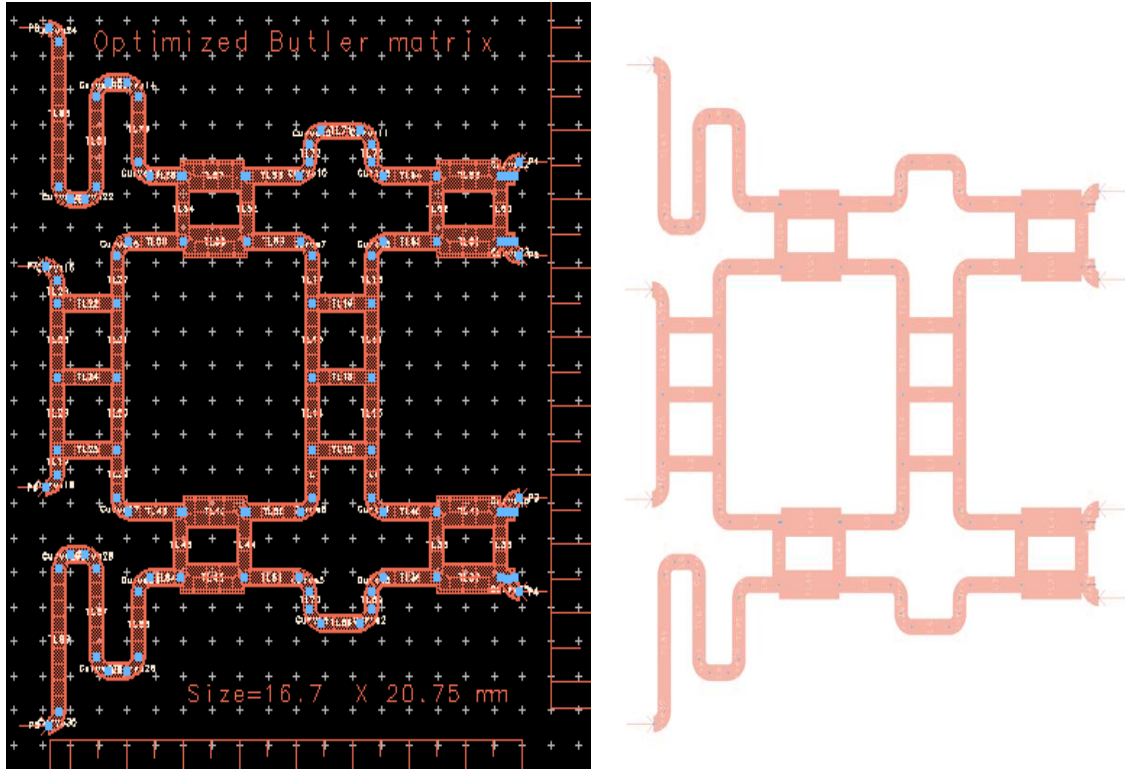


Figure 4.19 ADS optimized Butler Matrix layout.

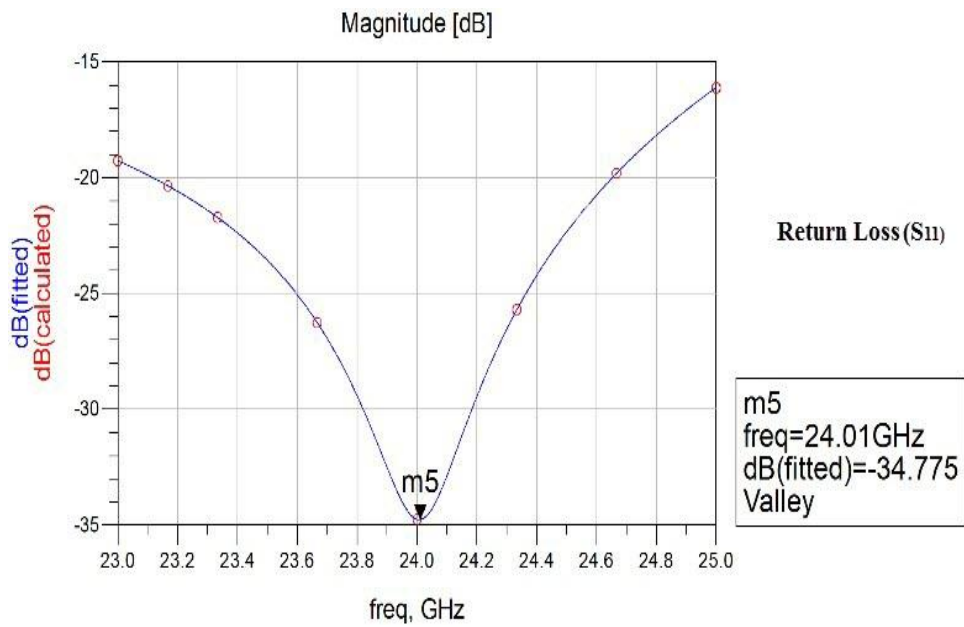


Figure 4.20 ADS first optimized goal the return loss (S₁₁) < -30 dB at 24 GHz.

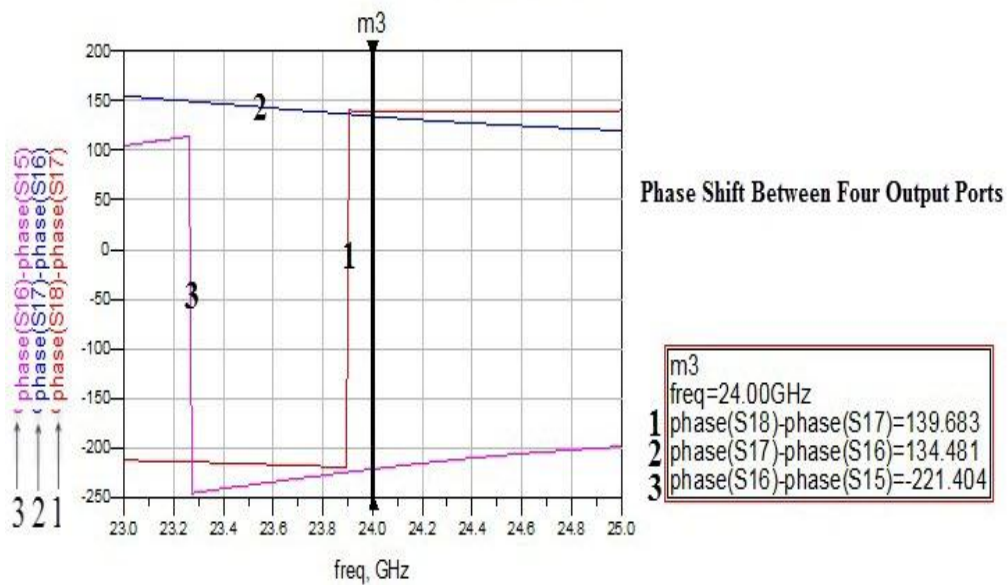


Figure 4.21 ADS second optimized goal outputs phase shifts (135°) at 24 GHz.

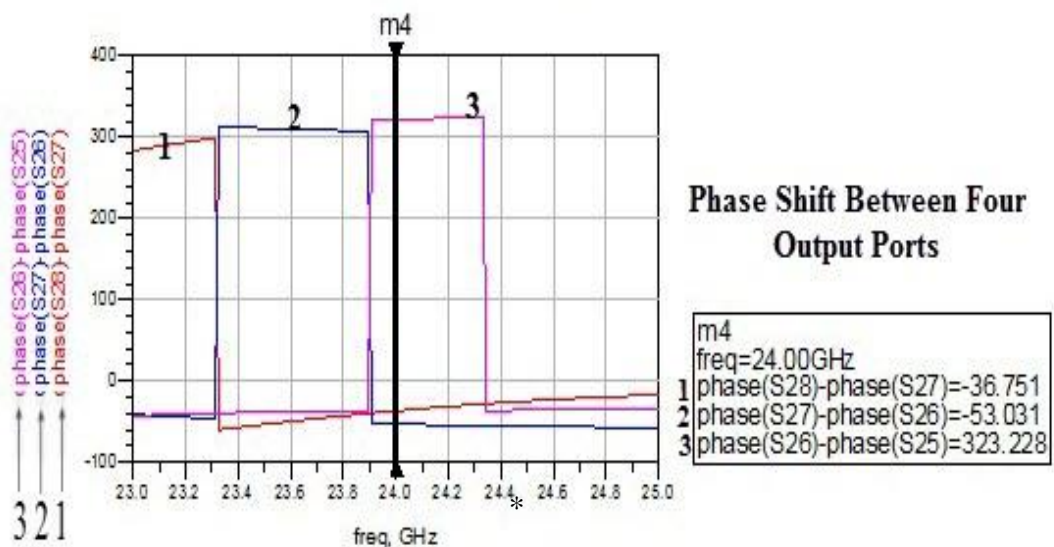


Figure 4.22 ADS third optimized goal outputs phase shifts (-45°) at 24 GHz.

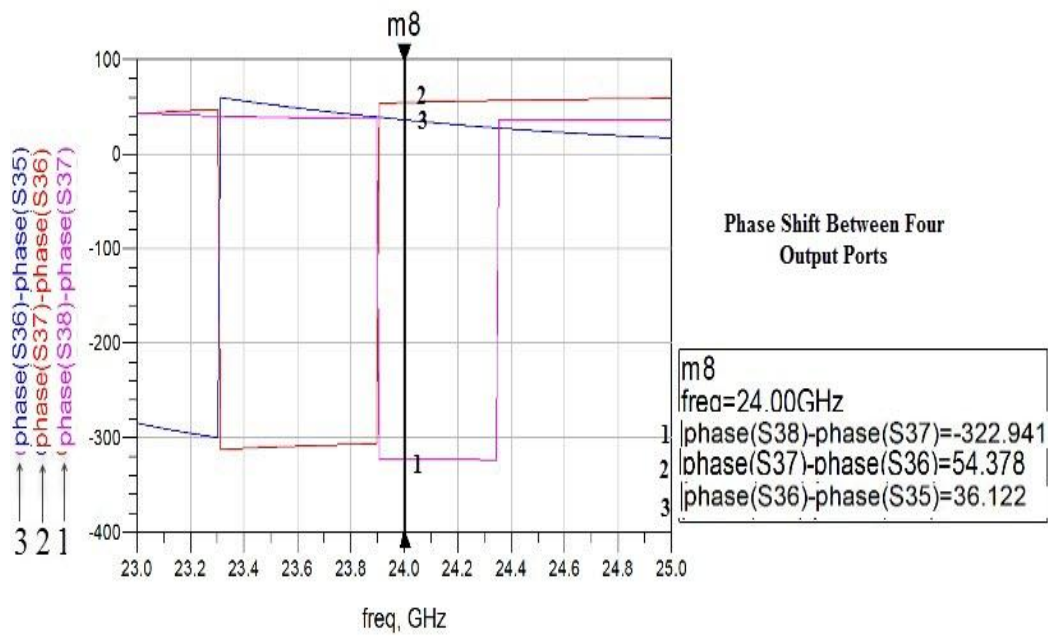


Figure 4.23 ADS fourth optimized goal outputs phase shifts (45°) at 24 GHz.

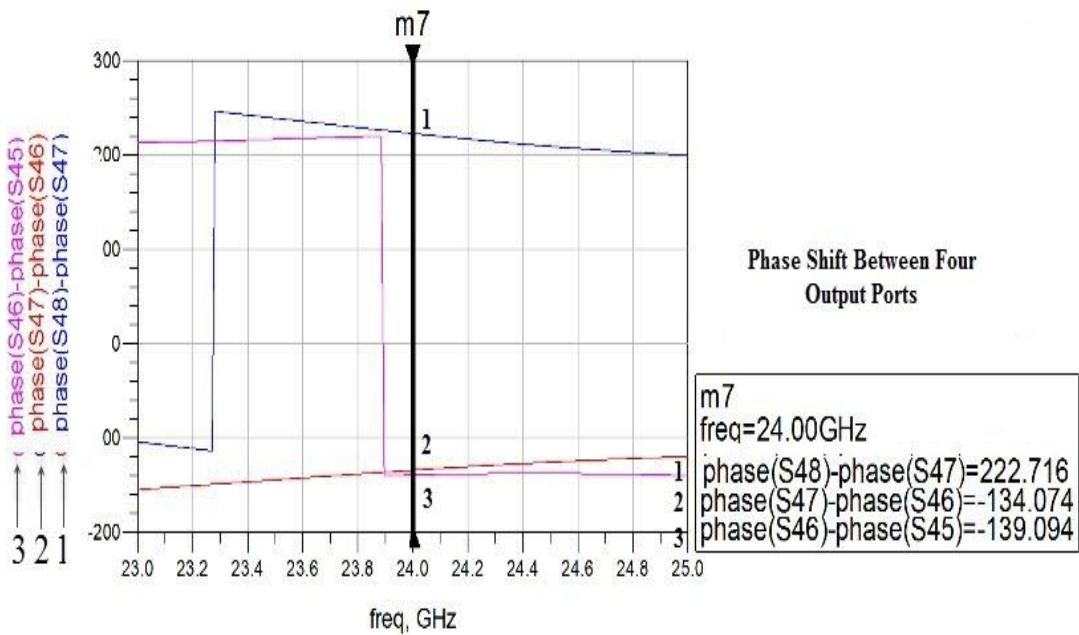


Figure 4.24 ADS fifth optimized goal outputs phase shifts (-135°) at 24 GHz.

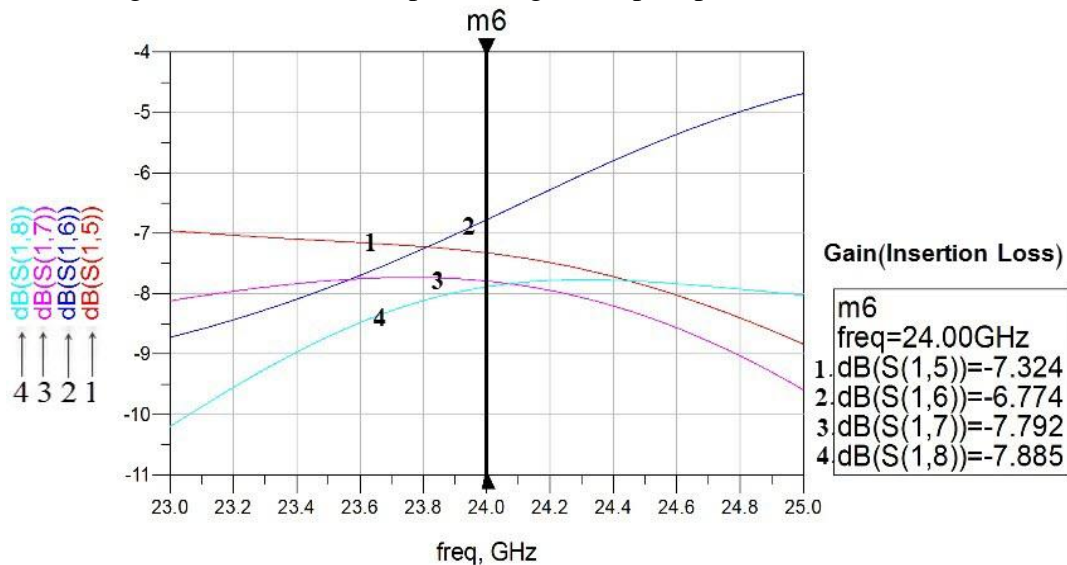


Figure 4.25 ADS sixth optimized goal insertion loss at 24 GHz.

As seen in table 4.9 best results that achieved our desired goals were taken and listed.

Table 4.9 ADS optimized Butler Matrix simulated results

First Goal:	Return Loss (S_{11}) at center Frequency 24 GHz	-34 dB
Second Goal: Phase Shift	Phase (S_{18})-(S_{17})	139.6°
	Phase (S_{17})-(S_{16})	134.4°
	Phase (S_{16})-(S_{15})	138.6°
Third Goal: Phase Shift	Phase (S_{28})-(S_{27})	-36.7°
	Phase (S_{27})-(S_{26})	-53.0°
	Phase (S_{26})-(S_{25})	-36.8°
Fourth Goal: Phase Shift	Phase (S_{38})-(S_{37})	37.1°
	Phase (S_{37})-(S_{36})	54.3°
	Phase (S_{36})-(S_{35})	36.1°
Fifth Goal: Phase Shift	Phase (S_{48})-(S_{47})	-137.2°
	Phase (S_{47})-(S_{46})	-134.0°
	Phase (S_{46})-(S_{45})	-139.0°
Sixth Goal: Gain (Insertion Loss)	dB (S_{14})	-7.3
	dB (S_{15})	-6.7
	dB (S_{16})	-7.7
	dB (S_{17})	-7.8
Seventh Goal:	System Size	16.7 mm x 20.7 mm
Eighth Goal:	Output Ports Distance	6.68 mm

Table 4.9 illustrated the final optimized simulated butler matrix results without antennas, it can be seen that the overall return loss was below -30 dB, the outputs phase shift was $\pm 45^\circ, \pm 135^\circ$ with phase error 6° . Best insertion loss was -6.7 dB with 1dB error. The distance between antennas was considered to be $\frac{\lambda}{2} = 6.68$ mm, the overall optimized size was 345 mm^2 .

4.12 Design of butler matrix with antenna array by ADS 2011

Now after the Butler Matrix was designed, it was integrated with four inset fed antennas. Some self-tuning was used in the design to achieve the main eight goals listed in previous section. See the final design in figure 4.26.

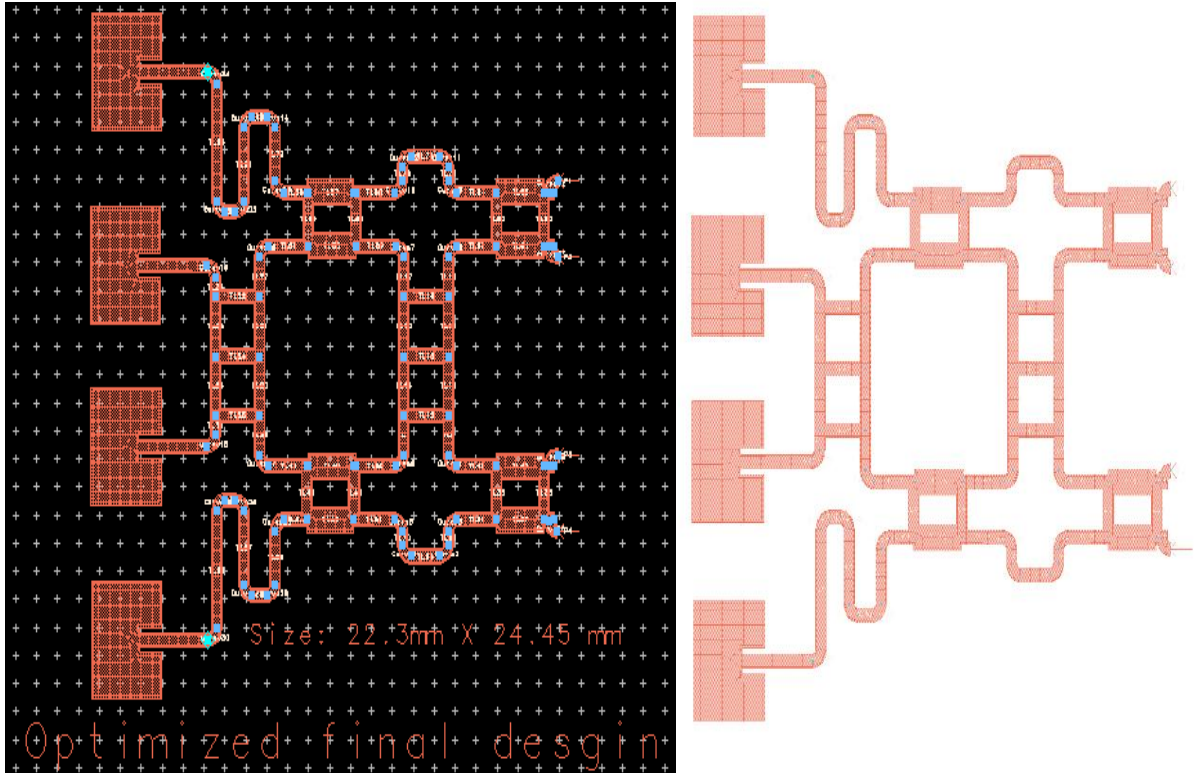


Figure 4.26 ADS Final optimized design layout.

Now we want to draw the far field radiation pattern when individual input port is fed to test the beam steering functionality. ADS momentum visualization tool was used to observe the pattern with far field cut at $\theta = 0^\circ$, and $\phi = 90^\circ$.

1. When port 1 is fed, the far field is shown in figure 4.27, the max power radiated for main lobe was at -43° .

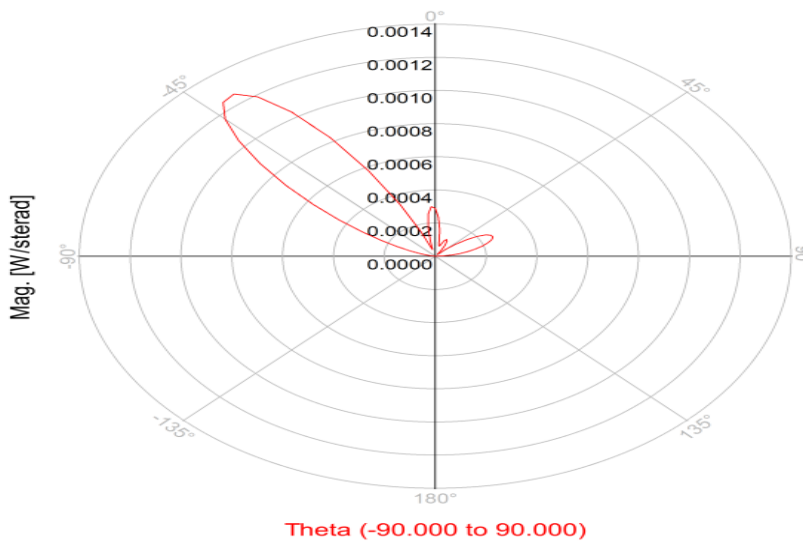


Figure 4.27 Radiation pattern when port 1 is fed.

2. When port 2 is fed, the far field is shown in figure 4.28, the max power radiated for main lobe was at +13°.

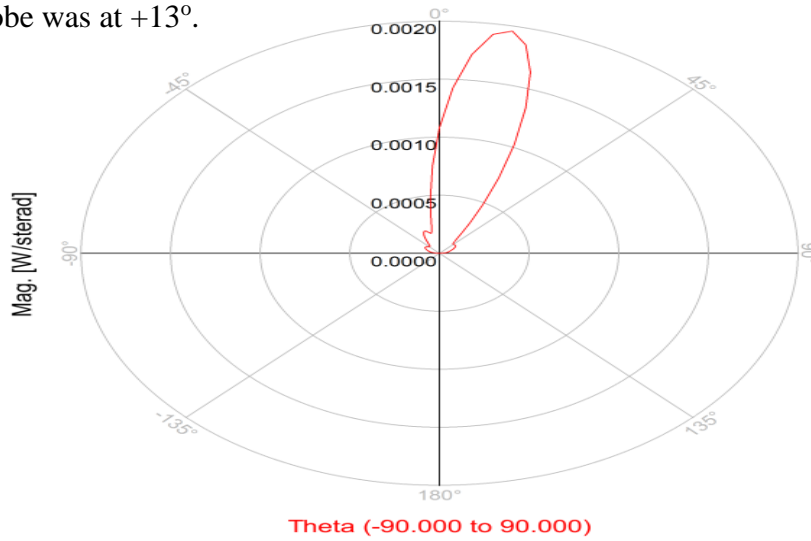


Figure 4.28 Radiation pattern when port 2 is fed.

3. When port 3 is fed, the far field is shown in figure 4.29, the max power radiated for main lobe was at -13°.

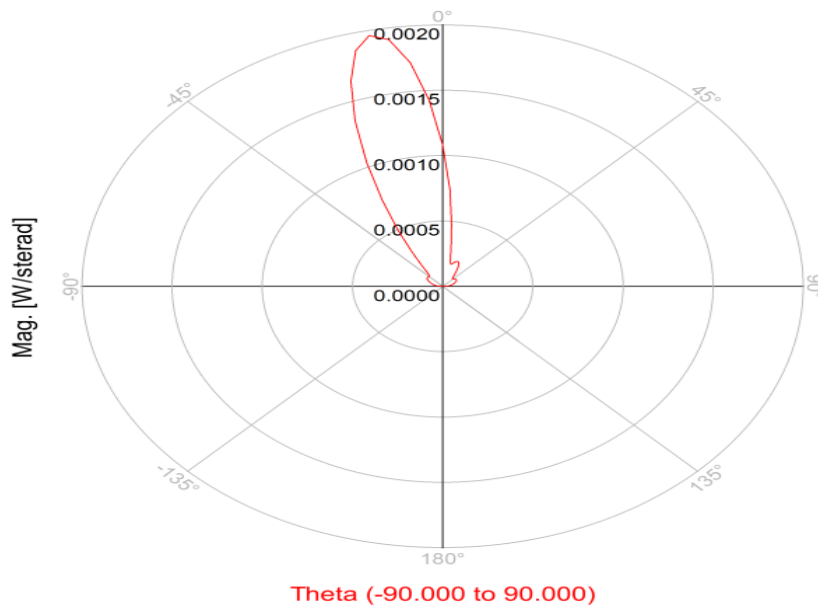


Figure 4.29 Radiation pattern when port 3 is fed.

4. When port 4 is fed, the far field is shown in figure 4.30, the max power radiated for main lobe was at $+43^\circ$.

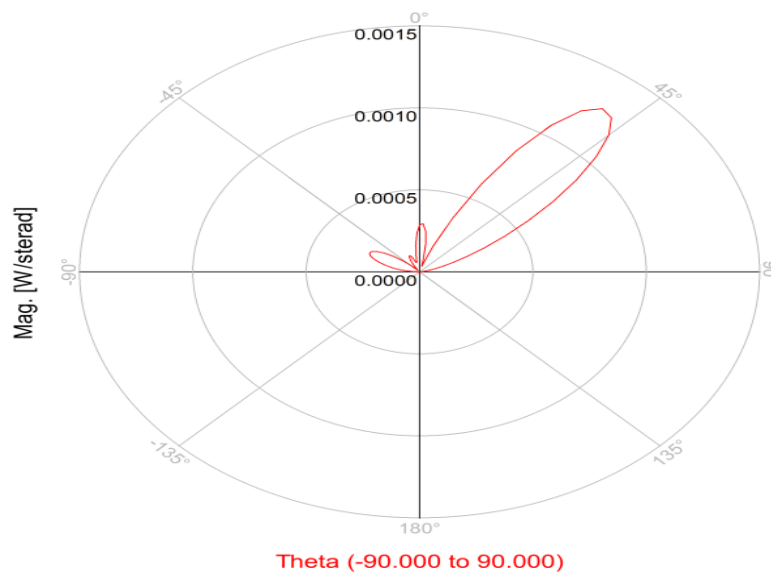


Figure 4.30 Radiation pattern when port 4 is fed.

Figure 4.31 illustrated the far field radiation patterns when individual input port is fed, and explains the butler matrix beam steering functionality.

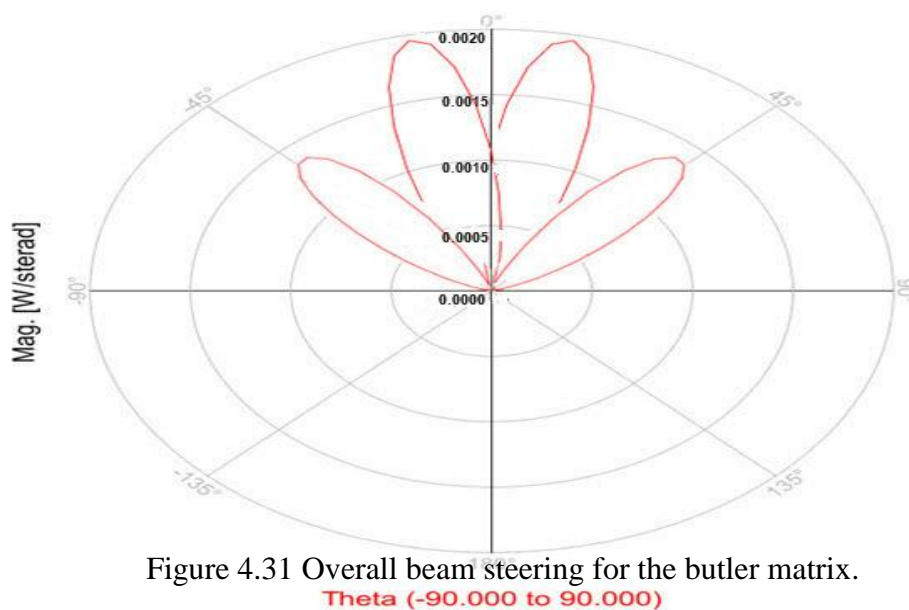


Figure 4.31 Overall beam steering for the butler matrix.

From figure 4.27 to 4.31, it is clearly depicts that the four beams generated by the butler matrix cover 86° .

The simulated Antenna parameters were listed in Table 4.10, when port 1 is fed.

Table 4.10 ADS simulated antenna parameters


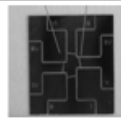
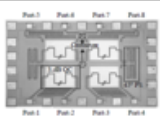
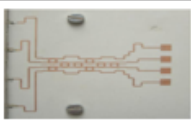


Antenna parameters	Values
Power Radiated	1.14 mw
Directivity	11.6194 dBi
Antenna Gain	9.623 dBi
Max Intensity	1.63 mw/streadians
Effective angle (steradians)	0.8655
Antenna efficiency	62 %

From table 4.10, the simulated response of the butler matrix with four antennas was listed assuming a signal is input at port 1, the maximum radiated power was -29 dB, the antenna efficiency was 62%, the maximum antenna gain reached 9.623 dBi, and the directivity was 11.6 dBi.

4.13 Contribution

Our results were listed and compared with previous studies in table 4.11. The return loss, size, steering angles, phase shifts and bandwidth are good compared with other studies.

Table 4.11 Results Comparison

Parameters	Design of a 4x4 Butler Matrix for Vehicle Radar Beam forming Antenna systems at 24 GHz	A novel wide-band Butler matrix for vehicle radars at 24GHz	A 24-GHz CMOS Butler Matrix MMIC for Multi-Beam Smart Antenna Systems	four-beam antenna array for 24 GHz applications fed by 4 x 4 butler matrix	Steerable Antenna Array at 24 GHz Using Butler matrices & Micro Electro Mechanical Systems-switches	A Compact 24-26 GHz integrated passive device-Based 4x4 Butler Matrix for Beam Forming Antenna Systems
Date	2014	IEEE 2008	IEEE 2008	IEEE 2013	IEEE 2012	APMC 2012
Simulator	ADS 2011	Sonnet v.10				EM
Range	22-25 Ghz		23-25 Ghz	0.8 Ghz		24-29 Ghz
Size	20 x 16 mm ²	20 x 17 mm ²	0.44 mm ²			2.2 x 1.9 mm ²
Return Loss	-34 dB	-18 dB	-19 dB	-20 dB		-20 dB
Phase difference	± 39°,±137°	± 47°,±133°	± 39°,±129°	± 44°,±137°	± 44°,±132°	± 43°,±137°
Steering angles	± 13°,±43°		± 14°,±49°	± 12°,±36°	± 14°,±46°	
Max peak to null power	-29.4 dB		35 dB			
Over all insertion loss	-7.3 dB	-7 dB	-8.26 dB	-7.5 dB		-8.2 dB
Bandwidth	3 Ghz		2 Ghz			2 Ghz
Draw						
Technology	Microstrip	Micro Machined	Micro-CMOS	Microstrip	Monolithic Microwave Integrated Circuits	Coplanar Waveguide Chip

References

- [1] A. Balanis, I. Ioannidis, Introduction to Smart Antennas, Morgan & Claypool Publishers, 2007, ISBN: 1598291777.
- [2] C. Sun, J. Cheng, T. Ohira, Handbook on Advancements in Smart Antenna Technologies for Wireless Networks, 1st ed., Information Science Reference, Hershey, New York, USA, 2009, ISBN10: 1599049880.
- [3] M. El-Tager, M.A. Eleiwa, "Design and implementation of smart antenna using butler matrix for ISM band", Progress in Electromagnetic Research symposium, Beijing, China, March 23-27, 2009, pp. 571-575.
- [4] J. Butler and R. Lowe, "Beam-Forming Matrix Simplifies Design of Electronically Scanned Antennas," Electronic Design, vol. 9, pp. 170-173, Apr. 1961.
- [5] Available on: "<http://www.home.agilent.com/en/pc-1297113/advanced-design-system-ads?&cc=PS&lc=eng>".
- [6] S. Ahmad, F.C. Seman, "4-Port Butler Matrix for Switched Multibeam Antenna Array", IEEE, Asia-Pacific Conference on Applied Electromagnetics Proceedings, Johor, Malaysia, December 2005, ISBN: 0-7803-9431-3.
- [7] A. Chavez, I. Garro, "A novel wide-band Butler matrix for vehicle radars at 24GHz.", IEEE, 18th International Conference on Electronics, Communications and Computers. School of EECS, Seoul National University, Korea, 2008, ISBN: 978-0-7695-3120-5.
- [8] P. Sanz, I. Slomian, "Four-beam antenna array for 24 GHz applications fed by 4 x 4 butler matrix", Microwave and Telecommunication Technology, 23rd Int. Crimean Conference, IEEE Catalog Number: CFP13788, 2013, ISBN: 978-966-335-395-1.
- [9] O. U. Khan, "Design of X-band 4x4 Butler Matrix for Microstrip Patch Antenna Array", telecommunication Conference, IEEE, 2006, ISBN: 1-4244-0548-3.
- [10] M. demerdash, A. Abdin, A. Mitkee, H. Elmikati, "Effect of Mutual Coupling on the Performance of Four Elements Microstrip Antenna Array Fed by a Butler Matrix", 29th National Radio Science Conference, Cairo, Egypt, 2012.
- [11] C. Tseng, "A Low-Cost 60-GHz Switched-Beam Patch Antenna Array with Butler Matrix Network", Antennas and Wireless Propagation Letters, IEEE, VOL. 7, 2008, ISSN: 1536-1225.
- [12] W. Bhowmik, S. Srivastava, "Optimum Design of a 4x4 Planar Butler Matrix Array for WLAN Application". Journal of Telecommunications, VOL 2, ISSUE 1, April 2010.
- [13] M. AbdKadir, M. Rose, M. Shah, D. Misman, M. Suaidi, M. Aziz, "4x4 Butler Matrix Design by Using Circular Bend", Asia Pacific conference on applied electromagnetic proceedings, IEEE, December, 2007, ISBN: 978-1-4244-1434-5.
- [14] T. Djera, N. J. G. Fonseca, "Design and Implantation of a Planar 4X4 Butler Matrix in substrate integrated waveguide Technology for Wide band high power applications", Progress in Electromagnetics Research B, Vol. 35, 29-51, 2011.
- [15] N. A. Muhammad, T. A. Rahman, "Beam Forming Networks Using Reduced Size Butler Matrix", Antennas and Propagation European conference, IEEE, 2010, ISBN: 978-84-7653-472-4.

- [16] A. Corona, M.J. Lancaster. "A high-temperature superconducting Butler matrix", Applied Superconductivity, IEEE Transactions on, Vol. 13, Issue. 4, Dec.2003.
- [17] M. Mujezinovic, M. Pecoraro, "4X4 X-Band Butler Matrices as Antenna Beamformers", Multi-Disciplinary Senior Design Conference, Rochester, New York, 2008.
- [18] RO4000®, Series Advanced Circuit Materials Division, data sheet, revised 1107-0.5CC .Publication #92-004, 2007.
- [19] M. Matin, A. Sayeed,"A Design Rule for Inset-fed Rectangular Microstrip Patch Antenna", Department of Electrical Engineering and Computer Science North South University, transactions on communications, January 2010, ISSN: 1109-2742.
- [20] L.Shani, "Design of microwave hybrid couplers using inter-coupled resonators", Communication, Master thesis, the University of Birmingham, 2012.
- [21] W.Li, C.Chu, S. Chang , "Switched-beam Antenna Based on Modified Butler Matrix With Low Side lobe Level" ,Electronics Letters, Volume 40, issue 5, 4th March 2004.
- [22] B. Pattan,"The Versatile Butler Matrix", Microwave Journal, Horizon House Publications, 2004.
- [23] Yi. Huang, Antennas from Theory to Practice, Wiley, Oct.2008, ISBN:-470-0-978 51028.
- [24] W.Gibson, "The Method of Moments in Electromagnetics", Chapman & Hall/CRC Taylor & Francis Group, New York, 2008, ISBN: 978-1-4200-6145-1.
- [25] Available on: "http://cp.literature.agilent.com/litweb/pdf/ads2008/mom/ads2008/Theory_of_Operation_for_Momentum.html."
- [26] M. hefrawy "Microstrip Antennas for Indoor Wireless Dynamic Environments", Microstrip Antennas, Intec, Ch16, ISBN 978-953-307-247-0, April 2011.
- [27] T.Chin, S.Chang, C.Chang, and J.Wu, "A 24-GHz CMOS Butler Matrix MMIC for Multi-Beam Smart Antenna Systems", IEEE Radio Frequency Integrated Circuits Symposium ,Department of Communications Engineering, Center for Telecommunication Research, National Chung Cheng University, Chia-Yi, 621, Taiwan, ,2008
- [28] M.Campo, W.Simon, R. Baggen, "Steerable Antenna Array at 24 GHz Using Butler matrices & MEMS-switches", IEEE conference, Kamp-Lintfort, Germany, 2012.
- [29] I. Haroun, T. Lin., D. Chang, C. Plett,"A Compact 24-26 GHz IPD-Based 4x4 Butler Matrix for Beam Forming Antenna Systems",Carleton University, Proceedings of APMC 2012, Kaohsiung, Taiwan, Dec. 4-7, 2012.

Chapter 5

Conclusion and Future Work

5.1 Conclusion

The Butler matrix can work as a beam-forming network permitting volumetric beams. In addition, each port will have the gain of the full array; it can be used for both receiving and transmitting signals in an antenna array. The beams may be deployed depending on the application functionality.

In this thesis Butler Matrix with patch antennas were designed as an application to work at 24 GHz for anti-crash car radar systems. Our system consists of (four inset-fed patch antennas, four 3 dB couplers, two-phase shifters, antenna path, and two 0 dB couplers (crossover)).

At first, mathematical equations were used to design each part in our system such as the patch antenna, 3dB coupler, 0dB crossover, antenna path and the phase shifter.

Then, ADS 2011 software based on MoM was used to design and simulate our system. ADS optimization methods were selected such as parameter sweep and automatic tuning to obtain the desired results.

Finally, after eight optimization goals were defined, best results were picked for overall system at 24 GHz, and the results were as follows: the return loss was below -34 dB, the realized antenna gain was 9.6 dBi, and the power radiated was -29.4 dB (1.14 mw).

Four azimuth coverage was 86° degree, the directivity was 11.6194 dBi, the max Power intensity was -27 dB, the optimum size was 16.7 mm x 20.7 mm, the phase shift between all output ports was $\pm 39^\circ$, $\pm 137^\circ$, and the overall insertion loss was -6.7 dB. With bandwidth more than 3 GHz.

5.2 Future Work

Our project can be developed to work in other frequencies for different applications. The number of input and output ports can be increased to get better beam-forming coverage area, and several types of antenna can be used in our system depending on the application.

It is intended to get the Butler Matrix with patch antennas fabricated and tested to validate the design method. The fabrication will be done in a place where fabrication and measurement equipment are available.